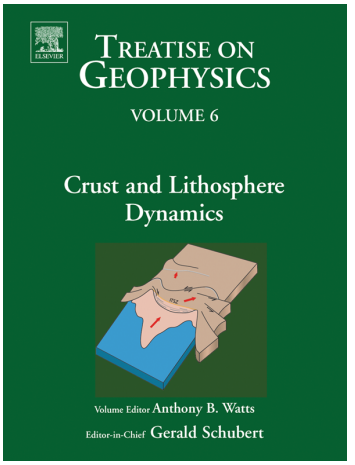

6.03 Plate Rheology and Mechanics

E. B. Burov, University of Paris, Paris, France

6.03.1 Introduction

The rheology and strength of the Earth's lithosphere has been a topic of debate since the beginning of the twentieth century when Joseph Barrell introduced the concept of a strong lithosphere overlying fluid asthenosphere (Barrell, 1914). This concept constitutes an integral part of plate tectonics (e.g., Le Pichon *et al*., 1973; Watts, 2001; Turcotte and Schubert, 2002) and the question of how the strength of the plates varies spatially and temporally is a fundamental one of wide interest in geology and geodynamics (e.g., Cochran, 1980; Jackson, 2002; Burov and Watts, 2006; *see* Chapter 6.01).

The strength of the plates depends on their structure and rheological properties exhibited in the particular geodynamic context. For a rock of given mineralogical composition and microstructure, the most important controlling parameters are pressure, temperature, strain, strain rate, strain history, pore fluid pressure, grain size, fugacities of volatiles, and chemical activities of mineral components (Evans and Kohlstedt, 1995). Goetze and Evans (1979) were the first to combine the data of experimental rock mechanics and extrapolate them onto geological time and spatial scales. They have introduced the yield strength envelope (YSE) for the oceanic lithosphere, which predicts the maximal rock strength as a function of depth. In the YSE rheology models, depth dependence of rock strength integrates multiple factors such as increase of both brittle and ductile strength with pressure, decrease of the ductile strength with depth-increasing temperature, lithological structure, and fluid content. The YSEs are used both to validate the rock mechanics data and to explain the mechanical behavior of lithospheric plates. The YSE concept proved to work fairly well for oceans where it explains the observed age and temperature dependence of plate response to surface and subsurface loads. Yet, the same concept faced a number of difficulties in continents (Burov and Diament, 1995). These difficulties have been the topic of recent discussions concerning the long-term rheology of continental plates (McKenzie and Fairhead, 1997; Burov, 2002; Watts and Burov, 2003; Maggi *et al*., 2000; Jackson, 2002; Handy and Brun, 2004; Afonso and Ranalli, 2004; Burov and Watts, 2006).

One of the major experimental rheology laws used for construction of YSEs is the Byerlee's law of brittle failure (Byerlee, 1978). Byerlee's law demostrates that the brittle strength is a function of pressure depth but not of the rock type (**Figure 1**). Byerlee has shown that various rocks exhibit similar relationship between the yield stress and normal stress, and that this relationship resembles Mohr–Coulomb plasticity that refers to the classical Amonton's law of friction (e.g., Nadai, 1963). The Byerlee's law was confirmed from multiple studies which have confirmed that most rocks have similar angle of friction (30–33°) and small dilatation angle (~10°). This explains why highly stratified rocks often behave as a mechanically uniform media: tectonic faults propagate at large distances at depth or horizontally, ignoring lithological stratification and inherited structures. The fault dip or the angle between conjugate faults is a function of the internal friction angle; it is thus possible to constrain the properties of brittle rocks from direct observations of fault/fracture geometries. These properties also do not depend on timescale. Hence, the parameters derived from laboratory experiments can be applied to geological spatial and temporal scales. Of course, anomalous inclusions, variations in porous pressure or stress concentrations can change fault geometries (e.g., Melosh, 1990; Lavier *et al*., 2000; Le Pourhiet *et al*., 2004; Tirel *et al*., 2004; Huismans *et al*., 2005). Explanation of the formation of low angle faults observed in some specific contexts presents a specific problem (e.g., Melosh, 1990). Yet, in most cases, the observation of 'abnormal' fault dips can be explained within the Byerlee's law. For example, the most common interpretations compatible with the Byerlee's law refer to local rotation of principal stress axis due to shear flow in the ductile crust (e.g., Melosh, 1990) or due to flexural rotation (e.g., Buck, 1988). Another common explanation for low angle faulting requires additional mechanisms of friction or cohesion softening applied to the Byerlee's law (e.g., Huismans *et al*., 2005).

Just opposite to the brittle properties, ductile rock strength strongly depends on rock type and other specific conditions such as grain size, macro- and microstructure, temperature, strain rate, and some other factors. In particular, the ductile behavior nonlinearly depends on strain rate and thus on the timescale of the deformation process. Laboratory experiments are conducted on human timescale (5–10 years). Their results are then extrapolated to a geological timescale ($>10^6$ years). This huge extrapolation cannot be justified from a mathematical point of view specifically because of nonlinear character of ductile deformation. Although the solid-state theory covers some creep mechanisms such as the diffusion creep or pressure solution (e.g., Poirier, 1985), the leading creep mechanisms such as dislocation creep are not sufficiently well understood (e.g., Hull and Bacon, 1984).

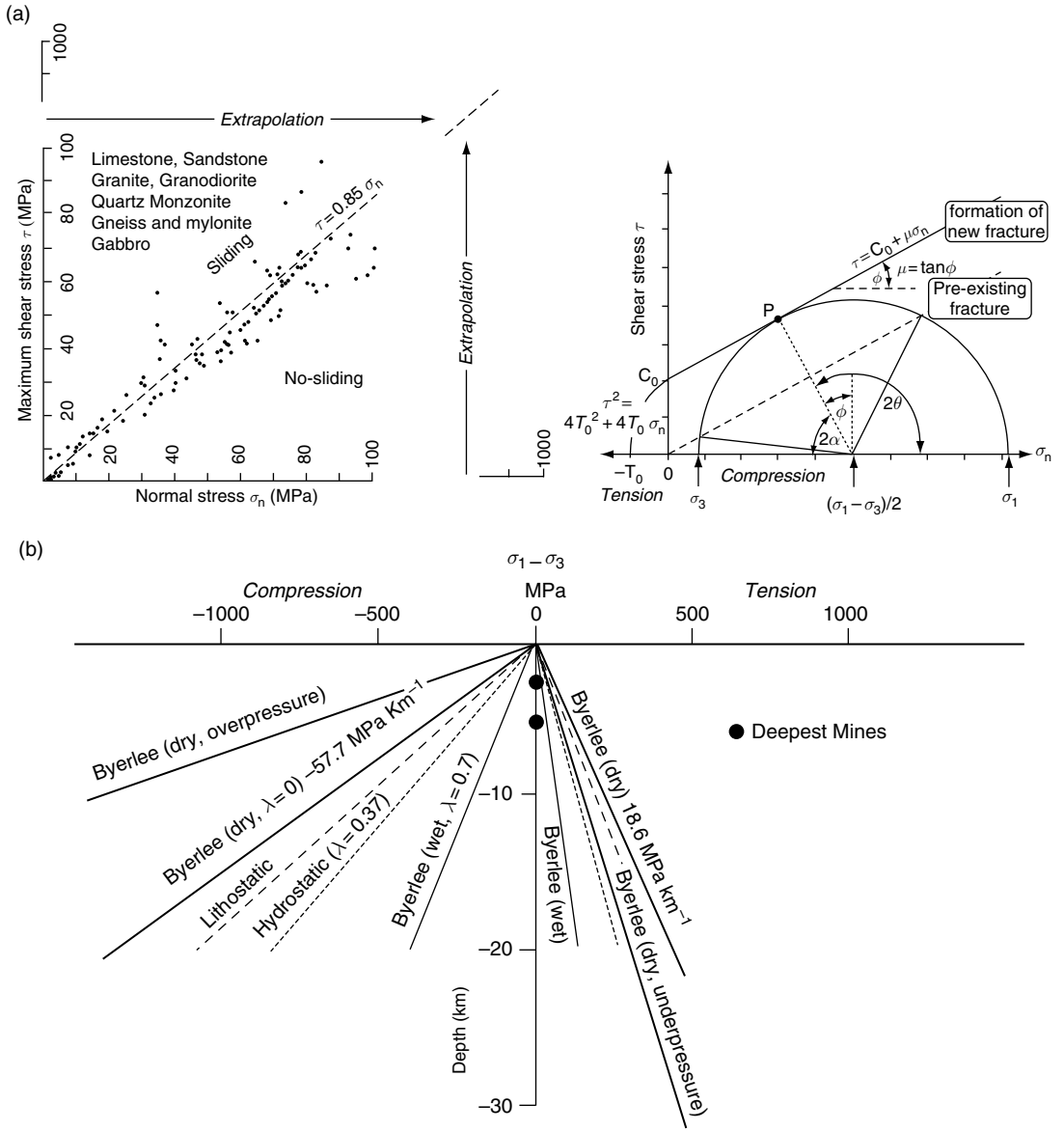

Figure 1 (a) *Right*: Experimentally established linear dependence between normal stress and shear stress for compressional failure of various rocks. These data demonstrate the applicability of Coulomb–Navier failure criterion $\tau = C_0 + \mu\sigma_n$ and relative independence of the Byerlee's law on rock type. Note, however, that this law has been validated only for first several kilometers of the upper crust (pressures of few MPa). It is commonly linearly extrapolated to more important depth/pressure conditions (up to 40–50 km depth or 1–1.5 GPa). *Left*: Two principal failure criteria (Coulomb–Navier et modified Griffith). Under general compression (here, $\sigma_n > 0$), Coulomb criterion predicts linear relation between normal stress σ_n and shear stress τ. Under general extension (here, $\sigma_n < 0$), modified parabolic Griffith criterion applies. C_0 is cohesion, T_0 is tension cutoff, μ is friction coefficient, β is friction angle, and σ_1 and σ_3 are principal stresses. 2α is angle between two conjucted faults forming under stress σ_1, $\phi = \pi/2 - 2\alpha$ is friction angle ($\mu = \tan\phi$). For most dry rocks $\phi = 30°$. It can be seen that Byerlee's law corresponds to Mohr–Coulomb plasticity with preexisting fractures. (a) Modified from Byerlee, JD., (1978) Friction of rocks. *Pure and Applied. Geophysics*., 116: 615–626. and Price NJ and Cosgrove JW (1990) *Analysis of Geological Structures.* New York: Cambridge University Press. (b) Dependence of brittle strength on depth/pressure: lithostatic pressure (if not stated otherwise), fluid pressure, and tectonically induced over- or underpressure. Note that rocks are weaker under extension than under compression, which explains frequent deep seismicity in overall weak rift zones. Tectonic extension or compression may change total pressure, and, consequently, brittle strength, by a factor of, respectively, 0.5–2; λ is pore pressure factor. From Watts AB (2001) *Isostasy and Flexure of the Lithosphere*, 458pp. Cambridge, NY: Cambridge University Press and Petrini K and Podladchikov Y (2000) Lithospheric pressure-depth relationship in compressive regions of thickened crust. *Journal of Metamorphic Geology* 18: 67–78.

Many of Arrehenius-type constitutive laws suggested for ductile rocks are rather approximations rather than physically formulated dependencies (e.g., Brace and Kohlstedt, 1980; Rutter and Brodie, 1991). The YSEs derived for the continental lithosphere for dry olivine rheology predict important strength for its mantle part. However, some studies (e.g., Jackson, 2002; Mackwell *et al.* 1998) suggest that mantle olivine is weak, while the cratons are thin and hot (equilibrium thermal thickness $a = z(1330^{\circ}) \sim 100$ km). Hence, it is suggested that the continental plate strength is concentrated in the crust. These propositions arrive from conflicting interpretations of rock mechanics and intraplate seismicity data. The latter is detected mainly above 40 km depth (Maggi *et al.*, 2000) both in continents and oceans. Maggi *et al.* (2000) and Jackson (2002) claim that all continental microseismicity originates in the crust. Yet, a recent thorough reassessment of the same data set (Monsalve *et al.*, 2006) demonstrates that continental microseismicity is bimodal, with crustal but also indisputably mantle locations as deep as 100 km. Nevertheless, most microseismic events occur above 40 km depth. In continents, this depth interval corresponds to the crust, whereas in the oceans it comprises both crust and the uppermost mantle lithosphere. The other studies (e.g., Watts and Burov, 2003; Handy and Brun, 2004) disagree with the idea of direct seismic depth–strength correlation. These authors point out that such correlation, if exists, should be rather inverse, since in the continuum mechanics failure is considered as a sign of weakness. They suggest that seismicity should be interpreted as a manifestation of mechanical weakness, not strength, of the seismogenic layer that fails at region-specific intraplate stress level. In this approach, crust–mantle decoupling and depth-growing confining pressure that inhibits brittle failure explain the absence of deep earthquakes. It should also be noted that seismicity refers to short-timescale behavior, which may be unrelated to long-term rheology because at this timescale the entire lithosphere should deform only in the brittle–elastic mode. Consequently, there may be no direct correlation between the seismic and long-term ductile behavior. Indeed, the observations of plate flexure below orogens (Watts, 2001) suggest that many continental plates have strong elastic cores (T_e), that are probably 2–2.5 times thicker than the seismogenic layer thickness, T_s. However, Jackson (2002), McKenzie and Fairhead (1997), and Zoback and Townend (2001) challenged the conventional rheology model for the continental lithosphere (dubbed the 'jelly-sandwich'). They stated that the model was incorrect, proposing instead a model based on the rheology envelope from Mackwell *et al.* (1998), in which the crust is strong, but the mantle is weak (dubbed the '*crème-brûlée*' model). This model suggests that continents are thin and hot (>800°C at 60 km depth) and have a water-saturated mantle.

The '*crème-brûlée*' model has arisen because of conflicting results from rock mechanics, earthquake, and elastic thickness (T_e) data. Even if its validity is highly debatable, it illustrates the lack of reliable constraints on the long-term rheology. Indeed, one can systematically improve the precision and inherent consistence of rock mechanics experiments but these data will not be able to provide a firm proof of their relevance to long-term deformation (Kohlstedt *et al.*, 1995). There is actually much confusion concerning the interpretation of brittle–elastic–ductile YSEs derived for the continental lithosphere. Even if the underlying rheology laws were robust, the common YSE profiles introduce additional strong uncertainties, because they are derived under strong assumptions as to the shape of the geotherm, pressure, strain, and strain-rate distribution with depth. For example, Jackson's (2002) suggestion that the depth of seismicity is limited by the depth of the brittle–ductile transition (BDT) arrives from interpretation of the YSEs derived for geological strain rate ($\sim 10^{-17} - 10^{-15}\,s^{-1}$). Yet, these YSEs become entirely 'brittle–elastic' if recomputed for seismic strain rates of $10^{1} - 10^{6}\,s^{-1}$. Indeed, as revealed by postglacial rebound data (e.g., Peltier, 1974; Peltier and Andrews, 1976), minimal ductile timesscales in the lithosphere–asthenosphere system are on the order of thousands years. Consequently, it would be oversimplistic to imply that the BDT depth may limit seismicity, at least in a direct way.

It becomes clear that independent large-scale constraints are needed to assess the long-term rheology of the lithosphere. In this chapter we summarize available experimental and observational data on lithosphere rheology and discuss possible ways of parametrization and application of data of the experimental rock mechanics for geological temporal and spatial scales.

6.03.2 Rock Properties as Derived From Rock Mechanics Data – Conventional Models

For small strains (e.g., cratons) and short timescales (e.g., seismic), rocks behave as an elastic material (**Tables 1–4**). Inelastic deformation occurs at long timescales or due to various defects present in the

Table 1 Commonly inferred parameters for diffusion creep, $n = 1$

Rock/mineral	A (s^{-1} Pa mm^m)	m	Q (kJ mol^{-1})	Comments
Dry Olivine	7.7×10^{-8}	1–3	536	Karato *et al.* (1986)
Wet Olivine	1.5×10^{-9}	1–3	498	Karato *et al.* (1986)

Karato S (1986) Does partial melting reduce the creep strength of the upper mantle? *Nature* 319: 309–310.

Table 2 Commonly inferred parameters of dislocation creep

Rock/mineral	A ($MPa^{-n}s^{-1}$)	n	Q (kJ mol^{-1})	Comments
Wet quartzite	10^{-4}	2.4	160	Brace and Kohlstedt (1980) Kirby and Kronenberg (1987); Kohlstedt *et al.* (1995)
Wet quartzite	1.1×10^{-4}	4	223	Gleason and Tullis (1995) (**Figure 3b**)
Dry quartzite	6.3×10^{-6}	2.4	156	Ranally and Murphy (1987)
Dry diabase	$10^{-3.7}$	3.4	260	Kirby (1983)
Dry diabase	2.0×10^{-4}	3.4	260	Kirby (1983)
Columbia diabase (weak)	190 ± 110	4.7 ± 0.6	485 ± 30	Mackwell *et al.* (1998) (**Figure 3b**)
Maryland diabase (strong)	8 ± 4	4.7 ± 0.6	485 ± 30	Mackwell *et al.* (1998)
Granite (wet)	2×10^{-4}	1.9	140	Mackwell *et al.* (1998)
Wet diorite	3.2×10^{-2}	2.4	212	Ranally (1995)
Dry mafic granulite	1.4×10^{4}	4.2	445	Wilks and Carter (1990)
Undried adirondac granulite	3.18×10^{-4}	3.1	243	Wilks and Carter (1990)
Undried pikwitonei granulite	1.4×10^{4}	4.2	445	Wilks and Carter (1990) (**Figure 3b**)
Dry olivine	10^{4}	3	520	Chopra and Paterson (1984)
Dry olivine	4.8	3.0	502	Evans and Kohlstedt (1995)
Dry dunite	4.85×10^{4}	3.5	535	Hirth and Kohlstedt (1996)
Microgabbro	5×10^{9}	3.4	497	Wilks and Carter (1990)
Wet Olivine (dunite)	275.6	4.45	498	Chopra and Paterson (1981)
Wet Olivine	4.876×10^{6}	3.5	515 ± 30	Hirth and Kohlstedt (1996)
Wet Aheim dunite	2.6	4.5	498	Evans and Kohlstedt (1995)
Dry Anita Bay dunite	4.5	3.6	535	Chopra and Paterson (1981)
Wet Synthetic San Carlos olivine	1.5×10^{6}	3	250	Karato *et al.* (1986)
Dry Synthetic olivine	5.4	3.5	540	Karato *et al.* (1986)
Wet Synthetic olivine	3.3	3.0	420	Karato *et al.* (1986)
wet Anita Bay dunite	955	3.4	444	Chopra and Paterson (1984)
wet Aheim dunite	417	4.48	498	Chopra and Paterson (1984) **Figure 3b**
Dry olivine	4.85×10^{4}	3.5	535	Chopra and Paterson (1981) **Figure 3b**
Olivine (Dorn's dislocation glide) at $\sigma_1 - \sigma_3 \geq 200$ MPa)			$\dot{\varepsilon}_0 = 5.7 \times 10^{11}\ s^{-1}$, $\sigma_0 = 8.5 \times 10^{3}$ MPa; $H^* = 535$ kJ mol^{-1}	

Table 3 Peierls plasticity

Rock/mineral	τ_0 (MPa)	$\dot{\varepsilon}$ (s^{-1})	Q (kJ mol^{-1})	Comments
Synthetic olivine	8500	5.7×10^{-11}	536	Karato *et al.* (1998)
San Carlos peridotite	9100	1.3×10^{-12}	498	Goetze and Evans (1979)

real rock. In particular, brittle failure results from crack growth and frictional slip (Byerlee, 1978; Lokhner, 1995), ductile flow results from grain boundary sliding, dislocations, or point or planar defects. In nature, however, there is no pure elastic, viscous, or plastic deformation.

Table 4 Summary of most common thermal and mechanical parameters of the lithosphere (also used in model simulations shown in this paper)

Type	Parameter	Value
Thermal	T_{z0}, surface temperature	0°C
	T_m, temperature at base of thermal lithosphere	1330°C
	k_c, thermal conductivity of the upper crust	$2.5\,Wm^{-1}°C^{-1}$
	k_{c2}, thermal conductivity of the lower crust	$2.0\,Wm^{-1}°C^{-1}$
	k_m, thermal conductivity of mantle	$3.5\,Wm^{-1}°C^{-1}$
	χ_c, thermal diffusivity of the upper crust	$8.3\times10^{-7}\,m^2\,s^{-1}$
	χ_{c2}, thermal diffusivity of the lower crust	$6.7\times10^{-7}\,m^2\,s^{-1}$
	χ_m, thermal diffusivity of mantle	$10^{-6}\,m^2\,s^{-1}$
	H_S, radiogenic heat production at surface	$9.5\times10^{-10}\,W\,kg^{-1}$
	h_r, radiogenic heat production decay depth constant	10 km
	H_{c2}/C_{c2} heat source term, lower crust	$1.7\times10^{-13}\,K\,s^{-1}$
	a, equilibrium thermal thickness of lithosphre	125–350 km
	Thermotectonic age of the lithosphere	150–500 My
Mechanical	ρ_c, density of upper crust	$2700\,kg\,m^{-3}$
	ρ_{c2}, density of lower crust	$2900\,kg\,m^{-3}$
	ρ_m, density of mantle	$3330\,kg\,m^{-3}$
	ρ_a, density of asthenosphere	$3310\,kg\,m^{-3}$
	Lamé elastic constants λ, G (Here, $\lambda = G$)	30 GPa
	ϕ, Byerlee's law / Mohr–Coulomb criterion – Friction angle	30°
	C_0, Byerlee's law / Mohr–Coulomb criterion – Cohesion	20 MPa
	A, m, n, Q, H, ductile flow-law parameters	Tables 1–3
	T_e, equivalent elastic thickness	0–110 km
	h_{1c}, h_{2c}, h_m, mechanical bottoms of the upper crust, lower crust and mantle, respectively	< 20; < 40; < 125 km, respectively
Divers	T_c, crustal thickness	7–70 km, 36 km (average in continents)
	T_s, seismogenic layer thickness	15–20 km; < 50 km

6.03.2.1 Elastic Properties

Elasticity arises from short-range interatomic forces that, when the material is unstressed, maintain the atoms in regular patterns. Stresses resulting from deformation are linear function of strain, and the initial geometry of the material is fully recoverable after stress/strain relief. Under stress the atomic bonding can be broken at quite small deformations leading to inelastic deformation. The elastic strain propagates with a speed of sound and goes ahead of viscous or plastic strain. This behavior is described by linear Hooke's law:

$$\sigma_{ij} = \lambda\varepsilon_{ii}\delta_{ij} + 2G\varepsilon_{ij} \qquad [1]$$

where λ and G are Lame's constants. Repeating indexes mean summation and δ is Kronecker's operator. λ and G are related to the incompressibility (bulk) modulus K_e:

$$K_e = \frac{1}{3}(3\lambda + 2G) \qquad [2]$$

An equivalent form of [1] is

$$\varepsilon_{ij} = E^{-1}\sigma_{ii}\delta_{ij} - E^{-1}\upsilon\sigma_{ij} \quad G = E/2(1+\upsilon);$$
$$\lambda = E\upsilon/((1+\upsilon)(1-2\upsilon)) \qquad [3]$$

where E is Young's modulus and υ is Poisson's ratio. A number of direct observations suggest that the lithosphere maintains elastic stresses over long periods of time. These observations demonstrate that lithospheric plates behave as rigid blocks or shells for tens and hundreds of million years. Plate tectonics is the most evident demonstration of this phenomenon for horizontal strains (De Mets *et al.*, 1990). For normal loading, plate flexure or regional isostasy studies demonstrate that plates behave as thin rigid plates of finite thickness called equivalent elastic thickness of the lithosphere (T_e). T_e varies from 0 km for very young areas (spreading centers) to 110 km for cratons (Watts, 2001). The continent average T_e is 30–50 km. For oceans T_e is proportional to square root of their age t (in My) (Le Pichon *et al.*, 1973) and is generally smaller than 50 km:

$$T_{e\,\text{oceans}} \sim 5t^{1/2} \qquad [4]$$

The age t of the oceanic lithosphere is a proxy of its thermal state and thus of its ductile strength. Hence, there is a little doubt that the integrated strength of the oceanic lithosphere is controlled and limited by its

ductile strength. In continental domain, T_e is controlled by several factors and cannot be estimated from simple relations (Burov and Diament, 1995).

6.03.2.2 Brittle or Plastic Properties

Rock failure may occur in different modes. One of them refers to tensile failure that results in fractures parallel to one of the axis of the principal stresses (σ_1, σ_3) and does not depend on confining pressure (Jaeger and Cook, 1976). However, tectonic fracturing is mostly related to shear failure, which is a pressure-dependent plastic behavior (**Figure 1**; Nadai, 1963). Brittle deformation in shear described by Byerlee's law refers to frictional sliding on the preexisting microfractures with either one or two fault planes forming an angle of $< 45°$ with the direction of the maximal compression. Several empirical plastic yielding criteria exist that predict activation of brittle–plastic deformation for given conditions (Von Mises, Tresca, Mohr–Coulomb, Drucker–Prager, etc.). The Coulomb–Navier failure criterion best represents the brittle behavior of rocks in geologically relevant contexts (Byerlee, 1978). This criterion refers to the Amonton's law of friction:

$$\tau = C_0 + \tan(\phi)\sigma_n \qquad [5]$$

where C_0 is the cohesive strength (<20 MPa), $\tan(\phi)$ is the internal friction coefficient, ϕ is the internal friction angle, τ and σ_n are, respectively, the shear and normal stress on a selected surface within material. According to Cauchy's formulation for a Cartesian basis (x, y, z) (e.g., Kachanov, 1971)

$$\begin{aligned}\boldsymbol{\sigma}_n = {} & \sigma_{xx}\cos^2(\boldsymbol{n},\boldsymbol{x}) + \sigma_{yy}\cos^2(\boldsymbol{n},\boldsymbol{y}) + \sigma_{zz}{}^2\cos(\boldsymbol{n},\boldsymbol{z}) \\ & + 2(\tau_{yx}\cos(\boldsymbol{n},\boldsymbol{x})\cos(\boldsymbol{n},\boldsymbol{y}) + \tau_{yz}\cos(\boldsymbol{n},\boldsymbol{y})\cos(\boldsymbol{n},\boldsymbol{z}) \\ & + \tau_{xz}\cos(\boldsymbol{n},\boldsymbol{z})\cos(\boldsymbol{n},\boldsymbol{x})) \end{aligned} \qquad [6]$$

where subscripts refer to the global Cartesian stress components. The shear stress on fault plane τ_n is $\tau_n{}^2 = X_n{}^2 + Y_n{}^2 + Z_n{}^2 - \sigma_n{}^2$, where X_n, Y_n, Z_n refer to the x, y, z components of $\boldsymbol{\sigma}_n$. Assigning the origin of z-coordinate to Z_n we obtain two-dimensional (2D) Mohr circles ($\theta = \text{angle}(\boldsymbol{n}, \boldsymbol{x})$):

$$\begin{aligned} \sigma_n &= \sigma_{xx}\cos^2\theta + \sigma_{yy}\sin^2\theta \\ \tau_n^2 &= X_n^2 + Y_n^2 - \sigma_n^2 \\ \sigma_n^2 + \tau^2 - \sigma_n(\sigma_{xx} + \sigma_{yy}) + (\sigma_{xx}\sigma_{yy}) &= 0 \end{aligned} \qquad [7]$$

Measurements *in situ* are referred to (σ_1, σ_3) frame (**Figure 1**):

$$\begin{aligned} \sigma_n &= 1/2(\sigma_1 + \sigma_3) + 1/2(\sigma_2 - \sigma_3)\cos 2\theta \\ \tau &= 1/2(\sigma_2 - \sigma_3)\sin 2\theta \end{aligned} \qquad [8a]$$

σ_n and τ refer to a plane (e.g., fault plane) in which normal $\boldsymbol{n}$ forms an angle θ with the direction of σ_1; $\phi = 2\theta - \frac{1}{2}\pi = \frac{1}{2}\pi - 2\alpha$, where 2α is the angle between two conjugated shear planes $\alpha = \theta - \frac{1}{2}\pi$. The parabolic Griffith criterion extends Mohr–Coulomb criterion to the domain of tensile stress:

$$\tau^2 = 4T_0^2 + 4T_0\sigma_n \qquad [8b]$$

where $2T_0 = C_0$ is tension cutoff (**Figure 1**). Note, however, that [8b] is not Griffith criterion in *senso stricto*, as it is used in crack mechanics, but its variant used in conjunction with Mohr–Coulomb criterion. Intersection of the largest of the main Mohr circles (σ_1, σ_3) with the yield criterion yields failure stress and angles θ and α.

A third parameter, Ψ, dilatation angle, accounts for dilatation in shear that occurs due to sliding over interface asperities. Hence, Ψ characterizes the degree of compressibility ($\Psi = 0$ for incompressible rock). For simple shear Ψ is defined as the ratio of volume strain rate $\dot{\varepsilon}_{ii}$ to shear strain rate $\dot{\varepsilon}_{ij}$:

$$\tan\Psi = \frac{\dot{\varepsilon}_{ii}}{\dot{\varepsilon}_{ij}} \qquad [8c]$$

The Mohr–Coulomb constitutive law predicts shear zones at angle θ^* to compression axis (Vermeer and de Borst, 1984):

$$\theta^* = \frac{\pi}{4} + \frac{\phi + \Psi}{4} \qquad [8d]$$

which depends both on friction and dilatation angle.

Plasticity is associative if $\Psi = \phi$, or nonassociative if $\Psi \neq \phi$. More precisely, plasticity is nonassociative if the plastic potential function differs from the failure function. For Mohr–Coulomb or Drucker–Prager plasticity this is the case if $\Psi \neq \phi$. Most rocks are nonassociative: $\Psi < 10°$ and $\phi = 30°$–$40°$ (Vermeer and de Borst, 1984). This explains localization of shear bands due to the rheological instabilities, without material softening. These instabilities occur because the nonassociative materials do not deform homogeneously in post-peak stress regime, but bifurcate into two states: plastic deformation within a shear band and elastic unloading outside. This leads to stress discontinuity across the shear band and, consequently, to instability. Normal stresses parallel to the shear band decrease in post-peak regime, which results in decrease of vertical stress as well. This stress drop is called

'nonassociated softening' (Vermeer, 1990), in contrast to material softening, which implies that some intrinsic material parameters (cohesion, friction angle) are reduced as a function of strain.

Byerlee (1978) has experimentally demonstrated that for majority of rocks Coulomb failure criterion applies in the form (**Figure 1**)

$$\tau = 0.85\,\sigma_n, \quad \sigma_n \leq 200\,\text{MPa} \qquad [9a]$$

$$\tau = 50\,\text{MPa} + 0.6\,\sigma_n, \quad 1700\,\text{MPa} > \sigma_n > 200\,\text{MPa} \qquad [9b]$$

or, assuming

$$|\sigma_3| < |\sigma_2| < |\sigma_1| \qquad [10]$$

$$\sigma_1 = 4.7\sigma_3, \quad \sigma_3 \leq 114\,\text{MPa} \qquad [11a]$$

$$\sigma_1 = 3.1\sigma_3 + 177\,\text{MPa}, \quad 1094\,\text{MPa} > \sigma_3 > 114\,\text{MPa} \qquad [11b]$$

Byerlee (1978) has also shown that frictional properties of rocks are weakly dependent on rock type. This explains why tectonic faults may intersect heterogeneous structures. However, brittle strength depends heavily on pressure variations caused by tectonic stress or fluids. The latter are characterized by fluid pressure factor $\lambda = \rho_w/\rho$, where ρ_w is the density of water and ρ is the rock density:

$$\Delta\sigma = \sigma_1 - \sigma_3 = \alpha\rho g z(1-\lambda) \qquad [12]$$

where $\alpha = 1 - R^{-1}$ for normal faulting, $\alpha = R - 1$ for thrusting, $\alpha = (R-1)/(1+\beta\,(R-1))$ for strike-slip, with $R = \left((1+\phi^2)^{1/2} - \phi\right)^{-2}$ and $\tan\beta = (\sigma_2 - \sigma_3)/(\sigma_1 - \sigma_3) < 1$.

It is noteworthy that Byerlee's data can be also fitted using a weak power law (Lockner, 1995):

$$|\tau| = \sigma_n^{0.94} \qquad [13]$$

Deep drilling has provided direct evidence in support of Byerlee's law for the first few kilometers of the crust (1–14 km) (e.g., Zoback *et al.*, 1993). However, this law is probably not applicable for the depths exceeding 30–50 km (e.g., Kirby *et al.*, 1991). At high depth/pressure or temperature, brittle failure may switch to a semibrittle regime (e.g., Chester, 1995; Bos and Spiers, 2002). One of discussed possibilities refers to Peierl's plasticity (Goetze and Evans, 1979; see also next section) that takes place at high differential stresses (>100–200 MPa), when mixed dislocation glide and climb occur (Karato *et al.*, 1986; Karato, 1998). Parameters of Peierl's mechanism are not well known since they have been obtained only for two experiments (Goetze and Evans, 1979; Evans and Goetze, 1979) at room pressure. Synthetic parameters (e.g., Karato *et al.*, 1986; Karato, 1998) can be used only as rough estimates (**Table 3**). Despite the lack of experimental data for near-Moho and mantle conditions, there is a general agreement that brittle strength reaches maximal values at 30–50 km and does not grow below this depth (Kirby *et al.*, 1991, 1996). Some phenomena, such as discovery of apparently brittle ultra high-pressure pseudotachylytes in exhumed deep fault zones (Austrheim and Boundy, 1994), suggest that brittle failure may have been produced at great depth in large shear zones.

6.03.2.3 Ductile (Viscous) Properties

Viscous behavior applies when the deformational stress is a function of strain rate (**Figure 2**). The term 'ductile', often associated with strain-rate-dependent properties of the rocks, is not really related to a particular constitutive relationship but to the ability of materials to change form irreversibly without fracturing. Actually, if the strain-rate–stress dependence is negligible, the material is considered as ductile–plastic if it deforms irreversibly without fracture. When the ductile deformation is characterized by linear strain-rate–stress dependence, one speaks of Newtonian viscous deformation. When this dependence is nonlinear, the term 'non-Newtonian viscosity' is applied. At temperatures >300°C, strain-rate-dependent nonlinear dislocation creep is dominant. At very high temperatures (>1330°C), the deformation is likely to be dominated by linear diffusion creep (note, however, that a number of studies have suggested that the upper mantle is partly driven by the dislocation creep (Van Hunen *et al.*, 2005).

6.03.2.3.1 Diffusion and dislocation creep

In contrast to brittle deformation, the ductile deformation is extremely rock-type dependent (e.g., Kirby and Kronenberg, 1987). Even small variations of mineral composition may result in quite different ductile properties (Kirby and Kronenberg, 1987; Mackwell *et al.*, 1998; Brace and Kohlstedt, 1980; **Tables 1** and **2**). The mechanisms of ductile deformation are highly versatile: diffusion creep, numerous mechanisms of the dislocation creep (dislocation climb, glide, screw, edge, etc.), pressure solution, etc. The diffusion creep (Nabarro–Herring or Coble creep (Ashby and Verall, 1978)) is

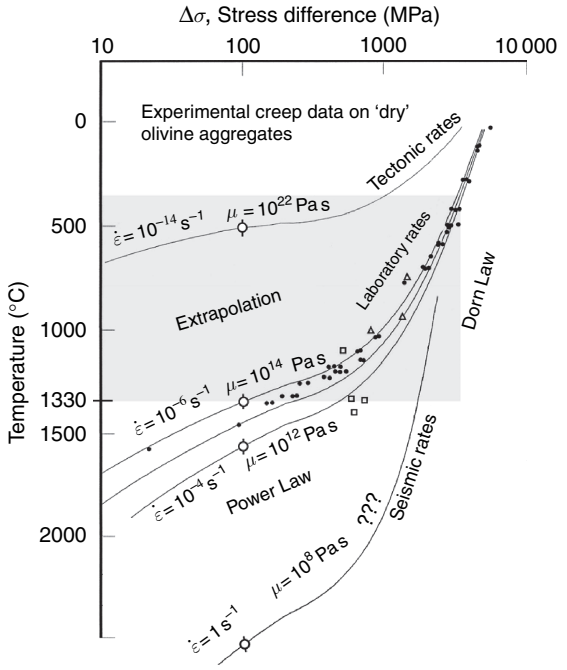

Figure 2 Typical example of experimental data on ductile flow in rocks (olivine aggregates, power, and Dorn flow laws for different temperature–stress domains). Shown also are predicted viscosity values, μ, for 100 MPa stress level (open circles). Note sensitivity to strain rate $\dot{\varepsilon}$ and rock composition (triangles, squares, and black dots correspond to different variants of principally the same olivine aggregates). The typical strain rates used in experiments (10^{-6}–$10^{-4}\,s^{-1}$) are 10 orders of magnitude higher than those in nature (10^{-14}–$10^{-17}\,s^{-1}$), which poses a serious question on the possibility of extrapolation of these data onto geological timescales. Hypothetical extrapolation of experiential data to seismic timescales (1 s) predicts very low viscosity values, yet at this timescales creep takes place at temperatures that are higher than maximum lithospheric temperature (1330°C). Consequently, it is unlikely that seismic movements can activate ductile creep in lithospheric mantle. Modified from Goetze C and Evans B (1979) Stress and temperature in bending lithosphere as constrained by experimental rock mechanics. *Geophysical Journal of the Royal Astronomical Society* 59: 463–478.

associated with temperature-dependent directional diffusivity of rocks and minerals under applied stress. This mechanism is grain-size dependent (**Table 1**):

$$\dot{\varepsilon}^d = A\,a^{-m}\Delta\sigma^n \exp(-H(RT)^{-1}) \qquad [14]$$

where $\dot{\varepsilon}^d$ is the shear strain rate, A is a material constant, a is a grain size, m is a diffusion constant, n is power law constant, $\Delta\sigma = \sigma_1 - \sigma_3$, R is Boltzmann's gas constant, H is creep activation enthalpy ($H = Q + PV$, where Q is activation energy, P is pressure, and V is activation volume), and T is temperature in K. For olivine-rich rocks at high-temperature–low-stress conditions, $m = 3$ and $n = 1$ so that the constitutive law is linear Newtonian. At high stresses and moderate temperatures <1330°C, $m = 0$, and $n = 3$ the creep rate is dominated by dislocation creep (Power law, Dorn law). The power flow law is strongly non-Newtonian (**Table 2**) for $\Delta\sigma < 200$ MPa:

$$\dot{\varepsilon}^d = A\Delta\sigma^n \exp(-H(RT)^{-1}) \quad \text{for} \quad \Delta\sigma < 200\,\text{MPa (Power law)} \qquad [15]$$

$$\dot{\varepsilon}^d = \dot{\varepsilon}_0 \exp(-H(1-\Delta\sigma/\sigma_p)^2/RT) \quad \text{for} \quad \Delta\sigma > 200\,\text{MPa (Dorn law)} \qquad [16]$$

where $\dot{\varepsilon}_0$ and σ_p are, respectively, maximal strain rate and Peierl's stress' (lattice resistance to dislocation glide, on the order of several GPa). For tectonically relevant $\Delta\sigma/\sigma_p$ ratios (<0.1), Dorn's is close to plastic behavior (Peierl's plasticity) and tends to limit ductile strength in high-stress regimes (**Figure 2**). This law is not sufficiently well studied (based on only few experiments) and its application is subject to largest uncertainties (Goetze and Evans, 1979).

The effective viscosity μ_{eff} for power flow law can be defined from

$$\tau_{ij} \equiv \mu_{\text{eff}}\,\dot{\varepsilon}^d_{ij} \qquad [17]$$

which yields

$$\mu_{\text{eff}} = \dot{\varepsilon}^{d(1-n)/n}_{ij} \mathrm{A}^{-1/n} \exp\left(H(nRT)^{-1}\right) \qquad [18]$$

The laws [15] and [16] are derived for uniaxial states. They should be converted, with possible reservations, to a form valid for triaxial states, via second invariant ($\mathcal{J}_2$) of strain rate $\dot{\varepsilon}^d_{ij}$ and geometrical proportionality factors:

$$\mu_{\text{eff}} = \dot{\varepsilon}^{d(1-n)/n}_{\text{II}} (\mathrm{A}^*)^{-1/n} \exp\left(H(nRT)^{-1}\right)$$
$$\dot{\varepsilon}^d_{\text{II}} = (\mathcal{J}_2(\dot{\varepsilon}^d_{ij}))^{1/2} \quad \text{and} \quad \mathrm{A}^* = \frac{1}{2}\mathrm{A}\cdot 3^{(n+1)/2} \qquad [19]$$

where $\dot{\varepsilon}^d_{\text{II}}$ is the effective shear strain rate. The diffusion creep takes over for small grain size that is specific for highly sheared material (ductile shear zones) or for very high temperatures. Grain-size reduction is believed to be an important mechanism of rock softening and localization in mantle shear zones or in the upper mantle (Karato *et al.*, 1986). Creep mechanisms are strongly dependent on water, water fugacities, and mineralogical and melt content (Karato, 1986).

6.03.2.3.2 Pressure solution, cataclastic flow, Peierl's plasticity, and other mechanisms

There are a number of ductile flow mechanisms some of which may occur at low-temperature conditions. Pressure solution is the one that may occur above the depth of BDT, at temperatures below 200°C. This mechanism refers to enhanced solubility of minerals under stress/pressure. Application of mechanical stress provokes directional solution of minerals, for example, silica, which leads to volume change equivalent to deformation:

$$\dot{\varepsilon}_{\mathrm{II}}^{d} = 12\delta\rho_{\mathrm{w}} D_{\mathrm{s}} \sigma(h^3 \rho\sigma_0)^{-1} \qquad [20a]$$

where δ is width of the grain boundary, ρ_{w} is density of solvent (water), D_{s} is the diffusion coefficient, σ is stress, h is the initial dimension of the crystal, ρ is the density of the soluble mineral (e.g., silica), and σ_0 is maximal stress. For silica, $\sigma_0 \sim 500$ MPa is a stress needed for perfect solubility in water at $T = 500$°C. Some recent experimental studies (e.g., Gratier *et al.*, 2006) have found that the eqn [20a] should be corrected to include an exponential term depending on temperature and σ. The resulting flow law is weakly nonlinear power law with $n = 1.7$.

Cataclastic flow or semibrittle flow in porous rocks or at fault surfaces is another well-known example of 'cold' ductile behavior that occurs in high-strain regime. Cataclastic flow is associated with strain-rate-dependent reduction of friction. It refers to distributed microfractures at grain level, such that at a mesoscopic level or hand specimen scale the rock appears to flow. This flow is often associated with semibrittle flow and treated in conjunction with crystal–plastic flow (Chester, 1988):

$$\tau = \tanh(\alpha\sigma_n)\left(\beta^{-1}\ln\left(\dot{\varepsilon}B^{-1}e^{(Q/RT)}\right)\right) + (1-\tanh(\alpha\sigma_n))\tau_f \qquad [20b]$$

where α, β, B are material constants, and τ_{f} is frictional stress that corresponds to the Mohr–Coulomb stress (eqn [5]) at low deformation rates, and becomes rate dependent at higher rates (Rice and Tse, 1986):

$$\tau_{\mathrm{f}} = \sigma_n\left(\mu_{\mathrm{r}} - C\ln\left(\frac{\dot{\delta}}{\dot{\delta}_{\mathrm{r}}} + 1\right)\right) \qquad [20c]$$

where $\dot{\delta}$ and $\dot{\delta}_{\mathrm{r}}$ is shear displacement and reference shear displacement rate, respectively, C is a experimental constant, and μ_{r} is high-rate friction coefficient.

Peierl's plasticity (see also eqn [16]) applies when the stress in the rock reaches a specific limit called Peierl's stress. The latter is associated with Peierl's energy, which changes for a transition of a dislocation by a distance smaller than Burger's vector. At this moment the dominant creep mechanism becomes dislocation glide and climb. Extended constitutive equation for Peierl's plasticity is based on the Dorn's law (Goetze and Evans, 1979; Evans and Goetze, 1979):

$$\dot{\varepsilon}_{ij}^{d} = \dot{\varepsilon}_0 \exp\left(-\frac{Q + p(V - \beta\Delta V_{\mathrm{w}})}{RT}\left(1 - \frac{\tau_{ij}}{\tau_{\mathrm{p}}}\right)\right) \qquad [21]$$

where $\dot{\varepsilon}_0 = A\alpha$, A, Q, V, P, R, and T are defined in the same way as for the ductile creep laws (see eqn [16]), α is experimentally defined weakening parameter controlled by water content, β is adjustable experimental parameter, ΔV_{w} is molar volume change due to incorporation of hydroxyl ions in the main rock, τ_{p} is shear stress limit (~Peierl's stress) that characterizes transition to plastic failure. Regenauer-Lieb *et al* (2001) suggest that Peierl's plasticity and water-induced weakening may play a major role in localization of deformation at important depth or in subduction/collision zones. However, Peierl's rheology is poorly constrained, while Peierl's stress is significantly higher than typical tectonic stress, which limits the applicability of this law.

6.03.2.4 Lithospheric Structure and Goetze–Evans' Yield Strength Envelopes

By combining three major rheology laws (elastic, brittle, and ductile), Goetze and Evans (1979) have introduced the YSE for the lithosphere (**Figure 3**) defined as a differential stress contour $\sigma^{f}(z)$, or $\Delta\sigma_{\max}(z)$, such that

$$\sigma^{\mathrm{f}} = \Delta\sigma_{\max}(z) = \mathrm{sign}(\varepsilon)\min\left(\left|\sigma^{\mathrm{b}}(x,z,t,\dot{\varepsilon},\mathrm{sign}(\varepsilon))\right|, \left|\sigma^{\mathrm{d}}(x,z,t,\dot{\varepsilon})\right|\right) \qquad [22a]$$

where $\sigma^{\mathrm{b}}(x,z,t,\dot{\varepsilon},sign(\varepsilon))$, $\sigma^{\mathrm{d}}(x,z,t,\dot{\varepsilon})$ are the maximal brittle and ductile yielding stresses; $sign(\varepsilon)$ is a sign function equal to 1 for extension and −1 for compression, t is time and x refers to the possibility of not only depth (z) but also spatial strength variations. The differential stress $\Delta\sigma(\varepsilon)$ for the strain $\varepsilon = \varepsilon(z,t,\dot{\varepsilon})$ is

$$\Delta\sigma(\varepsilon) = \mathrm{sign}(\varepsilon)\min\left(\left|\sigma^{\mathrm{f}}\right|, \left|\sigma^{\mathrm{e}}(\varepsilon)\right|\right) \qquad [22b]$$

where $\sigma^{\mathrm{e}}(\varepsilon)$ is the value of elastic stress for the given strain ε. The lithosphere deforms elastically if $\sigma^{\mathrm{e}}(z,\varepsilon) < \sigma^{f}(z)$. This implies the existence of a pertinent elastic 'core', where inelastic strains are negligible. This core, associated with the equivalent

elastic thickness, T_e, provides main contribution to the integrated plate strength B:

$$B = \int_0^{\infty} \sigma^f(x, y, t, \dot{\varepsilon}) dz \leq \int_0^{\infty} \sigma^e(\varepsilon) dz \qquad [23]$$

Depth dependence of $\Delta\sigma_{max}(z)$ stems from many factors, including temperature, pressure, and composition. The YSEs are computed for a fixed background strain rate (typically, $10^{-15}\,s^{-1}$). As suggested by McAdoo *et al.* (1985) for oceanic lithosphere and by Burov and Diament (1992) for continental lithosphere, the YSEs can be linearized, which allows for simple parametrization of rheology laws from direct observations of flexure. Linearized YSEs were used in inelastic flexural models (McAdoo *et al.*, 1985; Burov and Diament, 1992, 1995, Appendix A). This has allowed us to predict T_e for regional studies, as a function of YSE, surface and subsurface loading, thermal distribution, plate structure, and other parameters. By fitting nonlinear flexural models to the observed deformation it has become possible to test and validate rheological profiles derived from experimental rock mechanics. These models have confirmed the validity of rheological envelopes for a number of regions (e.g., Central Asia (Burov and Diament, 1992; Watts and Burov, 2003); European lithosphere (Cloetingh and Burov, 1996)).

The formulation of the YSE and its interpretation in terms of the observed equivalent elastic thickness (T_e) of the lithosphere constitutes a major breakthrough in understanding of the long-term behavior of the lithospheric plates. Computed oceanic YSEs show a remarkable correlation with the measured values of T_e. The predicted depth of BDT also correlates with deepest microseismicity in the oceanic domain (e.g., Watts and Burov, 2003).

While the composition and thermal structure of oceanic plates is well established, it is not the case for the continental domains. Continents have a thick crust of diverse structure and properties that vary from region to region. In addition, it was argued (Jackson, 2002) that in continents, the resistance of mantle olivine is strongly reduced due to the presence of fluids (**Figure 3(b)**, **Table 2**). Yet, high water content has been detected in deep upper mantle below the lithosphere but not in the lithosphere itself (Katayama *et al.*, 2005). Close inspection of the YSE published by (Jackson, 2002) shows that it is not wet olivine that makes this YSE exceptionally weak but the assumption of a very thin hot continental lithosphere (800°C at 60 km depth, estimated equilibrium plate thickness $a = z(1330°C) \sim 100$ km). Such conditions may exist in a few places on the Earth but not in thick old Indian craton implied in Jackson (2002). Even wet olivine rheology preserves important strength (**Figure 3(b)**, right) in case of a geotherm computed for more relevant equilibrium plate thickness ($a = z(1330°C) \sim 200$ km) and with account for radiogenic heat sources.

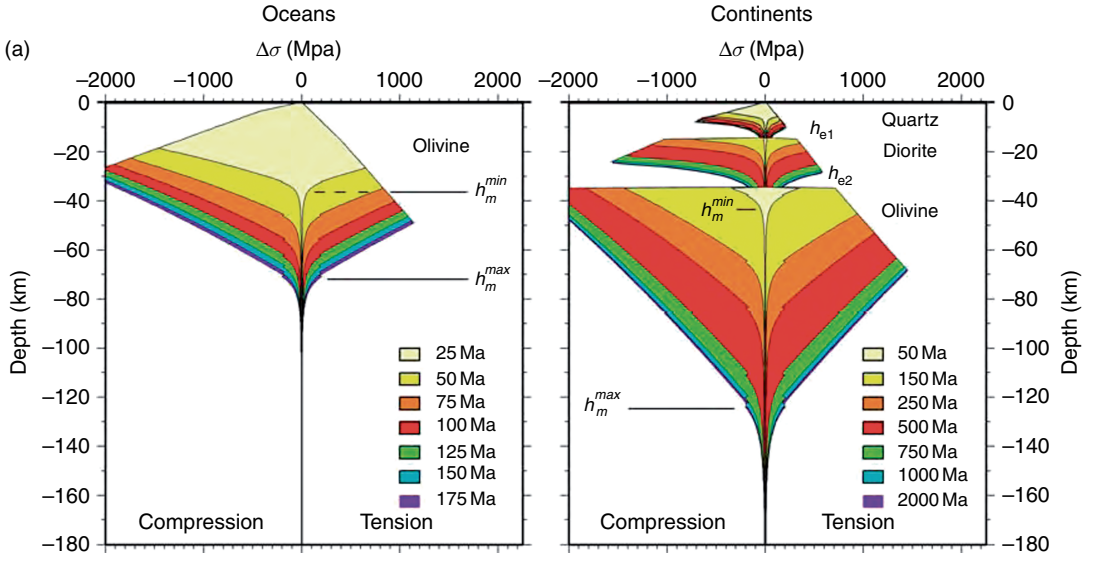

Figure 3 (*Continued*)

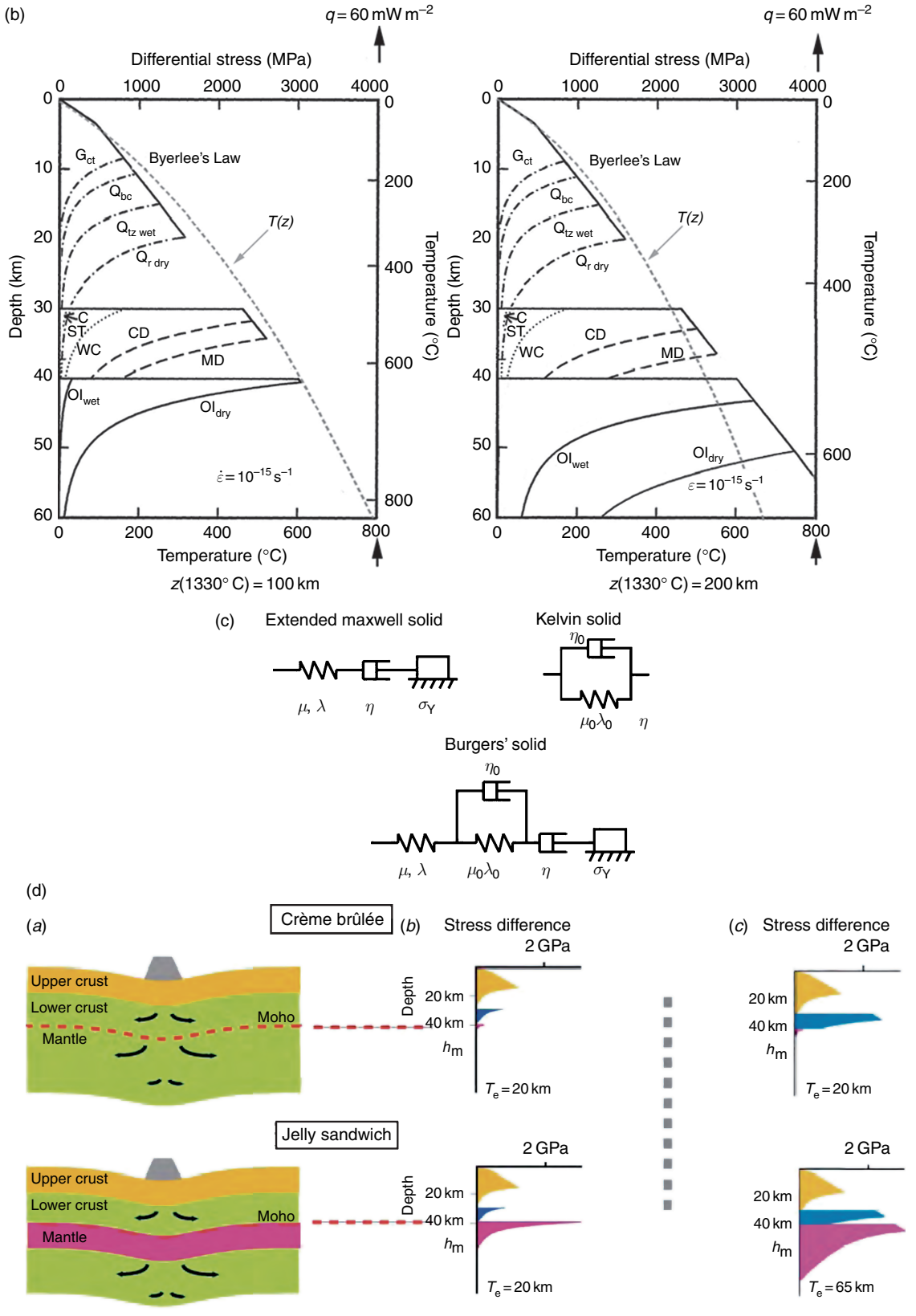

Figure 3 (*Continued*)

6.03.3 Constitutive Models

Elastic and brittle (plastic) rheologies are strain-rate independent whereas viscous rheology is strain independent. However, in the lithosphere, the behavior of elastic and brittle domains becomes strain-rate dependent via interaction with the viscous domain, which, in turn becomes strain dependent. Thus, even if the rheological parameters (elastic, ductile, or brittle) were well constrained, the next question would be how to combine these rheological terms in a constitutive model. There are various possible constitutive models based on either Maxwell, Voigt, or Kelvin model, or their various possible combinations (**Figure 3(c)**).

6.03.3.1 Maxwell Model

In a Maxwell solid, total strain ε^{M} equals a sum of the elastic strain ε^{e} and viscous strain ε^{v}:

$$\varepsilon_{ij}{}^{M} = \varepsilon_{ij}{}^{e} + \varepsilon_{ij}{}^{v} \quad [24]$$

or, in the incremental form

$$e_{ij}{}^{M} = e_{ij}{}^{e} + e_{ij}{}^{v} = S_{ij}/(2G^{M}) + \sigma_{ij}/(2\mu^{M}) \quad [25]$$

Figure 3 (a) Examples of rheological YSEs for oceans (as introduced by (Goetze and Evans, 1979)) and continents. The YSE is shown as a function of the thermotectonic age. The main difference between the oceanic and continental lithosphere refers to the thick crust and multilayered structure of the latter, which may lead to mechanical decoupling between the rheological layers and horizontal ductile flow in the intermediate or lower crust. (b) Influence of compositional variation, plate thickness $a = z(1330^{\circ}C)$ and fluid content on continental YSE computed for typical surface heat flow, q, of 60 mW m^{-2} but two different thermal models: equilibrium thermal plate thickness of 100 km (*left*: Champan, 1986)) and of 200 km (*right*: plate cooling model, Appendix 2, (Burov and Diament, 1995). CD, dry Columbia diabase; MD, dry Maryland diabase; WC, Pikwitonei granulate; ST and C, diabase from Shelton and Tulis (1981)) and Caristan (1982). The upper crust is wet quartzite from Gleason and Tulis 1995; Ol_{dry} and Ol_{wet},dry and wet dunite from Chopra and Paterson, 1984. Q_{bc} refers to dry quartzite from Brace and Kohlstedt (1982). G_{gt} is wet granite from Carter and Tsenn (1987). Qr is for extra strong dry quartz from Ranally (1995). Comparison of the YSE computed for two different thermal plate thicknesses demonstrates large ambiguities in estimation of the mantle strength: the continental heat flux used as a common surface boundary condition mainly affects crustal temperature distribution. The mantle part of the geotherm primarily depends on the position of the thermal bottom of the lithosphere. The left 'weak' YSE results from erroneous assumption that continents have the same or even smaller thickness then the oceans (Jackson, 2002). The use of the left YSE results in ridiculously small predictions of the mantle strength. Left part of the figure is based on (Mackwell *et al.*, 1998). The continental YSE based on the assumption of weak mantle rheology (left) are dubbed '*crème-brulée*' models whereas those that include strong crustal and mantle layers are dubbed 'jelly-sandwich' rheology. The failure envelopes shown in the left match those from Jackson (2002). The Jackson's (2002) envelopes are based on figure 4 from Mackwell *et al.* (1998). The parameters are given in **Tables 2** and **3**. (a) Modified from Burov EB and Diament M (1995) The effective elastic thickness (T_e) of continental lithosphere : What does it really mean? *Journal of Geophysical Research* 100: 3895–3904. (c) Various ways to combine rheological terms in constitutive models of materials: the extended Maxwell' serial model, Kelvin' parallel model, Burger's combined model, etc. The resulting properties of solids largely depend on how the rheological terms are interconnected. Knowledge of the parameters of each rheological term is not sufficient for prediction of the mechanical behavior of materials. (d) Schematic diagram illustrating contrastingly different models for the long-term strength of continental lithosphere (Burov and Watts, 2006). In the *crème-brûlée* model, the strength is confined to the uppermost brittle layer of the crust and compensation is achieved mainly by flow in the weak upper mantle. In the jelly-sandwich model, the mantle is strong and the compensation for surface loads occurs mainly in the underlying asthenosphere. (*a*) Models of deformation. The arrows schematically show the velocity field of the flow. (*b*) Brace–Goetze failure envelopes for a thermotectonic age of 150 My, a weak undried granulite lower crust, a uniform strain rate of 10^{-15} s^{-1}, and either a dry (jelly-sandwich) or wet (*crème-brûlée*) olivine mantle. h_m is the short-term mechanical thickness of the lithosphere and T_e is the long-term elastic thickness. Other parameters are as given in **Table 2**. The two envelopes match those in figures 5B and 5D of Jackson (2002). They yield a T_e of 20 km (e.g., Burov and Diament, 1995), which is similar to the thickness of the most competent layer. This is because the competent layers are mechanically de-coupled by weak ductile layers and so the inclusion of a weak lower crust or strong mantle contributes little to T_e. (*c*) Brace–Goetze failure envelopes for a thermotectonic age of 500 My. Other parameters are as in (*b*) except that a strong, dry, Maryland diabase has been assumed for the lower crust. The two envelopes show other possible rheological models: one in which the upper and lower crust are strong and the mantle is weak (upper panel) and another in which the upper and lower crust and the mantle are strong (lower panel). The assumption of a strong lower crust in the weak mantle model again contributes little to T_e because of decoupling, although T_e would increase from 20 to 40 km if the upper crust was strong at its interface with the lower crust. In contrast, a strong lower crust contributes significantly to the T_e of the strong mantle model. This is because the lower crust is strong at its interface with the mantle and so the crust and mantle are now mechanically coupled.

where e is $\partial\varepsilon/\partial t$ (incremental strain, or strain rate) and S is $\partial\sigma/\partial t$ (incremental stress, or stress rate). Here, stresses are equal in each of the rheological terms but strains may be different. The behavior of this solid is dominated by the term developing larger strain or strain rate. In case of instantaneous strain, the first reaction is elastic but on later stages stress decays due to viscous relaxation, at a rate given by Maxwell relaxation time τ_m:

$$\tau_m = \mu/E \quad [26]$$

If τ_m is considerably shorter than the life span of the system, then deformation is effectively viscous (small Deborah number). For the asthenosphere, τ_m is known from postglacial rebound data (e.g., Peltier, 1974). This time is about 10–100 years, implying effective viscosity of $(1–5) \times 10^{19}$ Pa s. In the lithosphere, τ_m is on the order of several million years, as indicated by data on volcanic island loading (Watts, 2001).

In 'extended' Maxwell viscoelastic-plastic models, the total incremental strain ε^{M_ext} equals a sum of the elastic, plastic, and viscous strain increments:

$$\varepsilon_{ij}^{M\_ext} = \varepsilon_{ij}^{M} + \varepsilon_{ij}^{p} \quad [27]$$

6.03.3.2 Kelvin Model

The alternative Kelvin (Voigt) model implies that the total stress equals the sum of the elastic σ^e and viscous stress σ^v:

$$\sigma_{ij}^{K} = \sigma_{ij}^{e} + \sigma_{ij}^{v} = 2\mu e_{ij}^{k} + 2G^{k}\varepsilon_{ij}^{k} \quad [28]$$

Its extended visco-elastic-plastic version is

$$\sigma_{ij}^{K\_ext} = \sigma_{ij}^{K} + \sigma_{ij}^{p} \quad [29]$$

In Kelvin solids, strains are equal in each of the rheological terms, but the stresses may be different. Although the minerals most probably do not behave as Kelvin solids at microscale, their aggregates and macrostructural assemblages may do.

6.03.3.3 Mixed Models

The observations of long-term loading such as sea mounts (Watts, 2001) demonstrate a complex behavior, which refers to initially Maxwell-type response with exponential stress drop followed (after several million years) by slowdown of stress relaxation so that long-term stress achieves some constant level. This behavior evokes a generalized linear (Maxwell + Kelvin) model, or Burger's model, which represents a serial combination of a Kelvin model with extended Maxwell model:

$$e_{ij}^{B} = e_{ij}^{M} + e_{ij}^{K} + e_{ij}^{P} \quad [30]$$

The viscous and elastic parameters of the Kelvin unit are not the same as of the Maxwell unit. It is possible that relaxation of postseismic deformation may be controlled by the Kelvin term, which may have a smaller viscosity than the Maxwell term (e.g., Pollitz *et al.*, 2001). Present failure to establish any links between the Kelvin and Maxwell viscosities restricts interpretation of postseismic data in terms of the long-term properties of the lithosphere–asthenosphere system.

6.03.4 Uncertainties of Experimental Rheology Laws

The uncertainties on the long-term rheological properties derived from the experimental rheology data have produced highly confusing propositions for the long-term rheological strength of the continental lithosphere (**Figures 3(b)** and **3(d)**). These uncertainties arrive from (1) uncertainties of rock mechanics data, (2) uncertainties of the thermal and other data used in construction of the YSEs, (3) poor knowledge of the deformation mechanisms that really take place at depth, (4) uncertainties on the constitutive models, and (5) additional (unaccounted) factors influencing rock strength such as frictional heating, pressure variations, fluid content, and chemical or thermodynamic transformations.

6.03.4.1 Uncertainties of Rock Mechanics Data

Elastic and Byerlee's brittle parameters are relatively well constrained, with accuracy of ± 10–30% for the relevant depth intervals. Although the validity of Byerlee's law is questionable for fault zones (e.g., Chester, 1995) or at depths below 30–50 km (Kirby *et al.*, 1991, 1996), this would primarily affect fault and seismic distribution but not large-scale deformation.

The ductile flow properties remain to be most uncertain, although the modern techniques of experimental rock mechanics allow for sufficiently robust and internally compatible measurements of creep parameters (e.g., Kohlstedt *et al.*, 1995). Yet, it is not

the precision of experiments but their applications to natural conditions that constitute major difficulties:

1. With rare exceptions, experiments refer to simplified conditions such as unixial deformation or torque, whereas the real rocks are deformed in several planes.

2. The experimental strain rates are on the order of 10^{-8}–$10^{-4}\,s^{-1}$ which is about 10^{10} times faster than the geological strain rates (10^{-18}–$10^{-14}\,s^{-1}$). The extrapolation of these data to geological timescale is mathematically 'illegal' because of the potential errors of this extrapolation spread over the whole relevant strength range.

3. The experiments refer to simple monophase minerals or selected 'representative' rocks. Extension of their results to real aggregate compositions has to be justified (e.g., Kohlstedt *et al.*, 1995). It is often assumed that the weakest of the most abundant mineral species defines the mechanical behavior of the entire rock. For granites, this refers to quartz or quartzite. It was shown, however, that very small amounts of weak phases such as micas or albites may result in significantly smaller strength than that of quartz or quartzite (see discussion in Burov (2002)). It was also noted that poly-phase aggregates are weaker than their constituents, as well as that different mineral species may take a lead in the experiments and nature (Kohlstedt *et al.*, 1995).

4. The experimental strain rates may vary in a different way from nature.

5. The experiments are conducted on small rock samples of homogeneous structure. At larger scales (>0.1–1 m), rocks may be structured. Their mechanical resistance may also depend on their macrostructure (Kohlstedt *et al.*, 1995; Ji *et al.*, 2000).

6. Water content influences rock strength. The experiments usually consider 'wet', 'undried' or 'dry' rock samples (Mackwell *et al.*, 1998). However, for each particular region, it is difficult to know whether the rock is dry, wet, or partially wet (e.g., Karato, 1986). It is also argued that the 'dry' experiments never reach the 'dryness' of some natural conditions (D. McKenzie, personal communication).

7. Volatile fugacities, and chemical and ther modynamic reactions modify the mechanical behavior of rocks. These factors are basically unknown in nature.

8. Creep mechanisms that take place in each particular experiment are not always well determined. It is not guaranteed that same mechanisms are activated in natural conditions (e.g., at slower strain rates).

9. Temperature–pressure (P–T) conditions of experiments do not represent natural P–T conditions or loading paths (e.g., Goetze and Evans, 1979). Basically it is only 'P' or 'T' condition which is respected at a time.

Due to these uncertainties, Brace and Kohlstedt (1980) and Kohlstedt *et al.* (1995) have suggested that real crustal rocks may be significantly 'softer' than the experimental estimates. As an encouraging point it should be noted, however, that the oceanic YSEs based on dry olivine flow law demonstrate a good correlation with the observed T_e values, age, and thermal state of the lithosphere (e.g., Watts, 2001). For continents, one can attempt to validate or re-parametrize rock mechanics data by using observations of long-term deformation, T_e data, and thermomechanical models (Watts and Burov, 2003; Burov and Watts, 2006).

6.03.4.2 Uncertainties of the Synthetic Yield Strength Envelopes

There are specific 'YSE uncertainties' arriving, in addition to the uncertainties of the rheology laws, from various assumptions on thermal distribution, background strain rate, plate structure, and rheological composition of the lithosphere.

Here, one of the most misleading assumptions is that of the homogeneous background strain rate. Analytical and numerical models (e.g., Kusznir, 1991; Burov and Poliakov, 2001) predict strong (orders of magnitude) vertical and horizontal variations of the strain rate in the deforming lithosphere – for example, in the ductile lower crust. As a result, the effective strength may deviate by up to 30% from that predicted from constant-rate envelopes.

The ductile behavior is extremely sensitive to temperature and presence of fluids. A slight variation in the background geotherm, thermal conductivity, or fluid content may 'transform', for example, hard dry quartzite (Kirby and Kronnebeg, 1987) into soft calcite (Kohlstedt *et al.*, 1995). In power-law fluids, shear stress weakly depends on the strain rate but strongly depends on temperature, T, and activation energy Q. Simple increase of Q by a factor of two 'converts' weak quartzite into hard olivine or clinopiroxene (**Table 2**). In the crust, behaviors predicted by strongest dry flow laws can be turned into those predicted by weakest wet flow laws by a small adjustment of the poorly constrained concentration of

radiogenic heat sources. Internal heat production, not accounted in the laboratory experiments, may also influence the long-term creep mechanisms (softening).

The geotherm, $T(z)$, not only controls the ductile strength of the lithosphere, but also, indirectly, its brittle strength through the influence of temperature on the depth of the BDT. Different assumptions on $T(z)$ produce important differences in the predicted strength (**Figure 3(b)**). In continents, age has no unique relation with thermal structure, and the surface heart flow is 'polluted' by up to 50% contribution from crustal radiogenic heat production (Turcotte and Schubert, 2002). Equilibrium thermal (or geochemical, seismic, gravimetric) thickness of continental plates, a (defined as the depth to 1330°C), is an important parameter needed for consistent introduction of bottom boundary conditions in thermal models. For continents, h may vary from 150 to 350 km. h controls the mantle part of the geotherm much more than the surface heat flux, q. This explains why for the same value of heat flux, q, and identical rheological parameters, some authors predict very hot geotherms and, consequently, weak mantle behavior (Jackson, 2002; Mackwell *et al.*, 1998) whereas the others (e.g., this study) predict colder geotherms and strong behavior. Seismic and seismic tomography data and geothermal data (e.g., Jaupart and Mareschal, 1999; *see* Chapter 6.05) suggest that continental lithosphere should be on an average thicker than the oceanic lithosphere (150–350 km compared to 100–125 km). However, there is a tendency to impose, for simplicity, same small thickness for continents and oceans ((Jackson, 2002); **Figure 3(b)**, right). This assumption results in largely underestimated (50–100%) mantle strength.

6.03.4.3 Uncertainties on Deformation Mechanisms in Nature

There is a growing understanding that ductile, elastic, or brittle deformation cannot be treated separately. In general, mixed behaviors should prevail. Semibrittle/semiductile behaviors can be developed near zones of BDT or large shear bands. A number of studies argue that under the upper crustal conditions, 'non-Byerlee' strain-rate-dependent frictional mechanisms may be activated simultaneously with the ductile creep. This leads to a weak, ductile-like constitutive law for the brittle regime. According to these studies (e.g., Chester, 1995), the upper crustal strength may be limited to maximal 50 MPa at 6–15 km depth. Observations of crustal rebound (Bills *et al.*, 1994) indicate that the strength of the upper crust may be strongly reduced below 3 depth, with estimated maximal viscosity below 10^{23} Pa s, which suggests stress levels less than 50 MPa. Many known natural examples show that ductile creep can start (even in pure quartz) at 5–6 km depth (S. Patterson (2002), personal communication). 'Conventional' quartzite rheology (Ranalli, 1995) used for the upper crust is about four times stronger than most of these recent estimates.

6.03.4.4 Role of Frictional Heating, Pressure, Fluid Content, and Other Factors

Fluid pressure reduces brittle strength (**Figure 1(b)**), and a small amount of fluids can (e.g., **Figure 3(b)**, **Table 2**) decrease ductile rock strength by a factor of 2–3 (e.g., Mackwell *et al.*, 1998). Yet, it is practically impossible to estimate fluid content *in situ*. The experimental data generally include only two sets for each type of rock: 'wet', or 'undried', and 'dry'. 'Dry' rock may still have traces of fluid and 'wet' rock may be 'wet' to a different degree. When fluid content is unknown, the prediction for rock strength remains indefinite, between the 'wet' and 'dry' state.

Frictional heating $\partial T_{\text{shear}}/\partial t$ at fault zones may decrease ductile or Peierl's strength, provoke metamorphic changes from harder to softer phases, or change fluid content (and thus strength) via influence on hydration/dehydration:

$$\partial T_{\text{shear}}/\partial t = frac \times (\rho C_{\text{p}})^{-1} \sigma_{\text{II}} \partial \varepsilon_{\text{II}}/\partial t \qquad [31]$$

Friction may produce up to 100°C temperature rise in the shear zones or subduction channel (Turcotte and Schubert, 2002). This would result in local 30–50% strength reduction in quartz-rich and metamorphic rocks.

Rock behavior is also conditioned by elastic properties. Although the criterions for brittle–plastic failure do not depend on elasticity, the viscose-elastic behavior does. Hence, behavior of the whole brittle–ductile–elastic system does, too. The elastic modules increase with pressure and density, yet this is basically ignored in the geodynamic models. These parameters control stress relaxation in the lithosphere and may be responsible for transient states lasting for several million years.

The behavior of the lithospheric plates is largely controlled by deformation at their boundaries (e.g., collision). These boundaries are characterized by specific conditions. In particular, subduction channel undergoes continuous phase, and thus rheology, changes. Unfortunately, there is only few data on the rheology of metamorphic rocks. The few ideas that we get from direct observations in the outcrops suggest that metamorphic rocks are much weaker than the host phase (e.g., micas; schists, serpentine, eclogite vs granulite).

6.03.4.5 Possible Ways to Parameterize Rheology Data for Geological Timescale

There might be several ways to constrain rock rheology for geological timescales (**Figure 4**):

1. Observations of deformation in response to tectonic loading:
   - Observations of isostatic compensation: flexure, estimates of the equivalent elastic thickness of the lithosphere, T_e (e.g., Burov and Diament, 1995, 1996; Watts, 2001).
   - Vertical motions related to postglacial rebound, lake and volcanic loading (e.g., Peltier, 1974; Passey, 1981; Watts, 2001).
   - Physical estimates of minimal integrated strength of the lithosphere required for (1) subduction, (2) for transmission of tectonic stresses over large spatial scales, and (3) for stability of large geological structures such as mounts over their respective life spans (e.g., Lanchenbruch and Morgan, 1990; Bott, 1993; England and Molnar, 1997, 2005).
   - Observations of lithospheric folding (wavelength as function of the integrated strength) Cloetingh *et al.* (1999); Gerbault *et al.* (1999); **Table 5**).
   - Indirect geophysical and geological data allowing to trace geometry of deformed lithosphere and anomalous (e.g., low viscosity or high water content) zones: attenuation of S-waves, petrology (P–T–t) paths, magnetotelluric sounding, gravity, observations of ductile and brittle behaviors in the outcrops, etc. (e.g., Molnar and Tapponnier, 1981; Chen and Molnar, 1983; Wever, 1989; Cloetingh and Banda, 1992;

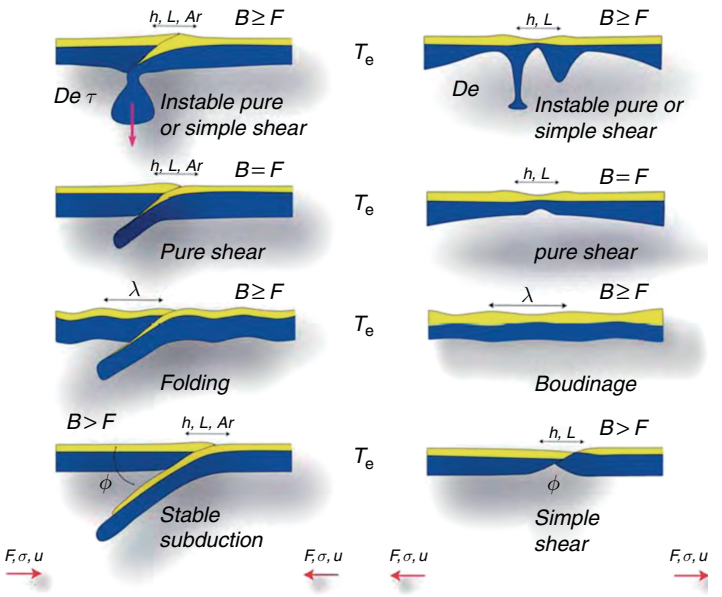

Figure 4 Observed modes of lithospheric deformation and related large scale parameters used for estimation of lithospheric strength and rheology: T_e,, F, σ, u, De, τ, h, L, λ, ϕ. $<\iota>T_e$ is equivalent elastic thickness. F, σ, u are respectively horizontal force, stress, and convergence/extension velocity that are linked to the lithospheric strength and possible deformation styles. De and τ are respectively Deborah number and relaxation/growth time related to viscosity contrasts in the lithosphere. λ is the characteristic wavelength of unstable deformation related to the thickness of the competent layers in the lithosphere. h, L are respectively the vertical and horizontal scale for process-induced topography supported by lithospheric strength, Argand number $Ar = \rho<\iota>ghL/F$. ϕ is subduction or major fault angle that can be indicative of the brittle properties and of overall plate strength.

Table 5 Estimates (Cloetingh *et al.* (1999) and references therein) for wavelengths of lithospheric folding (λ), effective elastic thickness (T_e), thermal age, t_0, the onset of folding (Ma), duration of folding (Ma).

λ (km)	T_e (km)	λ/T_e	Thermal age (Ma)	t_0, onset of folding (My BC)	Present state of folding	Type
200–250 (1)	< 40	>4–5	60	8	Active deformation	B
500–600(2)	50–70	10	400–600	60	preserved	N
200 (3)	30	6–7	200	60	preserved	B
200(present)-> 400–500 (preserved) (4)	25 (after recent reheating at 200 Ma)	8	>700	400–700	preserved	B
300–360 (5)	>15 *	>20	175–400	8–10	Active deformation	B
100–200 (6)	Not available, Approx. >30	4–6	>100	60	preserved	B/N
200 ? (7)	20–35	10–15	300	6	Active subsidence	N
200–250(8)	15	13	175	8–10	Active deformation	B/N
350–400 (9)	6–9 *	> 30	< 20	4–6	Active deformation	N
300 (10)	10–30	10	30	6–8	Active deformation	B/N
40(11)	20–25 *	2	< 20	6–8	Active deformation	N
50 (12)	20–25 *	2	20	6–8	Active subsidence	N
600 (13)	>100	6	>1200	1200	preserved?	B
60 (14)	<10	6	65	35–8 My	Active deformation	B/N

Numbers in brackets refer to data sources: (1) Indian Ocean, (2) Russian platform, (3) Arctic Canada, (4) Central Austaralia, (5) Western Goby, (6) Paris Basin, (7) North Sea Basin, (8) Ferghana and Tadjik Basin, (9) Pannonian Basin, (10) Iberian Basin, (11) Southern Tyrrhenian Sea, (12) Gulf of Lion, (13) Transcontinental Arch of North America; (14) Norwegian sea. 'B' means regular folding style, 'N' means 'irregular' and 'B/N' stands for the cases displaying both types of folding behavior. It is noteworthy that cases of abnormally high (>10) or low (< 4) λ/T_e ratios (marked with '$*$') correspond to hot (thermally reset) lithospheres, which implies dominant crustal folding. The high ratios often correspond to very weak lithospheres loaded by large amounts of sediment, which increases the wavelength of folding. Small λ/T_e ratios (< 4) may refer to plastic hinging achieved at large amounts of shortening, for which wavelength is a simple function of the amount of shortening and does not depend on h or T_e.

Govers *et al.*, 1992; Wei *et al.*, 2001; Austrheim and Boundy, 1994; Jolivet *et al.*, 1998).

- Direct mechanical or thermomechanical models testing the stability of geological structures or tectonic deformation styles as a function of implied rheological properties (e.g., Bird, 1991; Bassi, 1995; Brun, 2002; Toussaint *et al.*, 2004; Burov and Watts, 2006).

2. Observations of deformation in response to short-term loading:

- Distribution of intraplate seismicity (e.g., Maggi *et al.*, 2000; Jackson, 2002; Watts, 2001; Monsalve *et al.*, 2006; *see* Chapter 6.09).
- Tidal deformation (e.g., Bills *et al.*, 1994).
- Postseismic relaxation (e.g., Sabadini and Vermeersen, 2004; DallaVia *et al.*, 2005; *see* Chapter 6.09).
- Geodetic (GPS-INSAR) data (e.g., Montesi, 2004; England and Molnar, 2005).

The data based on observations of long-term deformation allow one to constrain a number of parameters such as T_e, F, σ, u, De, τ, h, L, λ, ϕ (**Figure 4**), where T_e is directly related to the integrated plate strength (B); F, σ, and u are, respectively, horizontal force, stress, and convergence/extension velocity that are ultimately linked to maximal stress/strain values supported by the lithosphere, as well as to possible deformation styles (e.g., continental subduction is virtually impossible for values of u below 2–3 cm yr^{-1} for three-layer lithosphere (Toussaint *et al*, 2004; Burov and Yamato, 2006) or 1 cm yr^{-1} for four-layer lithosphere (Yamato *et al.*, 2006)). De and τ are, respectively, Deborah number and relaxation/growth time of Rayleigh–Taylor instabilities related to viscosity and density contrasts in the lithosphere. λ is characteristic wavelength of unstable deformation (folding or boudinage), which is a function of thickness of the competent layers within the lithosphere. h and L are, respectively, characteristic height and horizontal size of process-induced topography, related to the plate strength and rheology. ϕ is subduction or major fault angle that can be indicative of the brittle properties and of the overall plate strength (subduction).

Interpretations of some short-term data are less certain. This concerns the intraplate seismicity and postseismic relaxation data, because there is no direct evidence that the mechanisms of short-term deformation are the same as the mechanisms of long-term deformation.

6.03.5 Rheology and Structure of the Oceanic Lithosphere

6.03.5.1 Goetze and Evans Yield Strength Envelopes – Age Dependence of the Integrated Strength

Yield stress envelopes (**Figure 3(a)**, left) for oceanic lithosphere are based on the Byerlee's law for the brittle part and on the dry olivine flow law for the ductile part. A single flow law is used as thin oceanic crust (basalts) does not need a separate law. The geotherms $T(z)$ used for computation of the ductile strength can be derived from half-space cooling plate model (Parsons and Sclater, 1977):

$$\frac{T-T_0}{T_{z0}-T}=\mathrm{erfc}\left(\frac{z}{2\sqrt{\chi t}}\right) \qquad [32a]$$

where t is time (age), χ is thermal diffusivity, *erfc* is complementary error function:

$$\mathrm{erfc}=1-\mathrm{erf}=1-\frac{2}{\sqrt{\pi}}\int_0^{\eta}\mathrm{e}^{-\lambda^2}\,\mathrm{d}\lambda \qquad [32b]$$

T_0 is the initial temperature (1330°C), T_{z0} is temperature at the surface (0°C). As can be seen from **Figure 3(a)**, the mechanical bottom h_m of the lithosphere follows the isotherm of 500°C:

$$h_\mathrm{m}\approx z(500^\circ\mathrm{C})\approx(\chi t)^{1/2} \qquad [33]$$

6.03.5.2 Rheology and Observations of Flexure (T_e Data)

The lithosphere responds to surface and subsurface loads by bending. Bending is characterized by vertical deflection, $w(x)$, and local radius of curvature, $R_{xy}(x)$, or curvature, $K(x)=-R_{xy}{}^{-1}=\partial^2 w/\partial x^2$. The amplitude and wavelength, λ, of bending depend on the flexural rigidity D or equivalent elastic thickness T_e ($D=E\,T_\mathrm{e}{}^3(12(1-v^2))^{-1}$). The flexural equation, when written in the form that uses bending moment $M_x(x)$, is rheology independent. The elasticity is thus used as a simplest rheological interpretation of bending strength. T_e and D are estimated by fitting the observed flexural profiles (Moho depression for continents or bathymetry for oceans) to the solution of thin plate equation:

$$\frac{\partial^2}{\partial x^2}\overbrace{\left(\underbrace{\frac{ET_\mathrm{e}^3}{12(1-v^2)}}_{D(x)}\underbrace{\frac{\partial^2 w(x)}{\partial x^2}}_{K(x)}\right)}^{M_x}+\frac{\partial}{\partial x}\left(F_x\frac{\partial w(x)}{\partial x}\right)+\Delta\rho g w(x)=\rho_c g b(x)+p(x) \qquad [34]$$

where F_x is horizontal fiber force, $\Delta\rho$ is the density contrast between surface material (topography/sediment) and asthenosphere, ρ_c is the density of surface material, $b(x)$ is topography elevation, and $p(x)$ is additional surface or subsurface load. For inelastic plates, T_e and D have sense of 'condensed' plate strength linked to the integrated plate strength B (eqn [23]). T_e is therefore a direct proxy for the long-term integrated strength of the lithosphere, B (see Watts, 2001). For example, for a single-layer plate of thickness h_m with $T_\mathrm{e}=T_\mathrm{e\_ocean}$

$$B=\int_0^{\infty}\sigma^f(x,y,t,\dot{\varepsilon})\mathrm{d}z$$

while

$$T_\mathrm{e\_ocean}=\left(12\left(\frac{\partial\sigma_{xx}}{\partial y}\right)^{-1}\int_{\frac{h_\mathrm{m}}{2}}^{\frac{h_\mathrm{m}}{2}}\sigma_{xx}^f z\,\mathrm{d}z\right)^{1/3};\quad T_\mathrm{e\_ocean}<h_\mathrm{m} \qquad [35]$$

where σ^f_{xx} is bending stress (Burov and Diament, 1995). For inelastic rheology, T_e is smaller than h_m and has no geometrical interpretation but is derived from the rigidity D and the flexural moment M. M and D are obtained from depth integration of bending stress σ^f_{xx}, which is a function of local plate curvature $K(x)=\partial^2 w/\partial x^2$ (e.g., Burov and Diament, 1995):

$$\sigma_{xx}^f(z,K)\approx\min(\sigma_\mathrm{b}(z),\sigma_\mathrm{d}(z),K(z-z_n(K))E(1-\mathrm{v}^2)^{-1})$$
$$D(x,K)=\left|\frac{M(x,K)}{K}\right|$$
$$T_\mathrm{e}(x,K)=\left(M(x,K)\frac{12(1-v^2)}{EK}\right)^{1/3} \qquad [36]$$

Here $z_n(K)$ is the 'floating' depth to the neutral stress-free plane: $z_n(K)\to 0.5h_m$ as $K\to 0$. By comparing observations of flexure in the regions of long-term surface loading such as ice, sediment, and volcanoes, to the predictions of simple elastic plate models, it has been possible to estimate T_e and thus B, in a wide range of geological settings. Oceanic flexure studies suggest that T_e is in the range 2–40 km and depends on load and plate age (**Figures 5(a)** and **5(b)**). These results are consistent with the predictions of rock mechanics, so that T_e values follow the age-controlled depth to 400–500°C (**Figure 5(c)**). The Brace–Goetze YSEs (Brace and Kohlstedt, 1980; Goetze and Evans, 1979) predict that strength should increase until the depth of the BDT, and then decrease in accordance with the brittle and ductile deformation laws. In oceanic regions, the failure curves are approximately symmetric about the

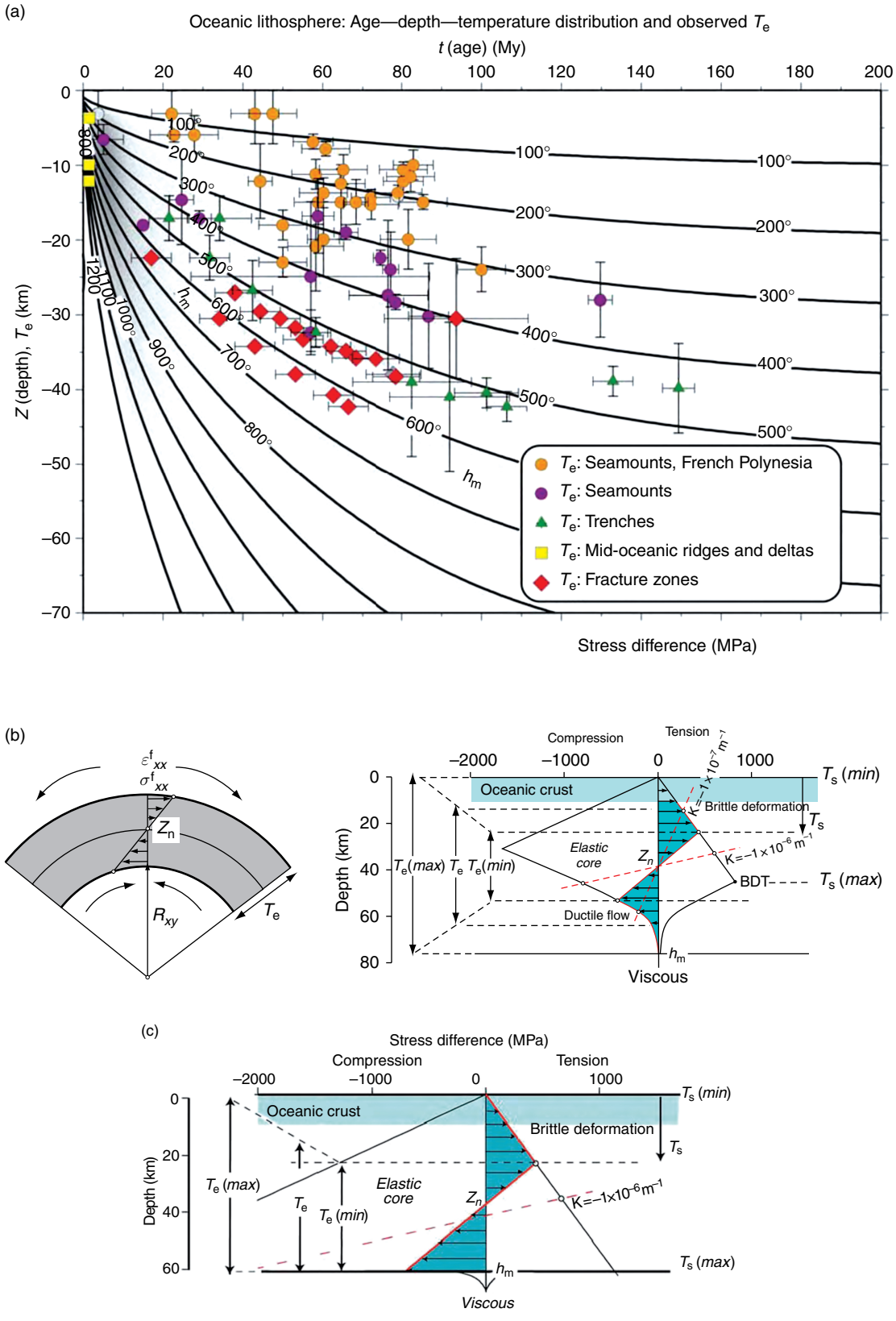

Figure 5 (*Continued*)

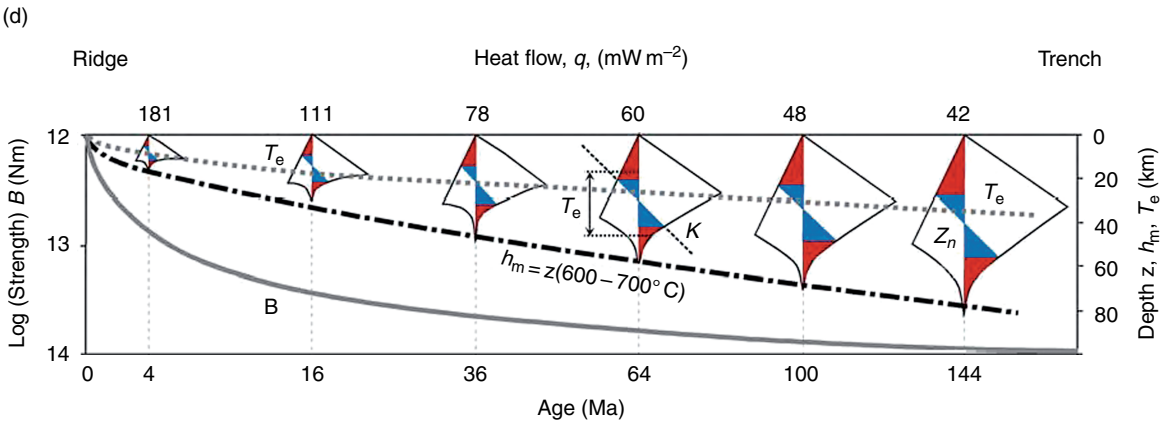

Figure 5 (a) Revealed correlation between the observed flexural strength T_e and age–temperature of the oceanic lithosphere. Thermal distribution is computed according to the plate cooling model (Parsons and Sclater, 1977; Burov and Diament, 1995). The T_e data are superimposed with computed geotherms. The relevant estimates refer to zones with normal thermal gradient such as fracture zones and trenches. Naturally, the cases of seamount loading cannot be fitted with the standard cooling model due to local thermal rejuvenation of the underlying lithosphere by hot-spot activity. However, locally tuned thermal models confirm T_e correlation with the depth of the geotherm 400–500°C , specifically for seamounts older than 10 My (Watts, 2001). (b) *Left*: Sketch of stress distribution due to bending of an ideal elastic plate. *Right*: Sketch of stress distribution in a bending viscoelastoplastic oceanic plate, and interpretation of the seismogenic layer, T_s ,and equivalent elastic thickness, T_e, of the oceanic lithosphere in terms of rheology (YSE) and its dependence on flexural stress gradient (based on (Watts and Burov, 2003)). ε^f_{xx}, σ^f_{xx}, and R_{xy} is flexural strain, stress, and local radius of flexure ($R_{xy} = -K^{-1}$). Thin solid line shows the YSE for 80 Ma oceanic lithosphere. The brittle behavior is controlled by Byerlee's law, the ductile behavior by olivine power-flow law ($n = 3$, $A = 7 \times 10^{-14}$ Pa^{-3} s^{-1}, $Q = 512$ kJ mol^{-1} (Kirby and Kronenberg, 1987a, 1987b)) and, the thermal structure by the cooling plate model (Parsons and Sclatter, 1977). The solid red line shows the stress difference for a load which generates a moment, M, of 2.2×10^{17} N m^{-1} and curvature, K, of 5×10^{-6} m^{-1}. The figure shows that the load is supported partly by an elastic 'core' and partly by the brittle and ductile strength of the lithosphere. The red dashed lines show the cases for K of 1×10^{-7} m^{-1} and 1×10^{-6} m^{-1} which bracket the range of observed values at trench-outer rise systems (Goetze and Evans, 1979; McNutt and Menard, 1982; Judge and McNutt, 1991)). The figure shows that T_s corresponds to the depth of the intersection of the moment-curvature curve with the brittle deformation field, but could extend from the surface, T_s (min), to the brittle–ductile transition (BDT), T_s (max). T_e, in contrast, could extend from the thickness of the elastic core, T_e (min), to the thickness of the entire elastic plate, T_e (max). Both T_s and T_e depend on the moment generated by the load and, hence, the plate curvature. Yet, T_s increases with curvature while T_e decreases. This figure represents an ideal case of pure bending stress in which T_e and T_s can be interrelated. Generally lithospheric regions where strain is sufficient to define T_s are in state of failure that may be largely produced by in-plane tectonic stress rather than by bending stress. In this case T_s and T_e anticorrelate or have no direct relation. (c) YSE based on '*crème-brulée*' rheology model: interpretation of the seismogenic layer, T_s and equivalent elastic thickness, T_e, under assumption of Jackson (2002) that the mechanical strength of the lithosphere is concentrated in the brittle layer. This case considers brittle–elastic lithosphere with zero-strength ductile part, for the same typical amount of flexure ($K = 5 \times 10^{-6}$ m^{-1}) and T_s value (20 km) as in the case shown in **Figure 7(b)**. The Figure demonstrates inconsistence of two simultaneous assumptions: of weak ductile mantle and $T_e = T_s$, due to geometric incompatibility between seismogenic layer (T_s) and elastic thickness (T_e). If $T_s = 20$ km than $T_e > 40$ km. (d) Variation of the mechanical strength, of integrated strength B and equivalent elastic thickness, T_e, of the oceanic lithosphere as function of age and thermal structure. T_e of the lithosphere actually depends on the gradient of bending stress related to local plate curvature, K. T_e approximately equals the size of the 'elastic core' plus half size of the underlying brittle zone and half size of the ductile zone beneath. Note that B correlates with T_e. Note also that T_e cannot be interpreted as a depth to some specific level in the lithosphere. Yet, it correlates well with h_m or geotherm to 400–500°C. After Watts AB (2001) *Isostasy and Flexure of the Lithosphere*, 458pp. Cambridge, NY: Cambridge University Press.

BDT where the brittle–elastic and elastic–ductile layers contribute equally to the strength. Since both T_e and BDT generally exceed the mean thickness of the crust (~7 km) there is a little doubt that the largest contribution to the strength of oceanic lithosphere comes from the mantle, not the crust.

McAdoo *et al.* (1985) used eqns. [36] to calculate the ratio of $T_e(K)$ to h_m for the middle value of oceanic thermal age of 80 Ma, a dry olivine rheology, and a strain rate of 10^{-14} s^{-1}. They showed that for low curvatures (i.e., $K < 10^{-8}$ m^{-1}) the ratio is 1, indicating little difference between the elastic thickness values. However, as curvature increases, the ratio decreases as $T_e(K)$ decreases. For $K = 10^{-6}$ m^{-1} the ratio is ~0.5, indicating a 50% reduction in the elastic thickness.

The tendency of the oceanic lithosphere to yield in the seaward walls of trenches can be understood in terms of simple mechanical considerations. Ideal elastic materials support any stress level. In the case of real materials, stress levels are limited by rock yield strength at corresponding depth. Flexural strain in a bending plate increases with distance from the neutral plane. Consequently, the uppermost and lowermost parts of the plate are subject to higher strains and may experience brittle or ductile deformation as soon as the strain cannot be supported elastically. These deformed regions constitute zones of mechanical weakness since the stress level there is lower than it would be if the material maintained elastic behavior and, importantly, there stress is lower than it would be on the limits of the elastic core that separates the brittle and ductile regions. The level of the brittle and ductile stress, however, is not zero. A load emplaced on the oceanic lithosphere will therefore be supported partly by the strength of the elastic core and partly by the brittle and ductile strength of the plate. The significance of T_e that has been estimated at trenches is that it reflects this combined, integrated, strength of the plate.

As the topography of Moho is accessible only from indirect observations, flexural models use various techniques allowing to compute the geometry of Moho or of the basement from the gravity anomalies. The departures of these anomalies from local isostatic models (e.g. Airy, Pratt), have long played a key role in the debate concerning the strength of the lithosphere. Modern isostatic studies follow either a forward or inverse modeling approach. In forward modeling, the gravity anomaly due, for example, to a surface (i.e., topographic) load and its flexural compensation is calculated for different values of T_e and compared to the observed gravity anomaly. The 'best fit' T_e is then determined as the one that minimizes the difference between observed and calculated gravity anomalies. In inverse (e.g., spectral) models, gravity and topography data are used to estimate T_e directly by computing the transfer function between them as a function of wavelength (e.g., admittance or coherence) and comparing it to model predictions. As for all potential field data, the inversion of gravity data has no unique solution. This makes some inverse flexural methods less reliable than direct models in complex continental settings.

In oceanic regions, forward and inverse modeling yield similar values of T_e. This is no better demonstrated than along Hawaiian-Emperor seamount chain. Forward modeling reveals a mean T_e of 25 ± 9 km while inverse (spectral) modeling using a free-air admittance method reveals 20–30 km (Watts, 1978). When the T_e estimates are plotted as a function of load and plate age (**Figures 5(a)** and **5(d)**) they yield the same result: T_e increases with the age of the lithosphere at the time of loading, being small (2–6 km) over young lithosphere and large over old lithosphere (>30 km).

6.03.5.3 Intraplate Seismicity (T_s), T_e, and the BDT

Intraplate seismicity is concentrated in a specific depth interval called seismogenic layer. The thickness, T_s, of this layer is in average 15–20 km and rarely exceeds 40–50 km both in oceanic and continental lithosphere, although deep-mantle earthquakes are also well detected (e.g., Déverchére *et al.*, 1991; Monsalve *et al.*, 2006). Brittle properties of the oceanic and continental lithosphere are not expected to be different, it is thus natural to suppose that the similarity of T_s in oceans and adjacent continents is suggestive of the tectonic stress transition from oceanic to continental domain. In spite of that, some authors suggest that T_s is related to long-term lithospheric strength, and not to the stress level, in the same way as T_e (Maggi *et al.* 2000; Jackson, 2002; **Figure 6**). These studies propose that both parameters are equivalent implying that strength of continental lithosphere resides in its brittle crust. This gave birth to the '*crème-brulee*' rheology model for continents (strong crust–weak mantle), which opposes the 'jelly-sandwich' rheology model (strong upper crust–strong mantle).

The mechanical considerations suggest that T_s has its own significance. It was previously concluded (e.g., Cloetingh and Wortel, 1986; Molnar and Lyon-Caen, 1988; Zoback, 1992; Bott, 1993; *see* Chapter 6.06) that average tectonic stresses do not exceed 100–600 MPa, and intraplate forces 10^{13} Nm. Byerlee's law predicts that brittle strength linearly increases with pressure and, hence, depth (**Figure 5**). Near the surface, brittle strength is 0–20 MPa while it is 100 times higher (2 GPa) in the mantle. The eqn [37] demonstrates that bending stress, and thus the probability to reach brittle strength limits, decreases while approaching the neutral surface. For any or both of the above two reasons, the upper crustal layers should fail easier than the lower mantle layers. At 50 km depth (the maximal depth of distributed seismicity), brittle rock strength is 2 GPa (**Figure 4**). Assuming 100 km thick lithosphere, one needs a horizontal tectonic force of 10^{14} Nm to reach this strength. This force is one or two orders of

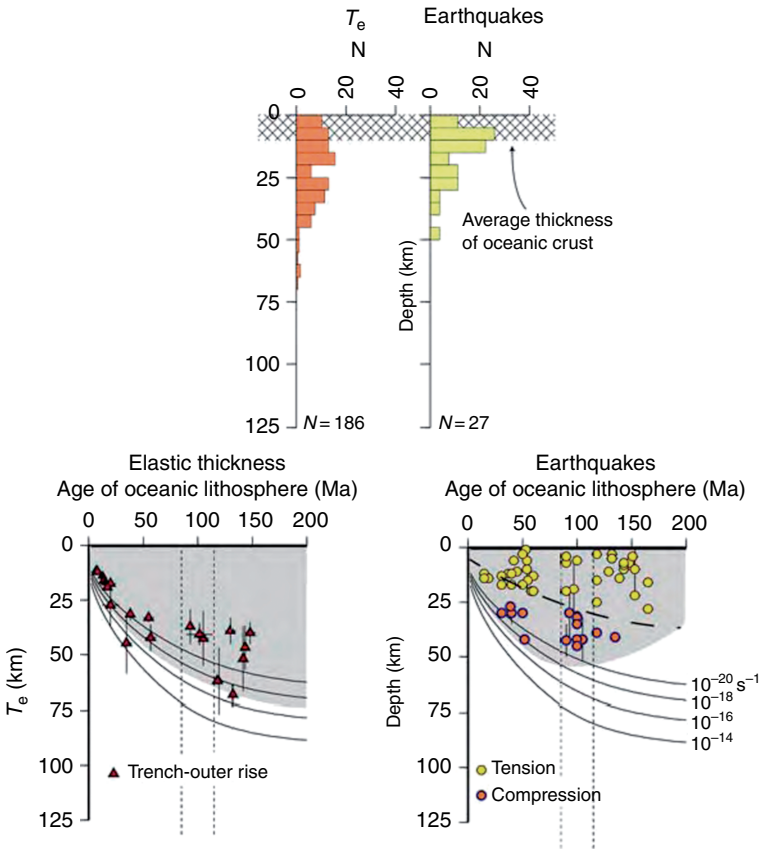

Figure 6 Summary of T_e and T_s estimates for deep-sea trench – outer rise systems (after (Watts and Burov, 2003)). Data based on Table 6.1 of Watts (2001) and Table 1 of Seno and Yamanaka, 1996). The T_e estimates have been corrected for curvature. Solid lines show the YSE based on the same rheological structure as assumed in **Figure 7**, a stress difference of 10 MPa, and thermal ages of oceanic lithosphere of 0–200 Ma.

magnitude higher than the estimates for intraplate forces. Stress level of 2 GPa may probably be reached only locally, when one combines tectonic stress with bending stress.

The discussions on rheology arrive not only from uncertainties of the rheology laws but also from conflicting results on T_e from some continental studies. But, it is agreed that oceanic T_e data are robust. Hence, through understanding $T_e - T_s$ relations for oceans we can progress with their understanding for continents. When all oceanic T_s data and T_e data are plotted on the same depth plot, there is an impression of correlation between T_s and T_e (**Figure 6**). Yet when one separates the extensional and compressional events, the correlation breaks down: extensional earthquakes are systematically found at two times smaller depth than the corresponding T_e values (Watts and Burov, 2003). Indeed, the Byerlee's law predicts that extensional failure requires nearly two times smaller stress, which leads to the conclusion that the earthquake depths are controlled by intraplate stress levels, and decrease with increasing integrated strength of the lithosphere B if $B > F$ (for a fixed F):

$$\begin{aligned} T_s &\approx \Upsilon(F/T_e + \sigma^f_{xx|z=T_s})/\rho g \\ T_e(\text{oceans}) &< \approx 0.7 h_m \end{aligned} \qquad [37]$$

The factor $\Upsilon = 0.6^{-1} - 0.85^{-1}$ comes from the eqn [9a], $\sigma^f_{xx|z=T_s}$ is flexural stress (eqn [36]) at depth $z = T_s$. Equation [37] shows that T_s decreases with increasing T_e. Thus, T_s and T_e do not correlate but anticorrelate if $F < B$ (i.e., if plate preserves integrity, e.g., in subduction settings). For unbent plate, T_s can be equal to T_e only if $T_e = (0.8F/\rho g)^{1/2}$. Since $F < 10^{13}$ Nm (per unit length) this implies $T_s < 15$–16 km, whereas T_e of the plate shown in **Figure 5** is 30 km, that is, $\approx 2T_s$. For smaller F, $T_s < 1/2T_e$. Flexural stress σ^f_{xx} may increase the value of T_s by

a factor of 2–3, but at the same time it would decrease T_e by the same factor (**Figure 5**). Thus two values, T_s and T_e, do not approach each other until the plate preserves its integrity ($F < B$). Maximal intraplate stress ($\sigma^f_{xx} + F/T_e$) is limited to 2 GPa (**Figure 5**). This yields $T_e < 40$–50 km, which is compatible with the observations (Maggi *et al.*, 2000).

As seen from **Figures 5** and **6**, strong mechanical core associated with T_e is centered at the neutral plane of the plate, z_m, whereas the seismogenic layer T_s is shifted to the surface. This is the reason why T_s cannot have same geometric interpretation as T_e. Since bending stresses are minimal near z_m, the earthquakes will be favored at some distance above or below it (**Figure 5(b)**). The brittle strength linearly increases with depth, thus the earthquakes must be more frequent above z_n. For an elastic plate or brittle–elasto–ductile plate, z_n is located roughly in its middle (**Figure 5**), at a depth $z \approx 1/2\ T_e(\max)$. In this case $T_s < 1/2\,T_e$. If plate strength is concentrated in the brittle–elastic layer T_s then earthquakes would occur at depths $< \approx (T_e(\max) - T_e)$ (**Figure 5(c)**). $T_e(\max) - T_e < 1/2\,T_e$ except for improbably strong flexure. Hence, in a brittle–elastic plate, the equity $T_s = T_e$ is impossible. T_s may equal T_e only in a plate with quasi-*symmetric* strength distribution, that is, comprising *equally* strong brittle and ductile part (**Figure 5(b)**), which is incompatible with *crème-brûlée* rheology model.

Rock mechanics data suggest that in addition to Byerlee's law, a semibrittle/semiductile strain-rate-dependent plastic flow may increasingly occur starting from 10–15 km depth, with a frictional component that is no longer significant at depths > 40–50 km (Ranally, 1995; Chester, 1995; Bos and Spiers, 2002). This also explains why intraplate seismicity both in the oceanic and continental lithosphere is limited to 40–50 km depth.

There are, of course, regions where earthquakes extend to great depths (>40 km), for example, in subduction–collision zones, including continents (Monsalve *et al.*, 2006). It is generally agreed (Scholtz, 1990; Kirby *et al.*, 1991) that this seismicity is not related to frictional sliding, at least not the Byerlee's law, but to some other metastable mechanisms. These mechanisms are only weakly related to rock strength. For example, it has been known for some time that, unlike shallow (i.e., depths <50–70 km) earthquakes, deep earthquakes produce very few aftershocks. This aftershock behavior is a strong argument that the earthquake-generating mechanism differs between shallow and deep earthquakes. The physical mechanisms of deep (>30–40 km) earthquakes are still to be understood but it is agreed that the differential stresses needed to initiate these earthquakes are smaller than the predictions of the Byerlee's law for dry rock at corresponding depth but are greater than that for shallow earthquakes (15–25 km depth) (Kirby *et al.*, 1991).

6.03.5.4 Constraints on the Long-Term Viscosity from Subsidence Data

Volcanic islands such as Hawaii present an ideal example of point loading that can be used to evaluate long-term lithospheric strength (Watts, 2001). Acting as almost instantaneous surface loading, islands produce local depressions, whose geometry and amplitude can be traced through time from stratigraphy data. It was shown that primary response of the lithosphere evokes integrated strength that is highly different from the strength established at long term. In general, the lithosphere exhibits high flexural strength within the first 10 My after loading (e.g., for Hawaii, $T_e(t=0) = 90$ km (Watts, 2001)), which progressively decays toward some asymptotic value (for Hawaii, $T_e(t \to \infty) = 30$ km, (Walcott, 1970)). It is remarkable that strength decay is exponential, as for a Maxwell solid, only within interval of a few million years; after that strength remains unchanged or slowly increases with time following common thermal age dependence. The subsidence data suggest that the characteristic relaxation times in the lithosphere are on the order of several million years. Compared to the Maxwell relaxation times in the asthenosphere (10–100 years) this suggests that the average lithosphere viscosity is 10^4–10^5 higher than the asthenospheric viscosity ($10^{19} - 5 \times 10^{19}$ Pa s). This yields a rough estimate of $10^{23} - 10^{24}$ Pa s for viscosity of oceanic lithosphere and suggests that elastic strain plays an important role in long-term deformation.

6.03.5.5 Large-Scale Lithospheric Folding

A number of observations (e.g., Weissel *et al.*, 1980) reveal periodical undulations of the sea floor in the zones of important intraplate compression such as Indian Ocean (see also discussion on continental folding in the following sections). These undulations evoke compressional instabilities that develop in stiff layers underlying a weaker matrix. The minimal stiffness (viscosity) ratio needed for development of folding is ~100 (Biot, 1961). The wavelength, λ, of

folding is roughly proportional to five thicknesses of the competent layer, h_m:

$$\begin{aligned}
&\lambda = 2\pi h_m(\mu_1/\mu_2)^{1/3} \text{ (viscous rheology, no gravity)}\\
&\lambda = 2\pi(F/\Delta\rho g)^{1/2}, F \approx B \approx 2\mu_1\dot{\varepsilon}h_m\\
&\quad \text{(viscous gravity folding)}\\
&\lambda = 2\pi(Gh_m/F)^{1/2} \text{(elastic buckling, no gravity)}\\
&\lambda = 2\pi(2D/F)^{1/2}, F \approx (4D\Delta\rho g h_m)^{1/2}\\
&\quad \text{(elastic gravity buckling)}
\end{aligned} \quad [38]$$

where μ_1 is average viscosity of the lithosphere and μ_2 is the viscosity of the asthenosphere. In case of the Indian Ocean, the observed λ is on the order of 250 km (Weissel *et al.*, 1980), which needs a 50 km thick stiff layer. This value agrees with the eqn [37] and is close to T_e estimates for Indian Ocean (40–50 km, (Watts, 2001); **Figure 5**). The wavelength of folding thus can be used as a proxy for long-term strength of the lithosphere as well as T_e. Since folding develops in layered systems with competence contrasts higher than 100, we can conclude that the average viscosity of the oceanic lithosphere should be at least $10^{21} - 10^{22}$ Pa s compared to viscosity of the underlying asthenosphere (5×10^{19} Pa s). This provides only a lower bound on the mean viscosity of the lithosphere because λ is rather weakly dependent on μ_1/μ_2 in the range $10^2 < \mu_1/\mu_2 < 10^4$. Hence, μ_2 may vary from 10^{21} Pa s to 10^{24} Pa s.

6.03.6 Rheology and Structure of the Continental Lithosphere

6.03.6.1 Common Goetze and Evans' Yield Strength Envelopes

Similarly to the oceanic lithosphere, the continental YSEs are derived from common assumptions such as the rheological structure, crustal thickness, lithosphere thickness $a = z(1330°C)$, thermal structure, strain rate field, etc. Since the continental crust is much more versatile in its structure and composition than the oceanic crust, there is much larger variety of possible continental YSEs (**Figure 7**). In difference from the oceanic lithosphere, the thermal structure of continental plates is not well constrained since (1) they might have underwent several thermal events in their history, (2) the thermal thickness, a, of continents is not well defined, (3) about 50% of the continental surface heat flux is influenced by uncertain radiogenic heat production, surface processes, and spatial variations in thermal properties. The common thermal model refers to cooling of a multilayer plate heated from below ((Burov and Diament, 1992, 1995; Afonso and Ranalli, 2004), Appendix B). This model is characterized by time of cooling t (t = thermotectonic age), has a vertically heterogeneous structure, and accounts for radiogenic heat sources in the crust. In the absence of thermal events, thermal structure of the lithosphere becomes stationary after 400 – 700 Ma (e.g. Burov and Diament, 1995; *see* Chapter 6.05).

The assumed difference in the mechanical properties of the upper crust, lower crust, and mantle may lead to the appearance of weak ductile zone(s) in the lower crust that permit mechanical decoupling of the upper crust from the mantle (e.g., Chen and Molnar, 1983; Kusznir and Park, 1986; Lobkovsky and Kerchman, 1992; Bird, 1991). Crust–mantle decoupling occurs if the lower crust is weaker than mantle olivine at temperature at Moho boundary. The possibility of this decoupling implies the possibility of lateral flow in the lower crust, enhanced by dissipative heating, grain-size reduction, and probably by metamorphic changes (Lobkovsky and Kerchman, 1992; Burov *et al.*, 1993). For 'common' quartz-dominated crust, decoupling should be permanent, except thin (e.g., rifted) crust (<20 km). For other crustal compositions (diabase, quartz-diorite, etc., **Figure 7**) decoupling might take place in most cases, except very old cold lithospheres (age >750 Ma). Presence of fluids (wet/dry rheology) also promotes decoupling.

A number of independent data sources provide additional constraints on the choice of crustal rheology. These data include T_e and other deformation data, seismicity distributions (Molnar and Tapponnier, 1981; Chen and Molnar, 1983; Cloetingh and Banda, 1992; Govers *et al.*, 1992; Déverchère *et al.*, 1993); seismic reflectivity and velocity anomalies (P and S), attenuation of S-velocities associated with ductile zones or fluids (e.g. Kusznir and Matthews, 1988; Wever, 1989); petrology data (Cloetingh and Banda, 1992); data from magnetotelluric soundings, which serve as indicators of the presence of melts and fluids (Wei *et al.*, 2001).

6.03.6.2 Age and Other Dependences of the Integrated Strength of the Lithosphere

As for the oceans, T_e data are a main proxy for long-term strength of continental lithosphere. In continents, T_e ranges from 0 to 110 km and shows only partial relationship with age. Although the continental lithosphere should strengthen while getting colder with time (**Figure 7**), there is no such a clear T_e age

dependency in continents as in oceans (**Figure 8**). Many plates underwent thermal events that changed their thermal state in a way that it does not correlate with their geological age (e.g., Kazakh shield (Burov *et al*., 1990)), Adriatic lithosphere (Kruse and Royden, 1994)). On the other hand, after 400–750 Ma (**Figure 8**) temperature distribution in the lithosphere approaches stationary state and does not evolve with age. As mentioned, interpretation of the surface heat flux in continental domain is ambiguous because of uncertain crustal heat generation and thermal effects associated with erosion, sedimentation, and climatic changes. Surface heat flow mainly reflects crustal processes and should not be used to infer the subcrustal geotherm (England and Richardson, 1980).

The base of the mechanical lithosphere in continents, h_m, is referred to as isotherm of 700–750°C, below which the yielding stress is less than 10–20 MPa. The background strain rates are typically known within one-order accuracy. As can be seen from **Figure 7(b)**, such uncertainty is acceptable, since it affects the yield limits by not more than 10%.

The rheological meaning of T_e in the continents is not as clear as it is in the oceans (**Figures 7** and **8**). The T_e data show a bimodal distribution, with low values clustering at 30–40 km, and high values clustering at 80 km (Burov and Diament, 1995; Watts, 2001). The reason for this clustering probably refers to influence of plate structure: depending on the ductile strength of the lower crust, the continental crust can be mechanically coupled or decoupled with the mantle resulting in highly differing T_e. Burov and Diament (1992) have shown that for 'typical' continental lithosphere the weak ductile zones in the lower crust do not allow flexural stresses to be transferred between the strong brittle, elastic, or ductile layers of the 'jelly sandwich'. As result, there are several 'elastic' cores inside the bending plate. In such a multilayer plate stress levels are reduced, for the same amount of flexure, compared to a single plate. Consequently, T_e, which is a measure of

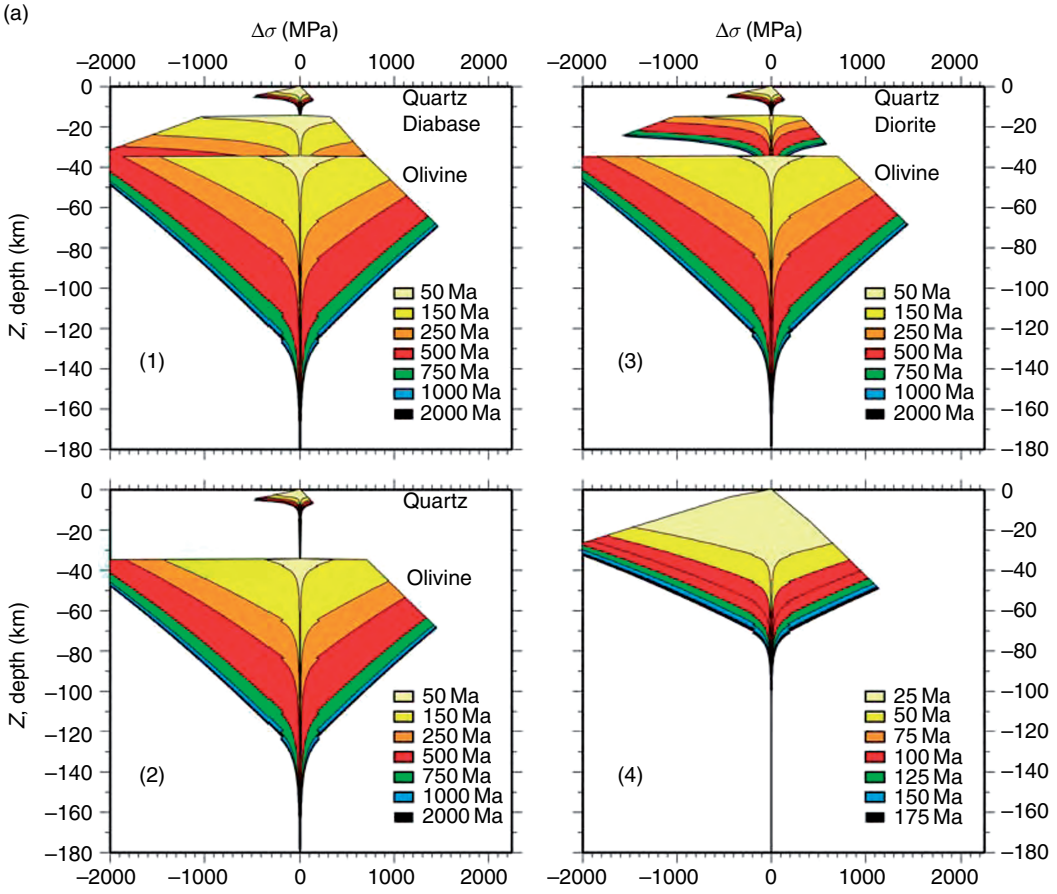

Figure 7 (*Continued*)

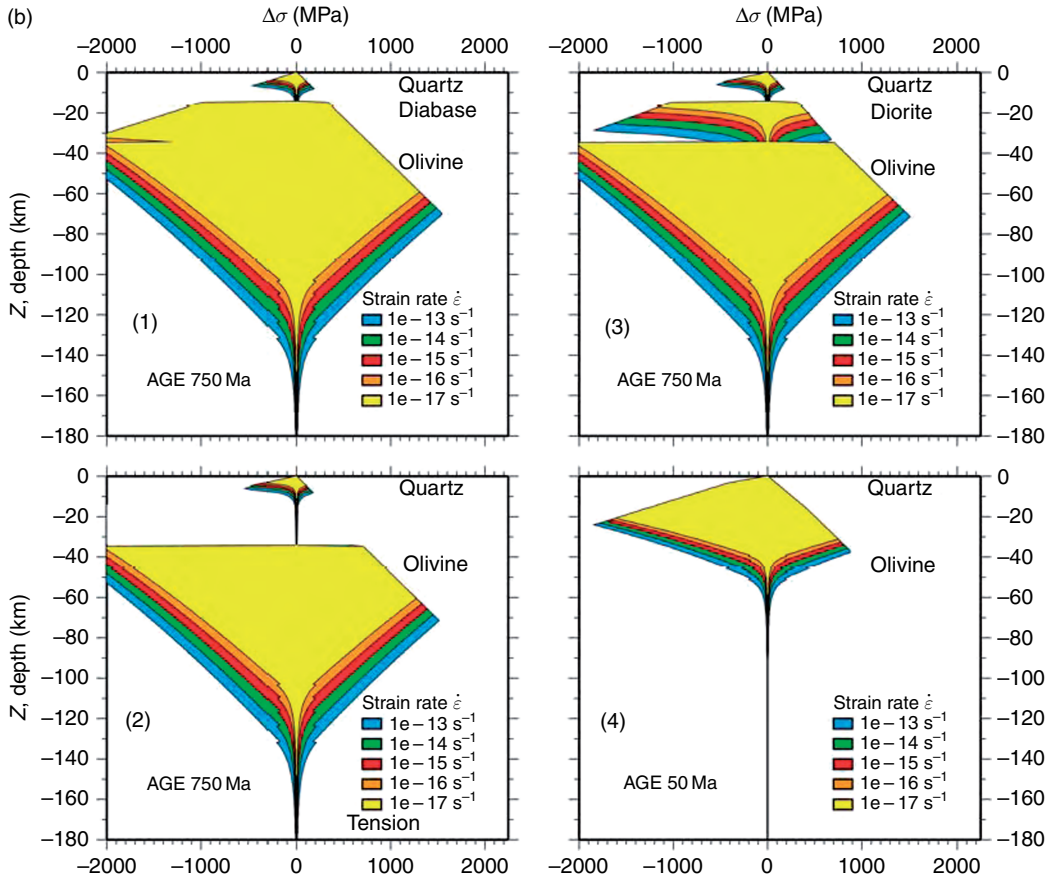

Figure 7 Continental YSE. Equilibrium thermal thickness 250 km. Upper crust is controlled by quartz rheology and mantle lithosphere is controlled by dry olivine rheology. (a) Continental YSEs as function of thermotectonic age and crustal composition. (b) Continental YSEs as function of the background strain rate and crustal composition. Cases 1,2,3 – rheological envelopes for different lower crustal compositions: diabase, quart-diorite, and quartz, respectively. For comparison, oceanic YSE (4) is shown in right bottom corner (thermal thickness 150 km). (a) After Burov EB and Diament M (1995) The effective elastic thickness (T_e) of continental lithosphere : What does it really mean? *Journal of Geophysical Research* 100: 3895–3904.

integrated bending stress, is also reduced. T_e of a multilayer plate reflects the combined strength of all the brittle, elastic, and ductile layers. Yet, it is not simply a sum of the thickness of these layers (h_1, h_2 … h_n) (**Figure 9(a)**, Appendices 1 and 2):

$$T_e(\mathrm{YSE}) \sim (h_1^3 + h_2^3 + h_3^3 + \cdots)^{1/3} = \left(\sum_{l=1}^{n} h_l^3\right)^{1/3} \quad [39]$$

For example, in case of two equally strong layers ($n = 2$) of total thickness h (e.g., crust and mantle), $T_e \approx 0.6h$ instead of h, that is, the integrated strength is reduced by a factor of 2 compared to a mono-layer plate (e.g., old craton with strong coupled lower crust). The meaning of T_e(YSE) in the continents thus becomes clearer. It reflects the integrated effect of all competent layers that are involved in the support of a load, including the weak ones.

If the multilayered continental lithosphere is subject to large loads, it flexes, and the curvature of the deformed plate, K, increases. T_e(YSE) is again a function of K and is given (Burov and Diament, 1995, 1996) by (**Figure 9(b)**).

$$T_e(\mathrm{YSE}) = T_e(\mathrm{elastic})\ C(K, t, h_{c1}, h_{c2}, \ldots) \quad [40]$$

where C is a function of the curvature K, the thermal age t, and the rheological structure. A precise analytical expression for C is bulky (Burov and Diament, 1992), although Burov and Diament (1996) provide a first-order approximation for a 'typical' case of continental lithosphere with a mean crustal thickness of 35 km, a quartz-dominated crust, and an olivine-dominated

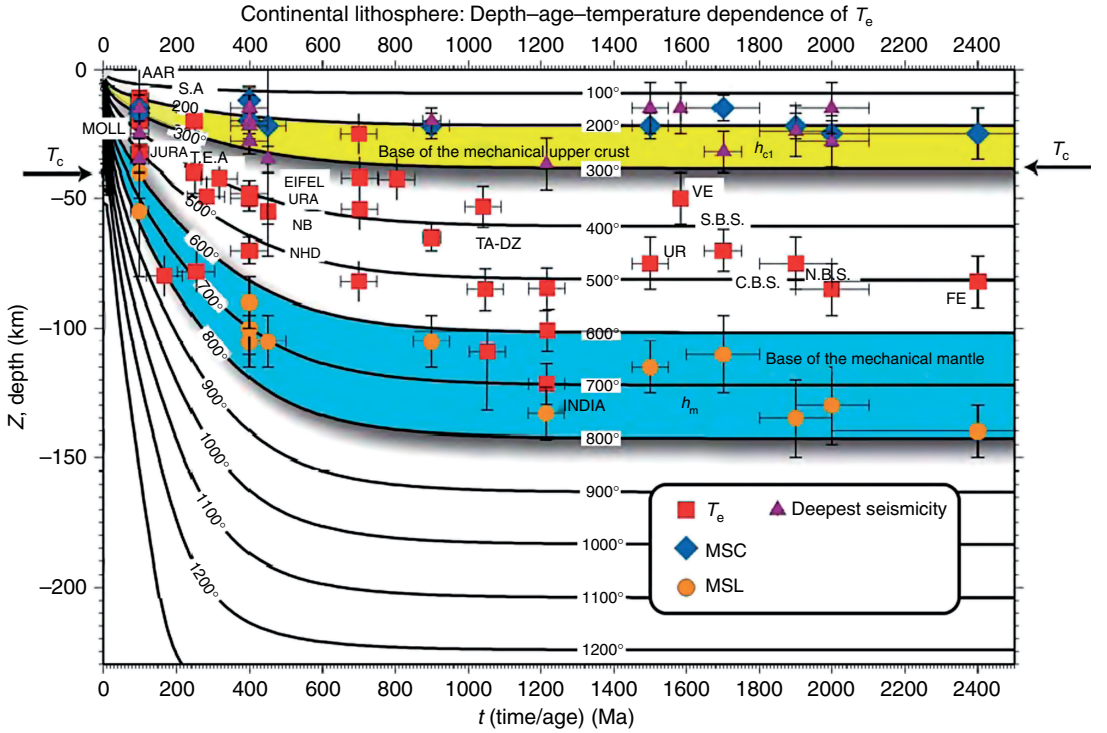

Figure 8 Compilation of observed elastic thickness (T_e) against age of the continental lithosphere at the time of loading and the thermal model of the continental lithosphere (equilibrium thermal thickness, $a = z(1330°C)$, of 250 km (Appendix 2). Also shown is the depth to the mechanical base of the lithosphere and maximal depths of seismicity (where available). The data refer to the studies that have taken into account – at minimum surface topography loads. Where available, we preferred estimates based on more robust forward models rather than on debated spectral estimates. In particular, McKenzie and Fairhead (1997) and Jackson (2002) used a specific variant of the FAA admittance that is valid for data referred to sea level. The T_e estimates obtained from this approach are not reliable in continents because this method ignores largest topography loads, such as mountains, and boundary forces (Watts and Burov, 2003; Lowry and Smith, 1994; Jordan and Watts, 2005; Burov and Watts, 2006). The lines are isotherms with account for radiogenic heat production in the crust. Filled squares are estimates of T_e in collision zones (foreland basins, thrust belts); filled circles correspond to postglacial rebound data. Isotherms 250°C–300°C mark the base of the mechanically strong upper crust (quartz). The isotherms 700°C–750°C mark h_m, the base of the competent mantle (olivine). Note that there are no significant changes in the thermal structure of the lithosphere after ~750 Ma, though there are significant reductions in T_e even for these ages. These reductions are obviously caused by differences in crustal structure and rheology. The notations are: Foreland basins/mountain thrust belts data: E.A, Eastern Alps; W.A., Western Alps; AD, Andes (Sub Andean); AN, Apennines; AP, Appalachians; CR, Carpathians; CS, Caucuses; DZ, Dzungarian Basin; HM, Himalaya; GA, Ganges; KA, Kazakh shield (North Tien Shan); KU, Kunlun (South Tarim); NB, North Baikal (chosen since this part of the Baikal rift zone is believed to represent a 'broken' rift currently dominated by flexural deformations); TA, Central and North Tarim; PA, Pamir; TR, Transverse Ranges; UR, Urals; VE, Verkhoyansk; ZA, Zagros. Post-glacial rebound zones: L.A., lake Algonquin; FE, Fennoscandia; L.AZ, lake Agassiz; L.BO, lake Bonneville; L.HL, lake Hamilton. Data sources: S.A., AN., CR., HM, NB, KA, TA, PA,KU, GA, AD, TA, W.A, E.A., DZ, AP, GA,TR,VE,FE (Burov and Diament, (1995) and references therin). Other data sources (ZA, L.A., L.AZ, L.BO, L.HL) (Watts, 1992, 2001).

mantle, which, they indicate, is valid for $10^{-9} < K < 10^{-6}$ m^{-1}. T_e(YSE) then simplifies to

$$T_e(\mathrm{YSE}) \approx T_e(\mathrm{elastic}) \times \left(1-(1-K/K_{\max})^{1/2}\right)^{(1/2+1/4(T_e(\mathrm{elastic})/T_e(\max)))} \quad [41]$$

where $K_{\max}$ (in m^{-1}) $= (180 \times 10^3\ (1 + 1.3\,T_e(\min)/T_e(\mathrm{elastic}))^6)^{-1}$, $T_e(\max) = 120$ km, $T_e(\min) = 15$ km, and T_e(elastic) is the initial elastic thickness prior to flexure, which can be evaluated from eqn [39].

We show in **Figure 9**, therefore, how T_e and T_s would be expected to change using the more precise analytical formulations of Burov and Diament (>1992, 1995) (Appendix 1). **Figure 9** illustrates how the thickness of the brittle and ductile layers evolves with different loads and, hence, curvatures. On bending, brittle failure and, hence, the potential for seismicity preferentially develops in the uppermost part of the crust. The onset of brittle failure in the mantle is delayed, however, and does not occur

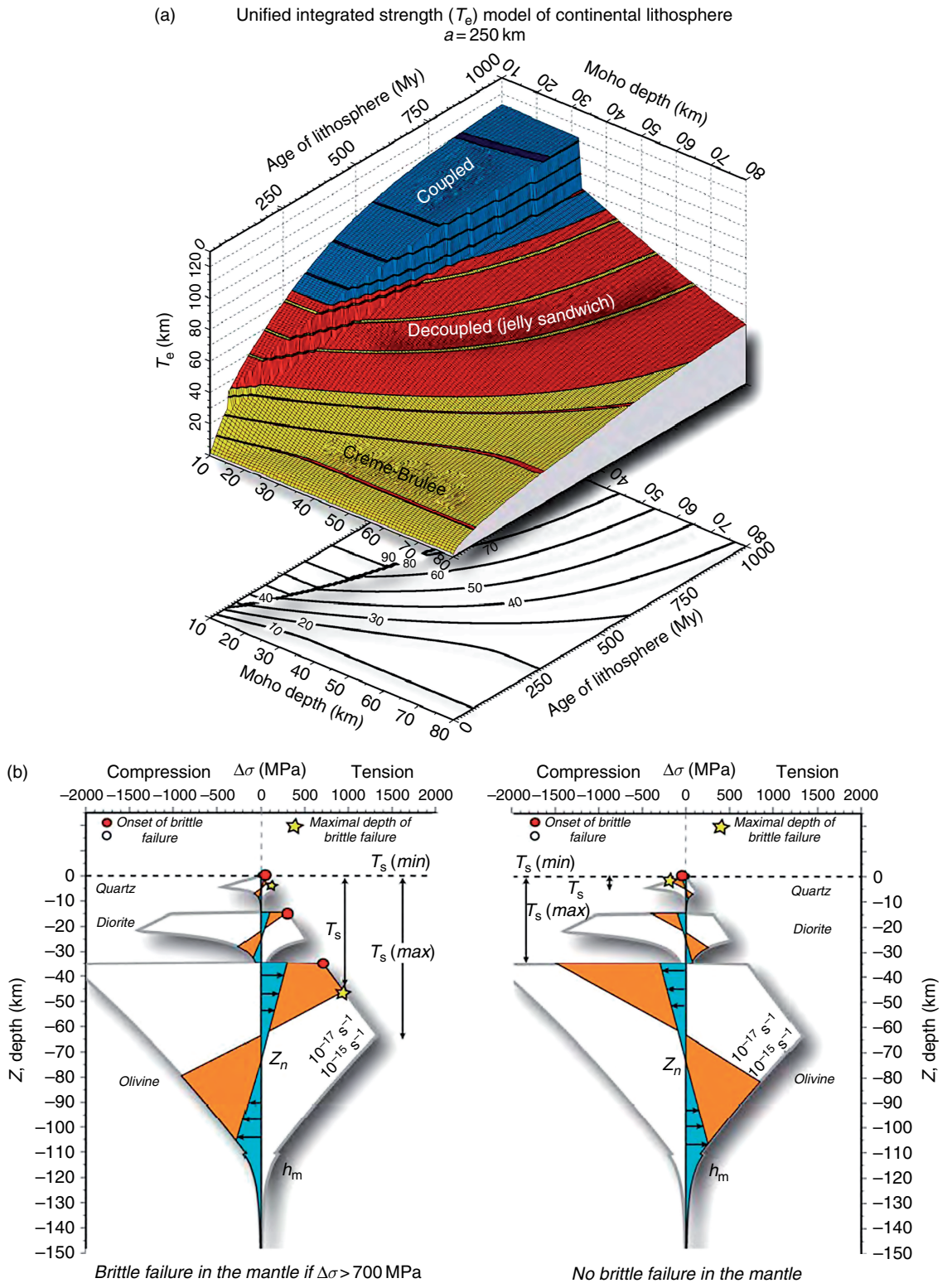

Figure 9 (*Continued*)

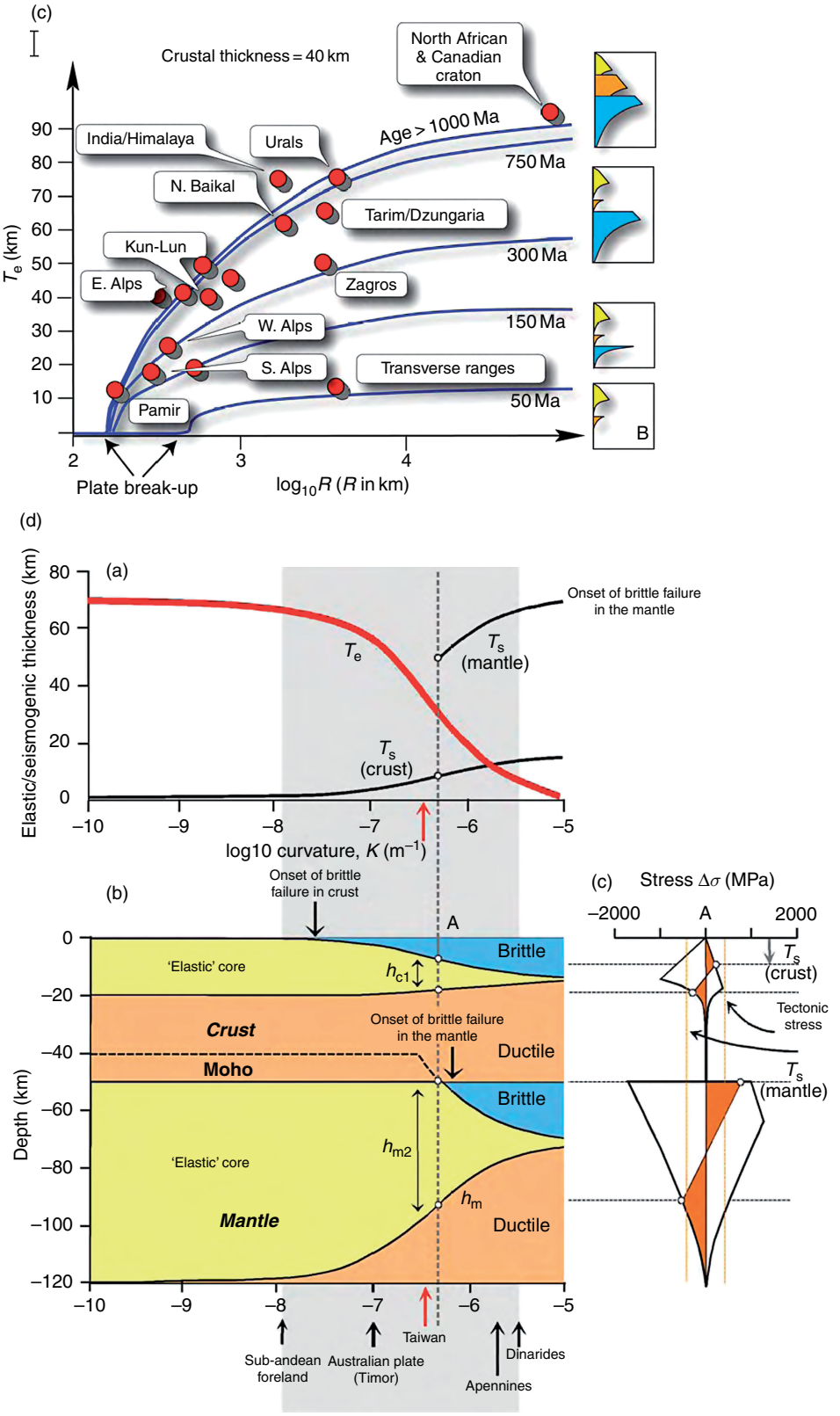

Figure 9 (*Continued*)

until the amount of flexure and, hence, curvature is very large. Observations of curvature in the regions of large continental loads provide constraints on the brittle strength of continental lithosphere. Curvatures range from $10^{-8}\,m^{-1}$ for the sub-Andean to $5 \times 10^{-7}\ m^{-1}$ for the West Taiwan foreland basins (Watts and Burov (2003) and references therein). The highest curvatures are those reported by Kruse and Royden (1994) of $4–5 \times 10^{-6}\ m^{-1}$ for the Apennine and Dinaride foreland. **Figure 9** shows, however, that plate curvatures of $10^{-6}\ m^{-1}$ may not be sufficiently large to cause brittle failure in the sub-crustal mantle, *unless* the flexed plate is subject to an externally applied tectonic stress. In the case illustrated in **Figure 9**, the stress required to cause failure in the sub-crustal mantle for this plate curvature is 350 MPa assuming 'dry' Byerlee's law. This is already close to the maximum likely value for tectonic boundary loads (e.g., Bott, 1993), suggesting that brittle failure, and, hence, earthquakes in the mantle will be rare. Instead, seismicity will be limited to the uppermost part of the crust, where rocks fail by brittle deformation, irrespective of the stress level. This limit does not apply, of course, to T_e. For curvatures up to $10^{-6}\ m^{-1}$, **Figure 9** shows that T_e is always larger than T_s. Only for the highest curvatures (i.e., $K > 10^{-6}\,m^{-1}$) will $T_e < T_s$ and, interestingly, will the case that $T_s > T_e$ arise. Of course, stress estimates shown in **Figure 9** depend on the assumed rheology. In particular, frictional strength at depth may be several times smaller than the prediction of the Byerlee's law in case of pore fluid pressure (reduction by a factor of 5, **Figure 1**). Yet the presence of fluids will also reduce the ductile rock strength by the same or higher amount. As a result the rock may chose to flow

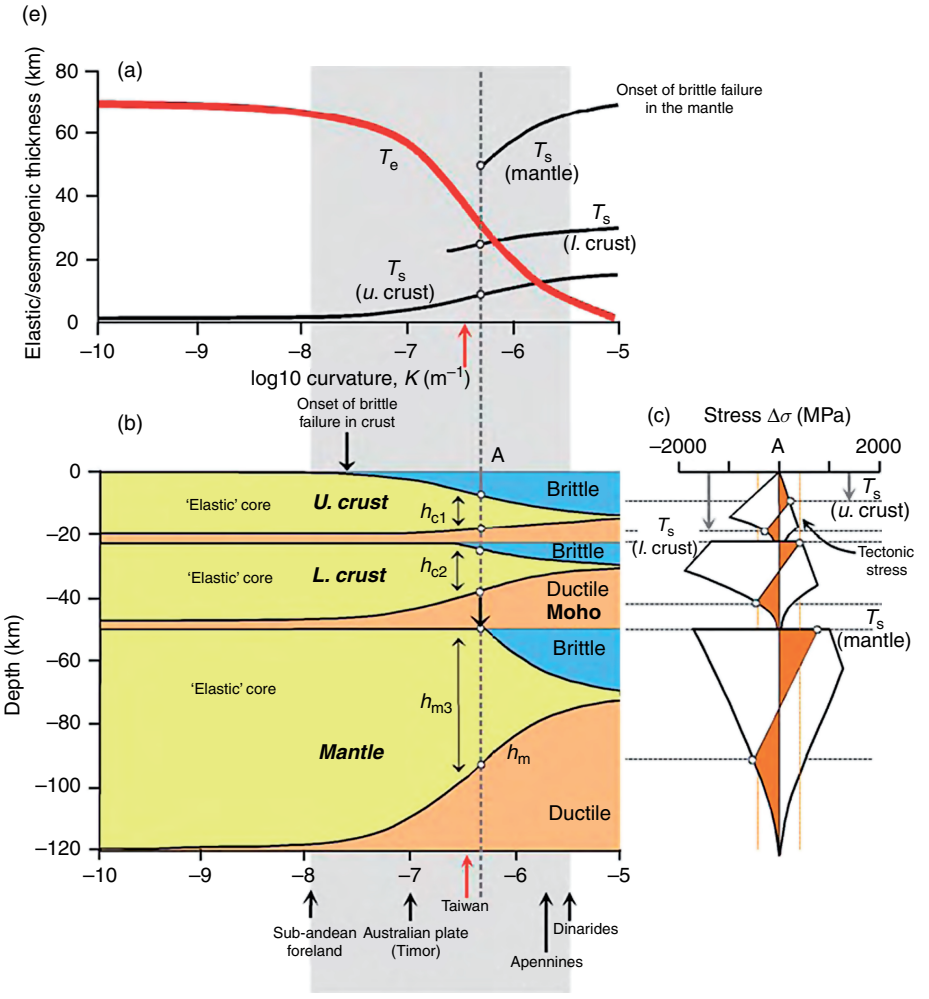

Figure 9 (*Continued*)

rather than to break; T_e will be reduced and plate curvature would be higher for the same load. It thus appears difficult to favor mantle 'seismicity' by simple brittle strength reduction due to the presence of fluids.

Finally, it should be noted that the dependence of T_e and T_s on the state of stress and plate curvature may result in strong lateral variations of T_e and T_s both at local and regional scale (**Figures 9(f)** and **9(g)**). The computations (Burov and Diament, 1995) demonstrate that surface loads (elevated topography or sedimentary loading; plate boundary forces) may result in strong lateral variations of both T_e and T_s. Surface or subsurface loading may decrease T_e (and increase T_s) by 30–50% (or more in case of initially weak plates). In particular, the lithosphere beneath mountain ranges or large sedimentary basins (rifts, forelands) may be significantly weakened resulting in more 'local' compensation of the surface loads. In subduction/collision zones, localized weakening due to plate bending under boundary forces may result in steeper slab dip and accelerated slab break-off. In case of weakened lithosphere (e.g., abnormal heat flux), loading may result in total failure of the plate (= local isostasy).

6.03.6.3 Seismicity, T_s, BDT, and Long-Term Strength

The considerations of previous section (**Figure 9**) suggest a dual role for the continental sub-crustal mantle. In regions of low curvature, the mantle may be devoid of earthquakes, but largely involved in the support of long-term flexural-type loads. In regions of high curvature, however, the mantle may be seismic, but the support of long-term loads is confined to the crust rather than the mantle. Despite differences in their timescales, we may therefore be able to use the presence or absence of mantle earthquakes, at least in the plate interiors, as a proxy for whether it is the crust or mantle that is mainly involved in the support of long-term loads. This discussion should be considered in strict relation to the common, but probably wrong (at least for great depths), assumption that pre-fractured 'Byerlee's' rock provides a

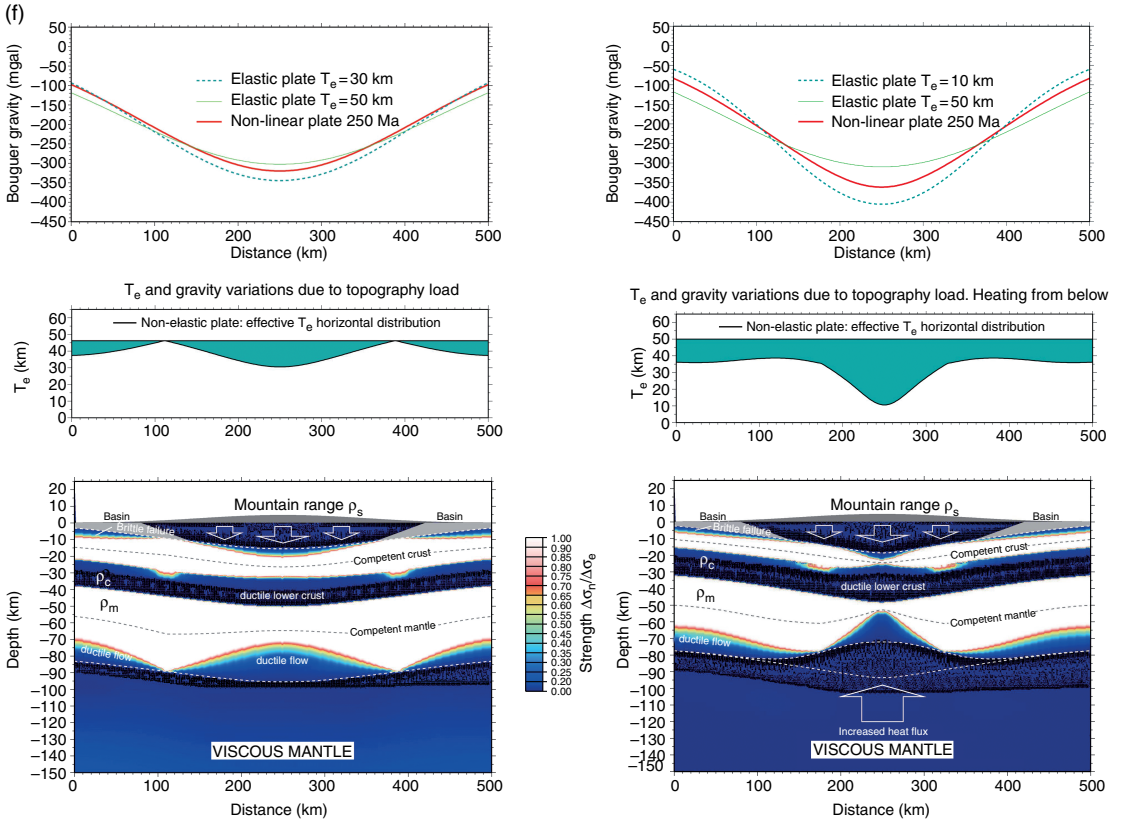

Figure 9 (*Continued*)

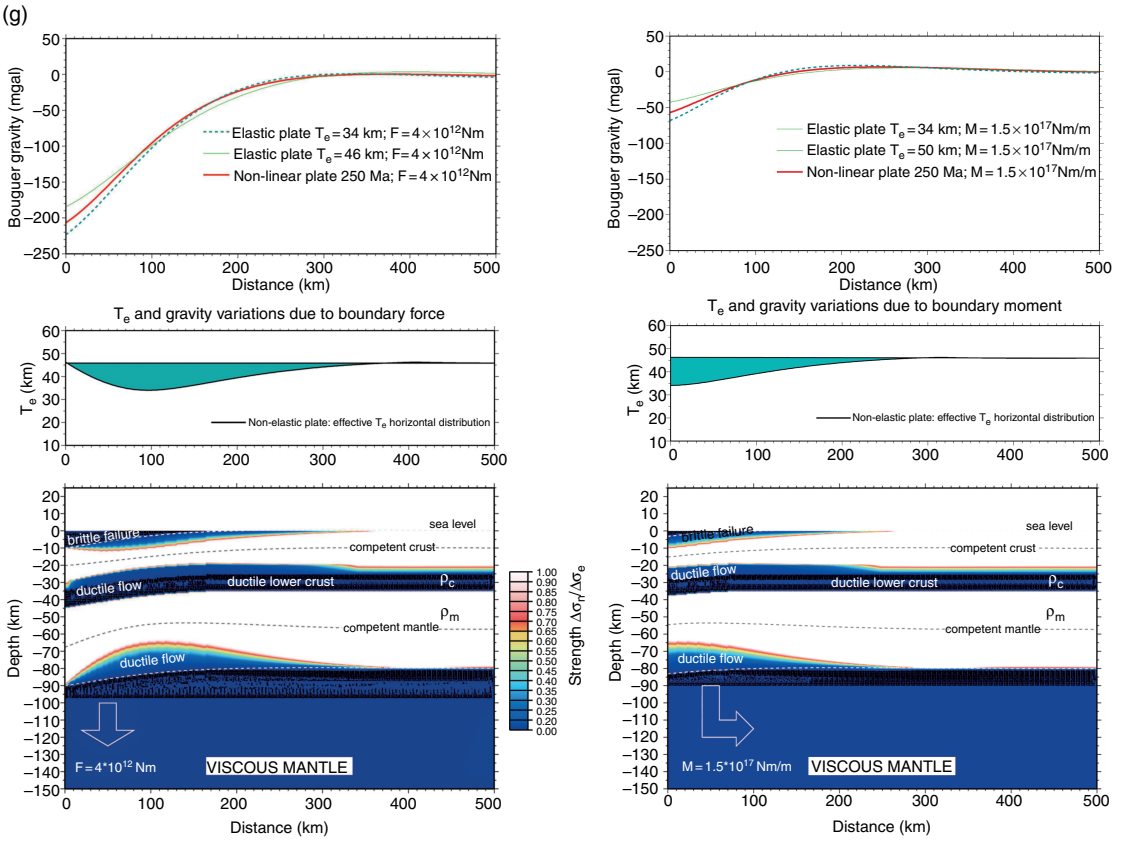

Figure 9 Predicted relationships between the rheology structure, age, plate curvature K, T_e, and, T_s for continental lithosphere. (a) Unified model of flexural strength of lithosphere, computed using equations of Appendix 1 and 2, for dry quartz upper crust, quartz–diorite lower crust, dry olivine mantle (**Tables 3** and **4**). Equilibrium thermal thickness, $a = 250$ km (Appendix 2). (b) Stress distribution within continental YSE for concave upward and concave downward flexure (see text). (c) Predicted dependence of continental T_e on age and curvature of the lithosphere, computed for normal crustal thickness, T_c, of 40 km and compared with the data for continental plates with normal crustal thickness. Right: geometry of corresponding YSEs (same composition as in **Figure 9(a)**). (d) T_e and T_s as function of curvature in a two-layer classical 'jelly-sandwich' plate (strong upper crust, weak lower and intermediate crust, strong mantle). (e) T_e and T_s as function of curvature in a three layer plate (strong upper crust, strong lower or intermediate crust, strong mantle). (f) Computed lateral strength (T_e) variations in continental lithosphere (strength envelope from **Figure 9(d)**) caused by surface loading (i.e., Gaussian mountain range 3 km height, Gaussian width 200 km), after (Burov and Diament, 1995). The color code corresponds to the ratio of the elastic stress for given amount of strain (elastic prediction) to the real stress value (inelastic correction). The zones characterized by stress ratio 1 are effectively elastic. The zones with smaller ratio correspond to inelastic deformation (= weakening), brittle or ductile. (g) Computed lateral strength (T_e) variations in continental lithosphere, loaded on the end (cutting force F, right, or flexural moment M, left (Burov and Diament, 1995). The color code corresponds to the ratio of the elastic stress for given amount of strain (elastic prediction) to the real stress value (inelastic correction). The zones characterized by stress ratio 1 are effectively elastic. The zones with smaller ratio correspond to inelastic deformation (= weakening), brittle or ductile.

more favorable background for activation of instable catastrophic sliding than geologically ductile rock. At seismic timescales all rock down to lower mantle behaves as an elastic or elastoplastic media. Any zones of mechanical weakness (fractures or ductile shear zones) may thus serve for nucleation of short-term brittle failure.

Figure 10 summarizes the data and the expected relationship between T_s and curvature for thermal ages of the continental lithosphere of 50, 500, and 1000 Ma. The circles show the maximum observed curvatures and, hence, the maximum likely value of T_s. In the de-coupled case, T_s does not exceed 15 km, which corresponds well with observations. Moreover, as for the oceans, T_e and T_s are more likely to anti-correlate than correlate. T_e always exceeds T_s, irrespective of thermal age and curvature. High T_e values limit the amount of curvature due to flexure and,

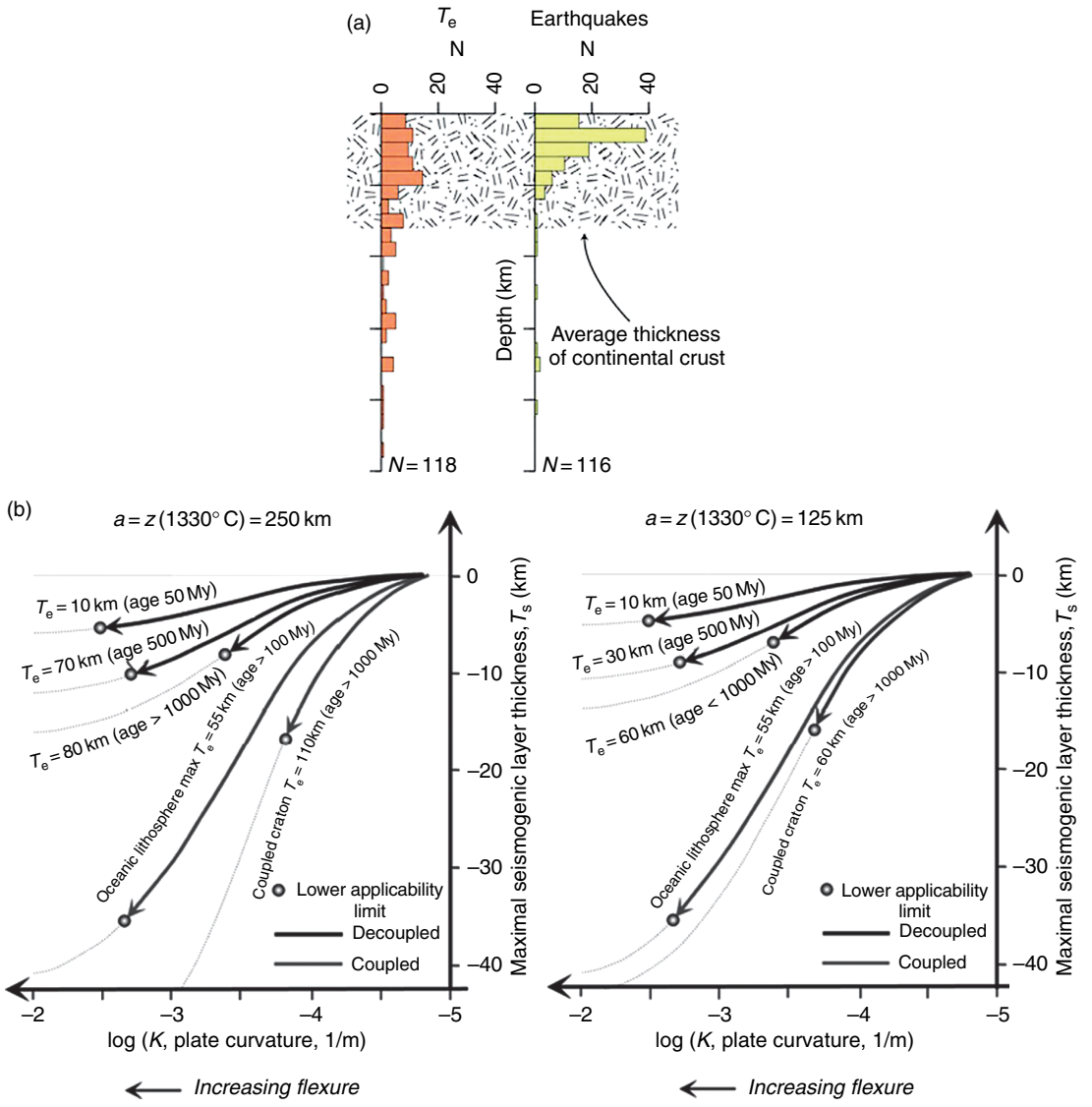

Figure 10 (a) Compilation of data on continental T_s compared with the data on T_e (based on (Watts and Burov, 2003)). (b) Relationships between the plate curvature, T_e and T_s for different ages of the lithosphere. Left: assumption of equilibrium thermal thickness of the lithosphere, $a = 250$ km. Right: $a = 125$ km. Black curves are for decoupled rheology, gray curves are for coupled rheology.

hence, the ratio of T_e to T_s increases with thermal age (and strength). The coupled case has the potential to yield higher values of T_s, but as T_e increases the curvature decreases. The ratio of T_e to T_s is therefore maintained. Interestingly, it is the oceanic lithosphere (**Figure 10**) that is associated with the highest values of T_s. The reason for this is that the oceanic crust is much thinner than its continental counterpart and Byerlee's friction law extends uninterrupted (by grace of the absence of weak zones such as ductile lower crust in continents) from the uppermost part of the crust into the underlying mantle.

Intraplate seismicity in continental areas is mainly located in the upper crust while it is often suggested that the lower crust or intermediate crust is too weak to deform in brittle regime (e.g. Chen and Molnar, 1983). A number of studies have indicated, however, the presence of seismic events in the lower crust as well as in the upper mantle (Shudofsky, 1985; Shudofsky *et al.*, 1987; Déverchére *et al.*, 1991; Cloetingh and Banda, 1992; Doser and Yarwood, 1994; Monsalve *et al.*, 2006). There is evidence from seismic reflection profiles that the continental Moho is sometimes offset by faults (Klemperer and Hobbs,

1991; Cloetingh and Banda, 1992; Burov and Molnar, 1998), although the significance of this observation is not entirely clear (*see* Chapter 6.11)

One of the explanations for little or absent mantle seismicity (Jackson, 2002) suggests that the mantle has low ductile strength and thus deforms in ductile regime at seismic timescale. This, we believe, is a confusion. Even if one admits that the mantle is fluid at geological timescale, it does not mean that it may flow at seismic timescale. Extrapolation of rock mechanics data (**Figure 2**) suggests that at seismic timescale, ductile creep cannot be activated within the lithospheric temperature–stress range: one needs temperatures higher than 1500–2000°C or stresses >1 GPa. On the other hand, there is little doubt that mantle is stronger than the asthenosphere, which viscosity is $\sim 5 \times 10^{19}$ Pa s for strain rate of $10^{-15}\,s^{-1}$. Recomputing flow stress for seismic timescale (eqn [14], strain rates of $10^{1}-10^{4}\,s^{-1}$) shows that even for such a 'weak' rheology, the yield stress must be on the order of 10–100 GPa, that is, 10 to 1000 times higher than any imaginable tectonic stress. This proves that the absence of seismicity cannot be regarded as a sign of 'weakness'. Finally, it should be kept in mind that seismicity is related to frictional release of elastic strain accumulated during the interseismic period (Scholtz, 1990). Hence, if one assumes that mantle is so weak that it prevents deep seismicity, then it should be characterized by Maxwell relaxation times on the timescale of postseismic rebound (from several seconds to 1 month). This would lead to an inconsistent conclusion that the lithosphere mantle is 3 orders of magnitude weaker ($\mu = 10^{16}$ Pa s) than the asthenosphere, where relaxation times are 100–1000 years.

The assumption of weak mantle rheology clearly does not hold in the areas where T_e is higher than crustal thickness ($T_e \sim 40$–110 km). For these areas the most obvious explanation for rare subcrustal seismicity is crust–mantle decoupling (**Figures 9–11**) and/or insufficient level of intraplate stress compared to high brittle strength due to strong confining pressure at Moho depth (Scholtz, 1990). According to Byerlee's law, the brittle rock strength, σ_b, scales as lithosptatic pressure, or $\sigma_b \approx 0.6\rho gz - 0.85\rho gz$. The level of intraplate stress is limited to several hundreds MPa. For stress level of 500 MPa, maximal seismic depth is 15 km. For exceptionally high stress levels of 1 GPa this depth extends to 30 km, that is still above normal Moho. In case of weak lower crust, transition of deviatoric stresses between crust and mantle is attenuated. Then, the mantle stress level is reduced, specifically in the case of bending. **Figure 9** shows, for example, that bending stresses may exceed ductile limits in the lower crust inducing flow and decoupling even in initially coupled system. The vertical gradient of bending stress can be calculated from the observed radius of plate flexure. Therefore, it is possible to predict the conditions for crustal or mantle seismicity from direct observations of flexure (Burov and Diament, 1992; Cloetingh and Burov, 1996). The horizontal far-field stresses that are detected, for example, in Europe (see Müller *et al.*, 1992), may also result in crust–mantle decoupling.

The rare cases of deep (lower crust or mantle) intraplate seismicity can be roughly classified as

1. zones of more or less homogeneous lower crustal seismicity (e.g., Albert rift, East Africa) (Shudofsky, 1985; Shudofsky *et al.*, 1987; Morley, 1989; Seno and Seito, 1994; Doser and Yarwood, 1994).
2. zones of localized seismicity, generally along deep faults (Baikal rift) (Déverchére *et al.*, 1991), Rhine Graben (Fuchs *et al.*, 1987; Brun *et al.*, 1991, 1992)).

Cases of deep seismicity are more frequent in extensional settings and more rare in collision settings. This confirms once again the idea that depth of seismicity is related to intraplate stress level. Indeed, the level of tectonic stresses is limited by available plate driving forces and by rock strength. One needs 2–3 times higher stress for brittle failure in compression than in tension (**Figure 1**), with or without fluid pressure. Under homogeneous compression, brittle rock strength, and thus stress needed to break the rock, may increase by a factor of 2, whereas under extension it may be reduced by a factor of 2 (Petrini and Podladchikov, 2000; **Figure 1**). Consequently for the same intraplate stress level, maximal seismic depth is 2–5 times more important for tension than for compression.

The differentiation between the zones of distributed and localized seismicity can be related to various conditions associated with seismogenic stress release:

1. *A more 'basic' composition* (Stephenson and Cloetingh, 1991; Cloetingh and Banda, 1992). In the areas where the lower crust has low temperature of creep activation (diabase, granulites, diorite, etc.), it may favor distributed cracking at depths corresponding to 300–400°C (20–35 km). There may be also instabilities caused by compositional differences in the lower crust.

2. *Variation of unstable-to-stable frictional slip on the deeply penetrating faults* (Tse and Rice, 1986). BDT refers to bulk rheological property, while the earthquakes are associated with frictional instabilities. Localized strain

rate acceleration along the faults may keep material brittle even at Moho depths (40–50 km). Deep mantle-penetrating faults are observed, for example, in the Northern Baikal rift (Déverchére *et al.*, 1993).

3. *Nonbrittle mechanisms of seismogenic stress release.* This may be referred, for example, to unstable phase changes, re-orientation of crystalline grids, and to few other mechanisms, which are subject of intensive discussions (Kirby *et al.* (1991); see also Govers *et al.* (1992) for a review). Partial or complete inapplicability of Byerlee's law at depths exceeding 40–50 km was outlined in a number of studies (e.g., Kirby *et al.*, 1991; Goetze and Evans, 1979).

6.03.6.4 Physical Considerations beyond the Observations of Flexure – Gravity Potential Theory

Simple physical considerations can be used to estimate minimal strength of the lithpospheric plates needed to support surface topography and tectonic loads, or to deform in accordance with the observed deformation styles. The tectonic forces are limited by the energy of plate driving motions and by lithospheric strength. The ratio of surface topography loads to horizontal tectonic forces (Argand number, *Ar*) indicates whether the mountain range is mechanically stable or it collapses under its own weight. The maximal short-term height, and thus weight of mountains, is limited by gravity forces and by brittle strength of surface rocks. The long-term height, and the amplitude of crustal roots, also depend on the long-term strength of the supporting crust and mantle. Based on these considerations, a number of authors (e.g., Artyushkov, 1973; Fleitout and Froidevaux, 1982; Dahlen, 1981; England and Houseman, 1989) have developed conceptually elegant models allowing to estimate the minimal average stress levels in the lithosphere. This approach is based on computation of intraplate gravity-driven stresses caused by horizontal variations in plate thickness and by density contrasts $\Delta\rho$. Isostatically compensated topography creates lateral pressure and potential energy misbalances that have to be balanced by horizontal tectonic stresses (σ_{xx}) to keep the topography at surface:

$$\int_0^{b_m} \Delta\rho g y \, dy = \int_0^{b_m} \sigma_{xx} \, dy = B_{min} \qquad [42]$$

This allows us to put lower bounds on the intergrated plate strength B_{min}. It was found that gravity-driven forces, and thus counterbalancing tectonic forces F and B_{min}, should vary from 10^{12} to 10^{13} N per unit length. Depending on plate thickness, this yields average intraplate stresses σ_{xx} of 10–100 MPa, on the order of values (yet smaller) obtained by Cloetingh and Wortel, 1986 from dynamic plate modeling.

6.03.6.5 Stability Theory – Rayleigh–Taylor Instabilities, or Survival of Cratons and Mountain Roots

The *crème-brûlée* and the alternative jelly-sandwich rheology model imply fundamental differences in the mechanical properties of mantle lithosphere. One can explore the stability of mantle lithosphere by posing the question "What do the different rheological models imply about the persistence of topography for long periods of geological time?" (Burov and Watts, 2006).

The mean heat flow in Archean cratons is $\sim$40 mW m^{-2}, which increases to $\sim$60 mW m^{-2} in flanking Phanerozoic orogenic belts (Jaupart and Mareschal, 1999). As Pinet *et al.* (1991) have shown, a significant part of this heat flow is derived from radiogenic sources in the crust. Therefore, temperatures at the Moho are relatively low ($\sim$400–600°C). The mantle must therefore maintain a fixed, relatively high, viscosity that prevents convective heat advection to the Moho. Otherwise, surface heat flow would increase to >150 mW m^{-2} which would be the case in an actively extending rift (e.g., Sclater *et al.*, 1980). Since such a high heat flow is not observed in cratons and orogens, a thick, cool, stable mantle layer should remain that prevents direct contact between the crustal part of the lithosphere and the convective upper mantle.

The negative buoyancy of the mantle lithosphere at subduction zones is widely considered as a major driving force in plate tectonics. The evidence that the continental mantle is $\sim$20 kg m^{-3} denser than the underlying asthenosphere and is gravitationally unstable has been reviewed by Stacey (1992), among others. Although this instability is commonly accepted for Phanerozoic lithosphere, there is still a debate about whether it applies to the presumably Mg-rich and depleted cratonic lithospheres. Irrespective of this, volumetric seismic velocities, which are generally considered a proxy for density, are systematically higher in the lithosphere mantle than in the asthenosphere. Depending on its viscosity the mantle lithosphere therefore has the potential to sink as a result of Rayleigh–Taylor (RT) instability (e.g. Houseman *et al.*, 1981; Buck and Toksöz, 1983).

One can estimate the instability growth time (i.e., the time it takes for a mantle root to be amplified by e times its initial value) using Chandrasekhar's (1961) formulation. In this formulation a mantle Newtonian fluid layer of viscosity μ, density ρ_m, and thickness d, is placed on top of a less-dense fluid asthenospheric layer of density ρ_a and the same thickness. (this formulation differs from that of Conrad and Molnar (1997) who used a fluid layer that is placed on top of a viscous half-space. However, both formulations are valid for instability amplitudes $<d$). The most rapidly growing instability wavelength λ, is Ad where $2.5 < A < 3.0$ and the corresponding growth time, $t_{\min}$, is $B\mu((\rho_m - \rho_a)gd)^{-1}$ where $6.2. < B < 13.0$ and g is the average gravity. One can evaluate $t_{\min}$ for a particular μ by assuming $(\rho_m - \rho_a) = 20\,\mathrm{kg\,m^{-3}}$ and $80 < d < 100\,\mathrm{km}$. If the continental mantle can support large stresses (>2 GPa) and has a high viscosity (10^{22}–10^{24} Pa s), as the jelly-sandwich model implies, then $t_{\min}$ will be long (>0.05–2 Ga), that is, comparable with age of cratons. If, on the other hand, the stresses are small (0–10 MPa) and the viscosity is low (10^{19}–10^{20} Pa s), as the *crème-brûlée* model suggests, then it will be short (0.2–2.0 My).

The consequence of these growth times for the persistence of surface topographic features and their compensating roots or anti-roots are profound. The long growth times implied by the jelly-sandwich model imply that orogenic belts, for example, could persist for up to several tens of million years and longer while the *crème-brûlée* model suggests collapse within a few million years.

We have considered so far a Newtonian viscosity and a large viscosity contrast between the lithosphere and asthenosphere. However, a temperature-dependent viscosity and power law rheology result in even shorter growth times than the ones derived here for constant viscosity (Conrad and Molnar, 1997; Molnar and Houseman, 2004). Moreover, if either the viscosity contrast is small or a mantle root starts to detach, then eqn [1] in Weinberg and Podladchikov (1995) suggests that the entire system will begin to collapse at a vertical Stokes flow velocity of $\sim$1 mm yr^{-1} for the jelly-sandwich model and $\sim$100–1000 mm y^{-1} for the *crème-brûlée* model. (note that these flow velocities depend strongly on the sphere diameter which is assumed here to be λ). Therefore, our assumptions imply that a surface topographic feature such as an orogenic belt would disappear in less than 0.02–2 My for the *crème-brûlée* model whereas it could be supported for as long as 100 My–2 Gyr for a jelly-sandwich model.

6.03.6.6 Dynamic Stability Analysis Using Direct Numerical Thermomechanical Models

In order to substantiate the growth times of convective instabilities derived from simple viscous models, and response of the lithosphere to horizontal shortening, Burov and Watts (2006) carried out sensitivity tests using a large-strain thermomechanical numerical model (FLAC-Para(o)voz v9) that allows the equations of mechanical equilibrium for a visco-elasto-plastic plate to be solved for *any* prescribed rheological strength profile (e.g., Cundall, 1989; Poliakov *et al.*, 1993). Similar models have been used by Toussaint *et al.* (2004), for example, to determine the role that the geotherm, lower crustal composition, and metamorphic changes in the subducting crust may play on the evolution of continental collision zones. Burov and Watts (2006) ran two separate series of tests (**Figures 12** and **13**) using rheological properties that matched cases with weak mantle rheology (*crème-brûlée*, **Figure 4**, left) and strong mantle rheology (jelly-sandwich, **Figure 4**, right), as well as some intermediate rheology profiles with weak or strong mantle. The goal of these experiments is to test what these and intermediate rheology models imply about the stability of mountain ranges and the structural styles that develop. The following sections show the results of stability tests and continental collision tests.

6.03.6.7 Experiments on Normal Loading (Topography), or Survival of Cratons and Mountain Roots

Figure 13 shows a snapshot of the deformation after 10 My in the experiments with normal (mountain) loading. The surface load is represented by a Gaussian-shaped mount, 3 km high, 200 km wide, of uniform density (2650 kg m^{-3}). As can be seen, for the *crème-brûlée* model the crust and mantle already become gravitationally and mechanically unstable after 1.5–2.0 My. By 10 My, the lithosphere disintegrates due to delamination of the mantle followed by its convective removal and replacement with hot asthenosphere. This leads to flattening of the Moho and tectonic erosion of the crustal root that initially supported the topography. The jelly-sandwich model, on the other hand, is stable and there are only few signs of crust and mantle instability for the duration of the model run (10 My).

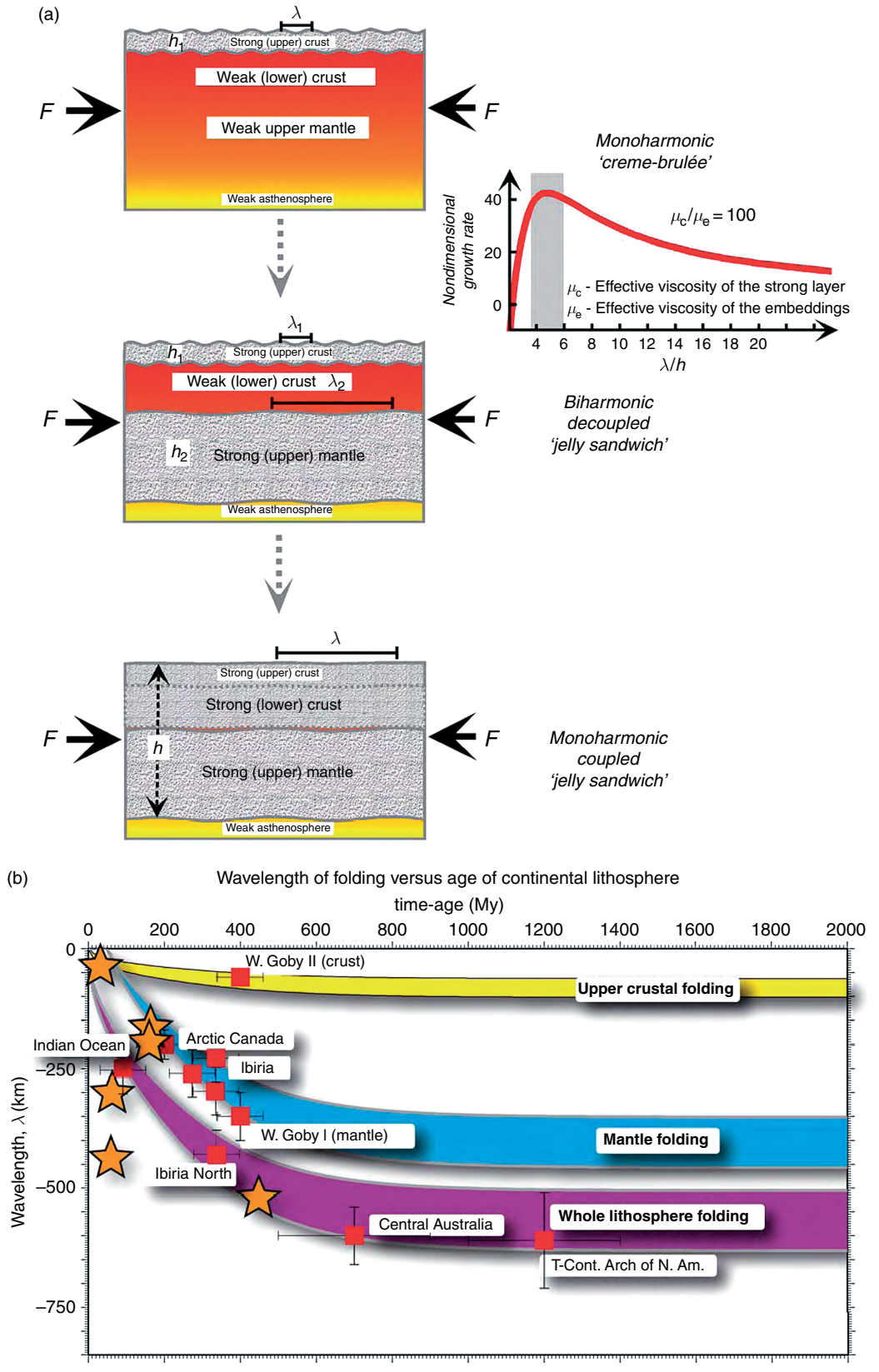

Figure 11 (*Continued*)

6.03.6.8 Experiments on Compressional Tectonic Loading (Subduction versus Collision)

Figure 14 shows the results of the collision tests for five different YSEs considered in Jackson (2002) and Mackwell *et al.* (1998) (see also **Figure 3**). **Figure 14(a)** shows a snapshot of the deformation after 300 km of shortening, which at 60 mm y^{-1} takes 5 My. The jelly-sandwich models (three upper cases) are stable and subduction occurs by the underthrusting of a continental slab that, with or without the crust, maintains its overall shape. In addition, the predicted deformation style in the accretion prism appears to be highly realistic (**Figures 14(b)** and **14(c)**; Burov and Yamato, 2006). The *crème-brûlée* models (two cases in the

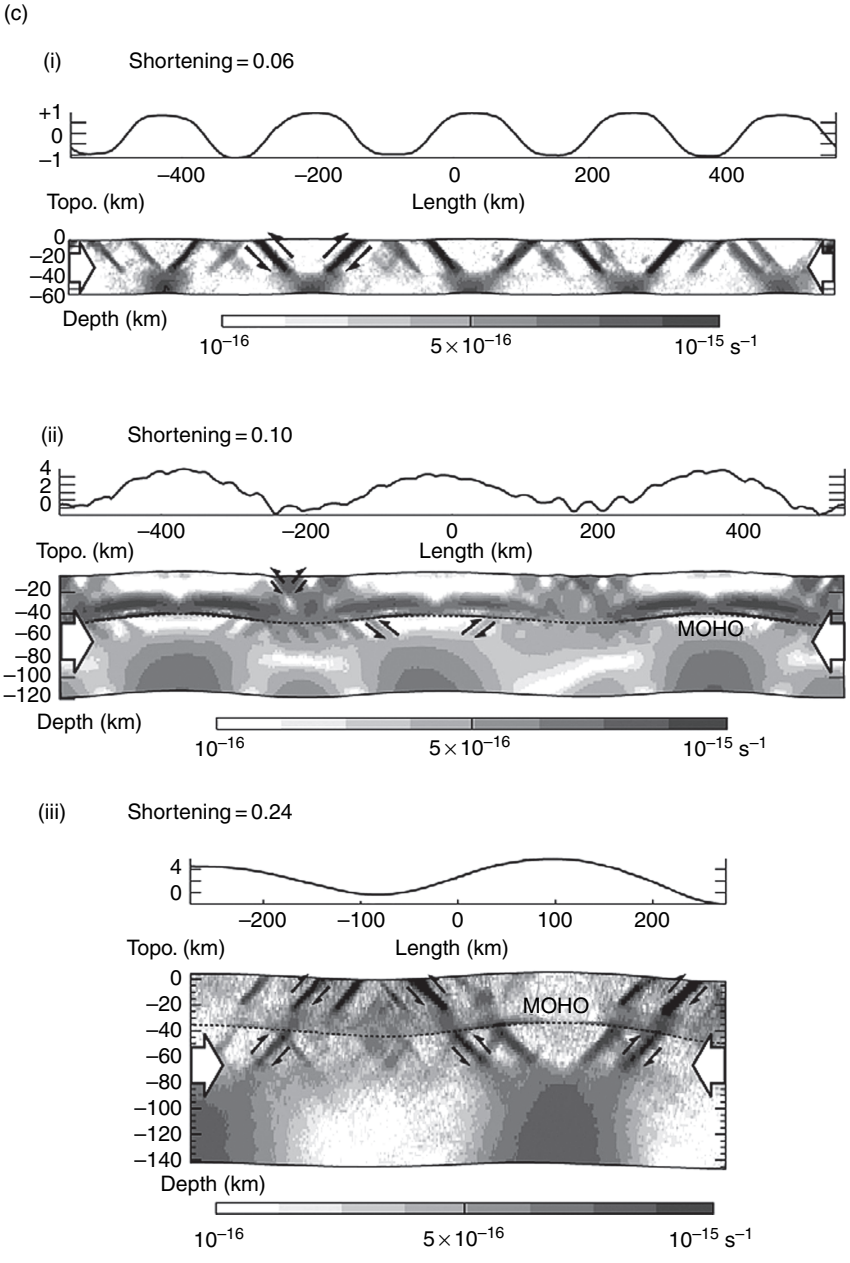

Figure 11 (*Continued*)

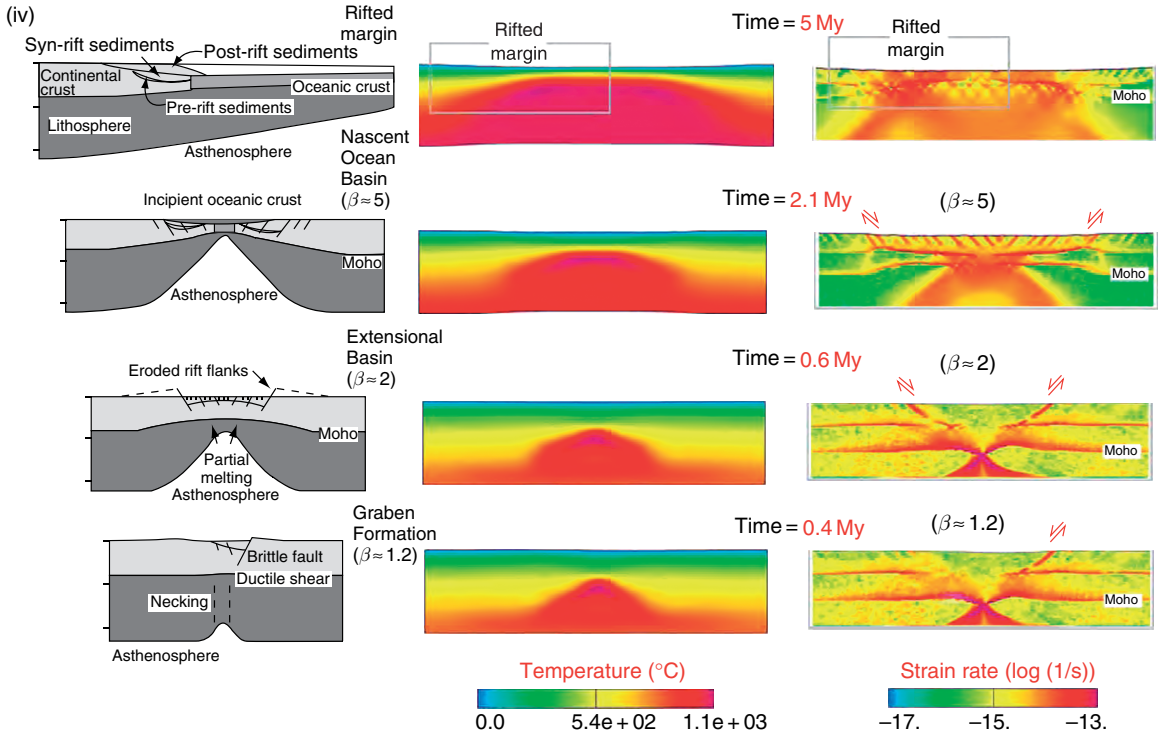

Figure 11 (a) Sketch of typical folding models for continental lithosphere (h_1 and h_2 are thicknesses of the competent crust and mantle, respectively). The system is submitted to compression by horizontal tectonic force F. In the case when the lower crust is weak ('*crème-brûlée*' rheology model), the upper crust may fold independently of the mantle part (wavelength λ_2), with a wavelength λ_1 (decoupled, or biharmonic folding), which corresponds to the 'jelly-sandwich' rheology model *senso stricto*). Very young (<150 Ma) and very old (>1000 Ma) lithospheres (single competent layer or coupled crust and mantle) develop monoharmonic folding. Note that we call 'jelly-sandwich' all rheological profiles that include both strong upper crust and mantle, thus the case of very old coupled lithosphere from the bottom of the Figure also corresponds to the 'jelly-sandwich' concept. Inset shows the analytical estimate for the growth rate of strongly non-Newtonian folding (coupled layers, non-Newtonian rheology) as a function of λ/h for a typical ratio of the effective viscosities of the competent layer and embeddings (100) (after Burov *et al.*, 1993)). Shaded rectangle shows the range of the dominating λ/h ratios (4–6). (b) The observed wavelength of folding (**Table 5**) as function of thermal age (calculated according to the model of Burov *et al.* (1993)). Numbers correspond to the ones used in the **Table 5**. Squares show the cases of 'regular' folding, whereas the stars mark 'irregular' cases (variable wavelengths, large amounts of shortening, important sedimentary loads, etc.). Different theoretical curves correspond to the crustal, mantle (supporting the presence of the decoupled rheology), and 'welded' folding. Modified from Cloetingh S, Burov E, and Poliakov A (1999) Lithosphere folding: primary response to compression? (from central Asia to Paris Basin). *Tectonics* 18: 1064-1083. (c) Topography and logarithm of strain rate field predicted from the direct numerical thermomechanical experiments on high-amplitude folding in brittle-elastic–ductile for oceanic lithosphere, in case 'i' ($T_e \sim 40$ km rheology profile 4 for 50–75 Ma in **Figure 7**(**a**)), and continental lithosphere in case 'ii' ($T_e \sim 60$ km, rheology profile 2 for 250 Ma in **Figure 7**(**a**)) and 'iii' ($T_e \sim 80$ km, rheology profile 2 for 750–1000 Ma in **Figure 7**(**a**)). All snapshots correspond to approximately 7 My since the onset of shortening (modified from (Gerbault *et al.*, 1999)). Cases 'ii' and 'iii' correspond to the 'jelly-sandwich' lithorheological structures from (a). The experiments confirm the ideas presented in (a) (e.g., biharmonic folding in case 'ii' with two different wavelengths developing together) and demonstrate the possibility of the development of large-scale folding despite concurrent intense brittle faulting. *De facto*, folding controls localization of brittle faults that tend to localize at the inflection points of folds. (d) Stable and unstable extension styles predicted from direct numerical elastic–viscous–plastic thermomechanical models (Burov and Poliakov, 2001), and compared with the typically observed extension styles. Application of common dry olivine flow laws for mantle lithosphere yields generally coherent results for predicted styles of rifting. Right: rifting styles as a function of the amount of extension (factor β) according to geological observations (Salvenson, 1978). Left: model predicted rifting styles (log strain rate) computed from elastic–viscous–plastic numerical model based on 'jelly-sandwich' rheology with strong upper crust (quartz) and upper mantle (olivine), after (Burov and Poliakov, 2001). The rheology profile used for thermomechanical modeling corresponds to 150–200 My profile 3 from **Figure 7**(**a**).

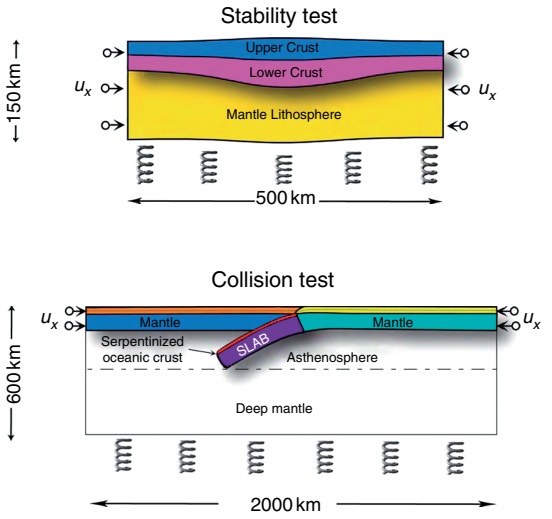

Figure 12 Setup of the numerical thermomechanical model aimed to study gravitational mechanical stability of the lithosphere (top) and evolution of continental collision (bottom). The numerical model is based on fully coupled thermomechanical large strain viscoelastoplastic numerical code Paro(a)voz v.9 based on the FLAC algorithm (Cundall, 1989). This code allows for explicit testing of ductile, brittle, and elastic rheology laws. The models assume a free upper surface and a hydrostatic boundary condition at the lower surface (depicted by springs in the figure). (a) The stability test was based on a mountain range of height 5 km and width 200 km that is initially in isostatic equilibrium with a zero-elevation 36 km thick crust. The isostatic balance has been disturbed by applying a horizontal compression to the edges of the lithosphere at a rate of 5 mm yr^{-1}. The displacements of both the surface topography and Moho were then tracked through time. (b) The collision test was based on a continent/continent collision initiated by subduction of a dense, downgoing, oceanic plate. Assumed a normal thickness oceanic crust is 7 km, a total convergence rate of 60 mm yr^{-1}, and a serpentinized subducted oceanic crust (Rupke *et al.*, 2002). Rheological properties and other parameters are as given in **Tables 2** and **3**.

bottom: one strong and another with weak lower crust), on the other hand, are unstable. There is no subduction, and convergence is taken up in the suture zone that separates the two plates. The *crème-brûlée* model is therefore unable to explain those features of collisional systems that require subduction such as kyanite and sillimanite grade metamorphism. The jelly-sandwich model, on the other hand, can explain not only the metamorphism and functioning of the fold-and-thrust structures (**Figures 14(b), 14(c)**, and **15**), but also some of the gross structural styles of collisional systems such as those associated with slab flattening (e.g., Western North America – Humphreys *et al.* (2003)), crustal doubling (e.g., Alps – Giese *et al.* (1982)), and arc subduction (e.g., southern Tibet – Boutelier *et al.* (2003)).

6.03.6.9 Stability Theory: Response to Large-Scale Compressional Instabilities (Folding)

Analysis of the record of recent vertical motions and the geometry of basin deflection for a number of sites worldwide suggests that lithospheric folding is a primary response of the lithosphere to recently induced compressional stresses (e.g., Burov *et al.*, 1993; Cloetingh *et al.*, 1999; *see* Chapter 6.11, **Table 5**, **Figure 11**). Despite the widespread opinion, it was shown (Cloetingh *et al.*, 1999; Gerbault *et al.*, 1999) that folding can persist over long periods of time (>10 Myr) independently of presence of in-homogeneities such as crustal faults (**Figure 11(c)**). The numerical experiments on brittle–elastic–ductile folding implemented in these studies show that formation of large-scale faults does not prevent folding. In turn, localization and spacing of the faults is controlled by the wavelength of folding (faults tend to localize at the inflection points of folds). As suggested on the base of analytical considerations (eqn [38], section on the oceanic folding), and confirmed by the numerical experiments, the characteristic wavelengths, λ, of small-amplitude folding are proportional to 5–10 × thickness of the competent layers and thus are indicative of the lithospheric strength:

$$\lambda < 5\text{–}10h \sim 5\text{–}10T_e \qquad [43]$$

These wavelengths are determined by the presence of young lithosphere in large parts of Europe or Central Asia or by that of old lithosphere in Canadian or Australian craton, as well as by the geometries of the sediment bodies acting as a load on the lithosphere in basins. The proximity of some of these sites to the areas of active tectonic compression suggests that the tectonically induced horizontal stresses are responsible for the large-scale warping of the continental lithosphere. The persistence of periodical undulations in Central Australia (700 Ma since onset of folding) or in the Paris basin (60 Ma) long after the end of the initial tectonic compression requires a strong rheology compatible with the effective elastic thickness values of about 100 km in the first case and 50–60 km in the second case (Cloetingh *et al.*,

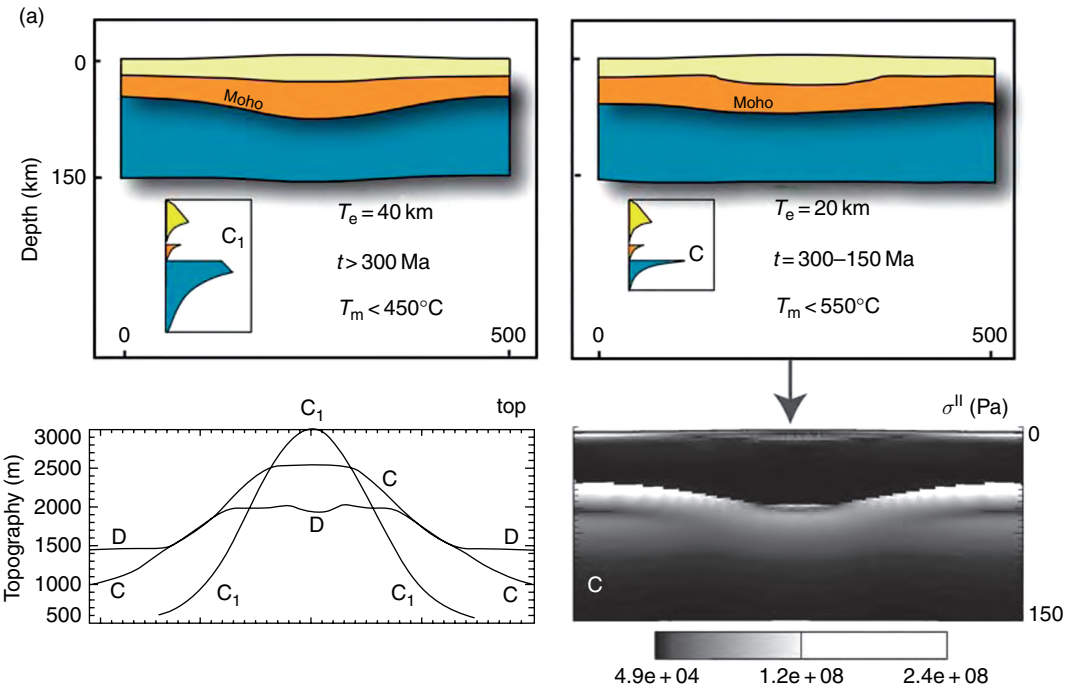

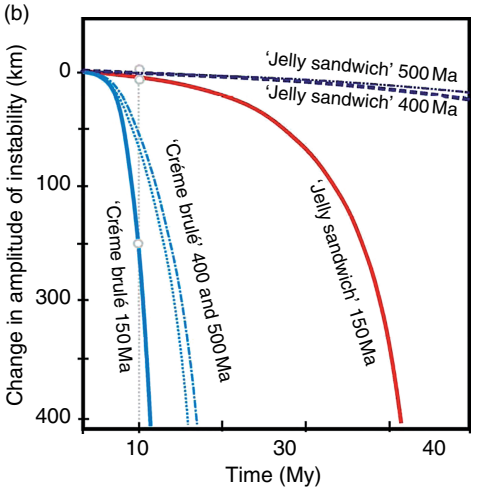

1999). **Figure 11** and **Table 5** show recent compilation of the observed wavelength of continental folding (Cloetingh *et al.*, 1999) compared to the predictions of analytical models (e.g., Burov *et al.*, 1993). In continental lithosphere, there may be several competent layers, which yield different folding wavelengths. In such cases, observed folding wavelengths allow one to separate between strong crustal and mantle layers. For example, in case of Central Asian lithosphere, two wavelengths are depictable: crustal (50–100 km) and mantle (300–350 km). These wavelengths suggest the existence of roughly 10-km-thick strong crustal 'core' and 30–50-km-thick strong mantle layer. In case of cratons (Central Australia), the folding wavelength reaches 600–700 km indicating a 60-km-thick competent layer. In both cases, thickness of strongest folded layer appears to be higher than the crustal thickness, confirming the idea that plates maintain considerable strength concentrated in their mantle part. The observations of folding suggest thicknesses of competent layers comparable with the corresponding T_e estimates (**Figures 7** and **8**). It is noteworthy, however, that there are some cases when λ/T_e ratios are abnormally high (>10) or low (<4). The high ratios mostly correspond to very weak lithospheres loaded by large amounts of sediment, which increases the wavelength of folding. The linear folding theory (eqns [38] or [43]) also do not apply in case of high amplitude-to-wavelength ratios (= basically small λ/T_e), because in this case, plastic hinging at the weakened inflection points results in transition from unstable to stable folding, for which the wavelength is a simple function of the amount of shortening and does not depend on h or T_e. Wavelength of folding may be additionally influenced by superposition of various geodynamic events, for example, post-compressional extension or mantle dynamics.

6.03.6.10 Extensional Tectonic Loading (Rifting)

A number of authors (e.g., Bassi, 1995; Huismans *et al.*, 2005; *see* Chapter 6.08) have studied possible rifting modes as a function of the rheological profile. The results show that narrow rifting mode is only possible in case of substantial mantle strength. If the lithosphere mantle is weak, the system switches to large rifting mode (e.g., Basin and Ranges) that may be characterized by periodic periodical instabilities such as boudinage. These models suggest that not only narrow rifting mode but also most other known rifting styles (except very wide delocalized rifts) require at least a 20–30-km-thick competent mantle layer. Application of common dry olivine flow laws in the direct numerical models of tectonic deformation yield generally coherent results for predicted rifting styles (**Figure 11(d)**). Certainly, strength in the mantle may not be always needed to get metamorphic core complexes developed. In this case, rather thick, weak lower crust may be required (Buck, 1988, 1991 *see* Chapter 6.08; Block and Royden, 1990). In this case it is suggested that the lack of a pronounced basin, associated with the large extension inferred for core complexes, may indicate that crust has flowed into the extending region. The crust in such cases would decouple the mantle from the surface so mantle strength would have very little effect on core complex development.

6.03.7 Relations between Short-Term and Long-Term Properties

6.03.7.1 Seismicity and Long-Term Deformation

Handy and Brun (2004) argue that seismicity is an ambiguous indicator of strength, that is, indicator of mechanical weakness of the relevant layer that is incapable to sustain tectonic or bending stress. The analytical and numerical models of previous sections

Figure 13 Thermomechanical numerical tests of the stability of a mountain range using the failure envelopes associated with the jelly-sandwich (figure 3(d), or figure 5(b) of Jackson (2002) and *crème-brûlée* (figures 3(b), 3(d), or figure 5(d) of Jackson (2002) rheology models. The thermal structure is equivalent to that of a 150 My-old plate. (a) Crustal and mantle structure after 10 My has elapsed. Middle of the figure shows surface topography evolution for rheologies C_1, C (jelly-sandwich), and D (*crème-brulée*), left, and effective shear stress distribution for the case C. Note rapid topography collapse in case D whereas cases C_1 and C are stable. (b) The amplitude of the mantle root instability as a function of time. The figure shows the evolution of a marker that was initially positioned at the base of the mechanical lithosphere (i.e., the depth where the strength = 10 MPa). This initial position is assumed to be at 0 km on the vertical plot axis. The sold and dashed lines show the instability for a weak, young (thermotectonic age = 150 My) and strong, old (thermotectonic age = 400 or 500 My old) plate respectively.

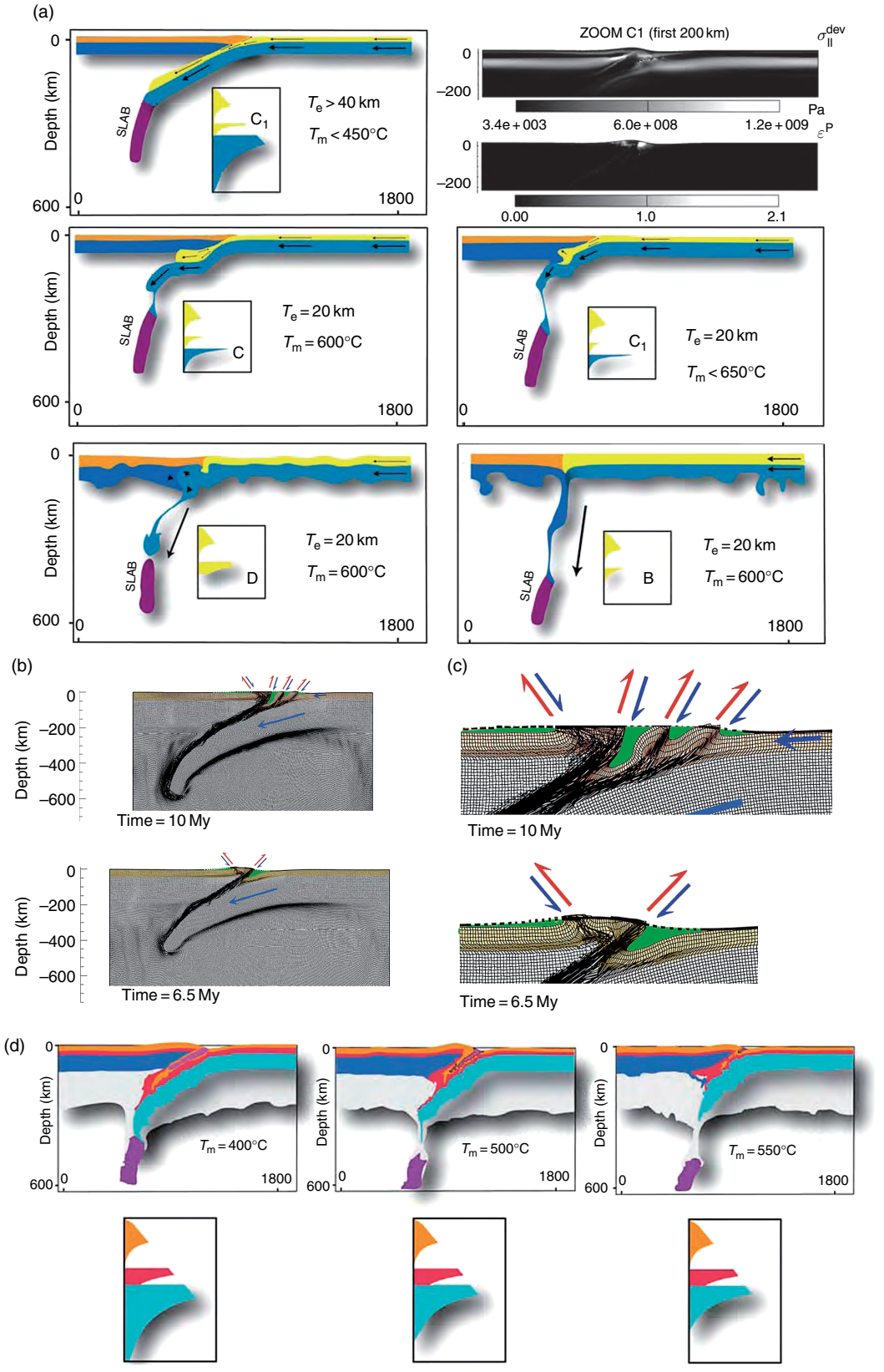

show that T_s is limited by current stress level (eqn [37]), and probably reflects the thickness of the uppermost weak brittle layers that respond on historical timescales to stresses by faulting and earthquakes. T_e, in contrast, reflects the integrated strength of the entire lithosphere that responds to long-term ($>10^5$ Ma) geological loads by flexure. A number of seismic tomography studies have also demonstrated that when compared with distribution of seismicity, tomography reveals that seisms are mainly limited by density or compositional boundaries, specifically those between the upper and lower crust. This may be related to stress drops caused by mechanical inconsistencies between these layers.

Seismic patterns do not allow for discrimination between the brittle and hypothetical nonbrittle (ductile) earthquakes. Although the practical absence of earthquakes beneath the seismic Moho remains enigmatic, the simplest explanation refers to the increase of the brittle strength with confining pressure depth. The other possible explanations for aseismic behavior of the mantle include stress relaxation due to crust/mantle decoupling; strengthening of the uppermost mantle due to downward bending (in downward bent rift basins); low or inhomogeneous horizontal intraplate stress. As shown in **Figure 9**, due to the typically thick continental crust and crust–mantle detachment, the bending stresses at the crust–mantle boundary are lower than the yielding strength, whereas the weight of the thickened crust increases the brittle strength of the mantle lithosphere.

From field observations it is argued (Handy and Brun, 2004) that earthquakes can be reasonably interpreted as a manifestation of a transient mechanical instability within shear zones. According to observations of outcropping fault surfaces, most shear zones have very specific rheological properties that distinguish them from normal rocks. In particular, in these zones, ductile melonytic creep is punctuated by ephemeral high-stress events involving fracture, frictional melting, and episodic local loss of cohesion.

6.03.7.2 Postseismic Relaxation Data and Long-Term Deformation

A number of studies interpret postseismic relaxation data in terms of the long-term viscosity of crust or mantle (e.g., DallaVia *et al.*, 2005; Pollitz *et al.*, 2001; Sabadini and Vermeersen, 2004). Most of these studies yield 'subsurface' viscosities of 5×10^{16} to 2×10^{19} Pa s. These values are generally smaller than the values of the asthenosphere visocosity derived from postglacial rebound data but considerably higher (eight orders of magnitude) than predictions of rock mechanics for seismic timescale (**Figure 2**). They are also three to six orders of magnitude lower than what can be inferred for long-term deformation from the data of rock mechanics, except some quartz-dominated lower crustal compositions. We conclude that these viscosity values are either not indicative of the long-term behavior, or are indicative of highly nonlinear behavior, which yields disproportionally small viscosities at high deformation rates. Since the postseismic deformation rates vary strongly with time, the effective viscosities should also vary in a broad range. Consequently, the notion of effective postseismic viscosity is rather senseless. The alternative

Figure 14 (a) Numerical tests of the stability of a continental collisional system using various possible failure envelopes (**Figures 3**(**b**) and **3**(**d**)). The figure shows a snapshot at 5 My of the structural styles that develop after 300 km of shortening. Insert to right of case C_1 shows zoom of first 200 km in depth, with the effective shear stress (top) and plastic brittle strain (bottom). Note that despite high mantle strength, no brittle (seismic) deformation occurs below Moho depth except subduction channel. (b) Deformation of the passive marker grid highlighting multiple thrust-and-fold structures forming at different stages of continental subduction, for the experiment corresponding to the rheology profile 'C1' from **Figure 14**(**a**). Formation of such structures requires a relatively low strength of the near-Moho zone in the lower crust (possibility of crust–mantle decoupling) and a strong mantle as a sliding surface. This explains the eventual complexity of some of the resulting *P-T-t* paths. For the sake of space, the image is cut horizontally at 650 km depth (the bottom is not shown). Green colour corresponds to sedimentary depots. (c) Zoom to the central part of **Figure 14**(**b**) (Burov and Yamato, 2006). Purple color corresponds to the created sedimentary matter, orange color marks the upper crustal material, red color marks the lower crustal material. The gradation of the scale bar is 50 km. (d) Experiments of **Figures 14**(**a**) (profile C_1), **14**(**b**) and **14**(**c**) repeated for the case of strong dry diabase lower crust (quartz–diabase–dry olivine rheology) at 5.5 My. Moho temperatures are respectively 400°C, 500°C, and 550°C. All other parameters and details are exactly the same as in the experiments from the **Figure 14**. Note important buckling of the plates imposed by the presence of strong diabase crust that results in mechanical coupling between the plates. Purple color corresponds to the sedimentary matter or to the oceanic slab, orange color marks the upper crustal material, red color marks lower crustal material. Blue (dark or light) color marks mantle lithosphere; grey color marks the asthenosphere.

explanation of the values of postseismic viscosity refers to interpretation in terms of primary Burger's viscosity (eqn [30]) that might be related to effective strain-rate-dependent deformation due to postseismic equilibration of fluid pressure in seismically modified fracture networks. In this case, these data are most probably not related to the long-term behavior.

6.03.7.3 Field Observations and Geophysical Data

Geophysical transects of plate margins and structural studies of exhumed fault rocks generally validate the rheology laws derived from experimental rock mechanics (Handy and Burn, 2004) assuming 'jelly-sandwich' parameters. Seismically observed crustal and mantle lithosphere structures largely evoke cases of ductile lower crust and stronger mantle lithosphere. In particular, this refers to the geophysical traverses NFP20 and ECORS-CROP across the Alps (Frei *et al*., 1990; ECORS-CROP group, 1989; Kissling and Spakman, 1996) and DEKORP-ECORS across the Rhine Graben (Meissner and Bortfeld, 1990; Brun *et al*., 1991, 1992). The Alpine part of the transects shows that the lower crust of the Apulian plate is detached from its underlying mantle and forms a north-tapering wedge between the downgoing European lithosphere and partly exhumed nappe edifice of the Alpine orogen (Handy and Burn, 2004). Burov *et al.* (1999) have previously studied the mechanical stability of this structure to find that high mantle resistance compatible with 30-km-thick competent mantle lithosphere layer is required to ensure its stability. Similar considerations concerning the presence of strong mantle can be driven out from seismic cross-sections of Rhine Graben, and those across the Altyn-Tagh fault system (Wittlinger *et al*., 1998) and Ferghana basin (Central Asia, (Burov and Molnar, 1998)), accross the Abitibi-Wawa belts and Kapuskasing uplift system in the Canadian craton (LITHOPROBE). In case of the Altyn-Tagh fault system, oblique convergence of the bounding plates is accommodated by the Altyn-Tagh strike-slip and thrust system indicating that the lithospheric mantle was displaced along the fault as a rigid media. The remarkable direct evidence of the high mantle strength refers to the Kapuskasing uplift (Burov *et al*., 1998). The Kapuskasing structural zone cuts structures of the Superior Province in the Canadian Shield: the Abitibi-Wawa granite–greenstone belts to the south and Quetico-Opatica metasedimentary belts to the north. The geophysical and seismic transect LITHOPROBE reveals enormous volumes of dense granulates thrust upward along the ancient Kapuskasing thrust fault that was active about 2700 My ago. Despite the weight of the granulite body, which exceeds that of an 'average' mountain belt, Moho boundary shows a very little depression with amplitude of a few kilometers, which requires T_e of 100 km and viscosities $>10^{24}$ Pa s. It was concluded that independently of crustal strength, mantle part of the lithosphere of the Canadian craton should include a strong layer of a minimal thickness of 60 km, and thus rheology corresponding to strongest of the dry olivine rheologies (**Table2**). This conclusion has been drawn (Burov *et al*., 1998) from the results of direct thermomechanical numerical experiments testing the mechanical stability of the Kapuskasing structure for a wide spectra of rheology laws. It is also noted that in the collision zones (e.g., Himalaya), the lower crust is practically never exposed to the surface. Since the lower crust is lighter than the mantle, the simplest explanation would be that it is dragged down by the downgoing mantle lithosphere, which requires high mantle strength.

6.03.8 Conclusions and Future Perspectives

Although the rheology laws based on data of rock mechanics may be partly representative for long-term and large-scale deformation, they need validation and re-parametrization for geological temporal and spatial scales. This particularly refers to crustal flow laws, due to the diversity of the mineralogical composition of the continental crust (Burov, 2002). Long-term rheological properties can be scaled on the basis of the observations of long-term/large-scale deformation such as reaction of the lithosphere to known geological loads (flexure, collision–subduction, folding, boudinage, rifting), tectonic deformation styles, seismic and geodetic data, postglacial rebound data, etc. The laboratory data should serve as a 'first guess' for construction of long-term rheological models. Parametrization of these data requires better constraints on some major structural parameters such as equilibrium thermal thickness of continents, $a = z(1330°C)$, and density contrasts between the lithospheric mantle and asthenosphere.

The data on the equivalent elastic thickness (T_e) and other large-scale data confirm that the rheology of the oceanic lithosphere is in acceptable agreement with rock-mechanics data for dislocation creep in dry olivine. For continents, rock-mechanics data are largely compatible with the observation that T_e varies from 0 to 10 km in young plates to 110–120 km in cratons. If $T_e > T_c$, the strongest rheological layer refers to the mantle and fits dry olivine rheology. If $T_e < T_c$ the strength is likely to be shared between crust and mantle. 'Jelly-sandwich' (decoupled) or 'dried jelly-sandwich' (coupled) rheology models appear to be most applicable for continents. The data and models suggest that for equivalent conditions, the integrated strength of continental mantle does not significantly differ from that of the oceanic lithosphere. After the thermal structure, the second major source for the diversity of the mechanical behavior of continental plates refers to the diverse structure and rheology of their crusts. Depending on the crustal strength and thickness, continents may be either stronger or weaker than the oceanic plates. 'Weak or moderate' continental plate strength ($T_e < 1–1.5\,T_c$) refers to the cases of 'generalized jelly-sandwich' rheology with ductile lower or intermediate crust (most orogenic belts and some cratons, plateaux, most post-rift basins). Strong 'dried jelly-sandwich' applies to old cratons ($T_e = 1.5–2.5\,T_c$) where the lower crust is strong and thus crust and mantle are mechanically coupled. '*crème-brulée*' rheology ($T_e < T_c$, strong crust–weak mantle) is extremely weak and may apply only for young or rejuvenated lithospheres or some active rift zones (e.g., Salton Sea, southern California; and Taupo volcanic zone, north island New Zealand).

The primary question related to the interpretation of the T_s data would be "why there is little or no microseismicity below 40–50 km depth, both in the oceans and continents?". The T_s data, we believe, are indicative of the limited tectonic stress level in the lithosphere and of small brittle strength of its upper layers compared to that of the deeper mantle. T_s is not a proxy for the integrated strength of the lithosphere or T_e. T_s rather anticorrelates with T_e if intraplate force $F < B$ (integrated plate strength). If $F = B$, the entire plate is in the yield state and T_e has no sense while T_s equals BDT depth. The only possible relation between T_s and T_e refers to the influence of T_e on the mean intraplate stress level: increasing T_e decreases the average stress and thus T_s. For a given value of tectonic force $F < B$, T_s decreases with increasing T_e. In most cases, simple consideration suggests, as a rule of thumb, $T_s \leq \Upsilon(F/T_e + \sigma^f_{xx})/\rho g \leq \frac{1}{2}T_e$ (eqn [37]). The only possibility for $T_s = T_e$ refers to nearly broken plates having equally strong brittle and ductile parts (e.g., rifting). This invalidates the proposition that plate strength is concentrated in the brittle part, except nearly broken plates.

The cross-compatibility of estimates of continental plate strength obtained from the observations of (1) flexure (for T_e values coming from the models accounting for all surface and subsurface loads), (2) folding, (3) mechanical stability models, and (4) field and indirect geophysical data, confirm YSE profiles derived for dry olivine and (with more reservations) granite upper crust. This applies to YSE profiles based on plate cooling model for 200–250 km thick lithosphere.

There is almost certainly no one type of strength profile that characterizes all continental lithosphere. It was shown that jelly-sandwich rheology models (and their variants that include strong mantle and various crustal structures) are mechanically compatible with long-term support of tectonic loads and major structural styles (e.g., **Figures 14** and **15**), whereas *crème-brûlée models*, or any models with weak mantle, are mechanically unstable. Thermomechanical modeling of lithospheric deformation suggests that the persistence of surface topographic features and their compensating roots require that the subcrustal mantle is strong and able to act as both a stress guide and a support for surface loads. It might be thought that it would not matter which competent layer in the lithosphere is the strong one. However, the models show that the density contrast between the crust and mantle is sufficient to ensure that it is the mantle, rather than the crust, which provides both the stress guide and support. In our view, subduction, orogenesis, or narrow to normal rifting require a strong mantle layer. We have found this to be true irrespective of the actual strength of the crust. Weak mantle is mechanically unstable and tends to delaminate from the overlying crust because it is unable to resist forces of tectonic origin. Once it does delaminate, hotter and lighter mantle asthenosphere can flow upward to the Moho. The resulting increase in Moho temperature would lead to extensive partial melting and magmatic activity as well as further weakening (e.g., Karato, 1986) such that, for example, subduction is inhibited and surface topography collapses in a relatively short interval of time.

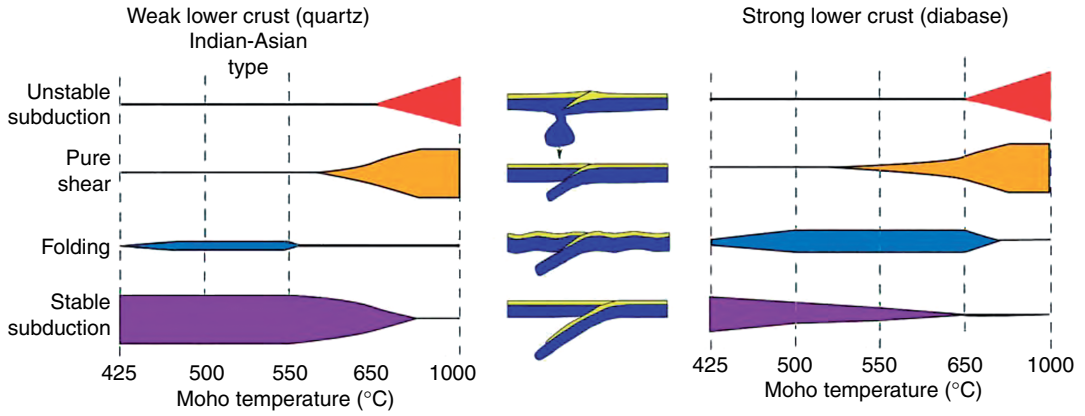

Figure 15 Comparison of shortening styles of continental lithosphere in case of weak lower crust (*right*) and strong dry diabase lower crust (left, rheology profile from **Figure 3(b)**). As also shown in **Figure 14(d)**, strong lower crust promotes largescale folding instead of subduction. Similarly to **Figure 14(a)**, Moho temperature characterizes the geotherm and thus the rheology profile.

Acknowledgment

This study was partly funded by Dyeti (INSU-CNRS) program.

Appendix 1: Flexure of Continental Lithosphere with Multilayered Nonlinear Rheology

The rheology-independent form of 2-D plate-bending equation is

$$-\frac{\partial^2 M_x}{\partial x^2}+\frac{\partial}{\partial x}\left(F_x\frac{\partial w}{\partial x}\right)+p_-=p_+ \qquad [44]$$

$$M=-\int_{h_m}\sigma_{xx}y\,\mathrm{d}y$$

where M_x is bending moment h_m is the total thickness of the plate, F_x is horizontal fiber force, w is the vertical deflection of the plate (bathymetry, geometry of Moho), p_- and p_+ are negative and positive normal loads, respectively. The equivalent elastic thickness T_e of a plate with arbitrary rheology (yet compatible with static bending) is

$$M=-D\frac{\partial^2 w}{\partial x^2}=-E\frac{T_e^3}{12(1-v^2)}\frac{\partial^2 w}{\partial x^2}$$

or [45]

$$T_e=\sqrt[3]{-M\frac{12(1-v^2)}{E}\left(\frac{\partial^2 w}{\partial x^2}\right)^{-1}}=\sqrt[3]{MK^{-1}G}$$

where E and v are the assumed elastic parameters, K is plate curvature, and $G=12(1-v^2)E^{-1}$.

For a single-layer plate (e.g., oceanic lithosphere, $T_e\le h_m$) composed of n mechanically coupled rheological layers of thickness h_i, $i=1,\ldots,n$:

$$T_e\approx h_1+h_2+\cdots=\sum_n h_i \qquad [46]$$

For a lithosphere composed of n mechanically decoupled layers

$$T_e\approx(h_1^3+h_2^3+\cdots)=\sqrt[3]{\sum_n h_i^3}<\sum_n h_i \qquad [47]$$

In case of equally thick decoupled layers ($h_1\approx h_2\approx h_3\ldots=h$), $T_e\approx n^{1/3}h$ instead of $T_e=nh$ for a coupled plate [46]. Layer decoupling thus reduces T_e by a factor of $n^{2/3}$, that is, by 40–50% for $n<4$. The effective rigidity $D(x, w''\ldots)$ of a plate with nonlinear rheology can be estimated as

$$D(\phi)\frac{\partial^2 w(x)}{\partial x^2}\approx -D(\phi)R_{xy}^{-1}=-M_x(\phi) \qquad [48]$$

Accordingly, $T_e=T_e(x, w'',\ldots)$ of such a plate is

$$T_e=\left(\frac{D(\phi)}{D_0}\right)^{1/3}=\left(-\frac{M_x(\phi)R_{xy}}{D_0}\right)^{1/3}\approx\left(\frac{M_x(\phi)}{D_0}\left(\frac{\partial^2 w(x)}{\partial x^2}\right)^{-1}\right)^{1/3} \qquad [49]$$

where $D_0=E(12(1-v^2))^{-1}$, $\phi=(x, w''\cdots)$. R_{xy} is local radius of bending $R_{xy}\approx-(w'')^{-1}=K^{-1}$. For a multilayer plate composed of $i=1,\ldots,n$ lithological layers with $j=1,\ldots,m_i$ rheological

zones (brittle, elastic, ductile, etc.) per each layer, D and T_e can be obtained from the following system:

$$\begin{cases} \dfrac{\partial^2}{\partial x^2}\overbrace{\left(D_0 T_e^3(\phi)\underbrace{\dfrac{\partial^2 w(x)}{\partial x^2}}_{K}\right)}^{M_x(\phi)} + \dfrac{\partial}{\partial x}\left(F_x(\phi)\dfrac{\partial w(x)}{\partial x}\right) \\ \qquad + p_-(\phi)w(x) = p_+(x) \\ T_e(\phi) = \left(\dfrac{M_x(\phi)}{D_0}\left(\dfrac{\partial^2 w(x)}{\partial x^2}\right)^{-1}\right)^{1/3} \\ M_x(\phi) = -\sum_{i=1}^{n}\sum_{j=1}^{m_i}\int_{z_{ij}^-(\phi)}^{z_{ij}^+(\phi)} \sigma_{xx}^{(j)}(\phi) z_i^*(\phi)\,\mathrm{d}z \\ F_x(\phi) = -\sum_{i=1}^{n}\sum_{j=1}^{m_i}\int_{z_{ij}^-(\phi)}^{z_{ij}^+(\phi)} \sigma_{xx}^{(j)}(\phi)\,\mathrm{d}z \end{cases} \quad [50]$$

The boundaries of the rheological zones z_{ij} are not predefined *a priori* but are computed, using an iterative procedure, as function of ϕ. Mechanical decoupling of rheological layers has three major consequences:

1. up to 50% reduction of the flexural resistance, T_e;
2. maintenance of high resistance to cutting loads;
3. T_e is mainly controlled by thickness of the strongest layer.

Appendix 2: Thermal Model of the Continental Lithosphere

The thermal structure of multilayer continental lithosphere is estimated using a half-space cooling model that incorporates radiogenic heat sources in the crust:

$$\begin{cases} \dot{T} - \chi_{c1}\Delta T = \chi_{c1}\rho_{c1}H_s k_{c1}^{-1} e^{-z b_r^{-1}}, & 0 \le z \le h_{c1} \\ \dot{T} - \chi_{c2}\Delta T = H_{c2} C_{c2}^{-1}, & h_{c1} \le z \le T \\ \dot{T} - \chi_m \Delta T = 0, & T_c \le z \le a \end{cases} \quad [51]$$

where the over-dot means differentiation with respect to time. h_{c1} is thickness of the upper crust, T_c is total crustal thickness (see **Table 4** for other parameters). The boundary and initial conditions are
$T(0, t) = 0$ (surface temperature)
$T(a, t) = T_m = 1350°C$ ($a \approx 250$ km is the depth to the thermal bottom, or 'equilibrium thermal thickness')
$T(z, 0) = T_m$ (homogeneous temperature distribution at the beginning).

The solution of the system (B1) is obtained under assumption of heat flux and temperature continuity across the upper and lower crust and mantle lithosphere.

References

Afonso JC and Ranalli G (2004) Crustal and mantle strengths in continental lithosphere: Is the jelly sandwich model obsolete? *Tectonophysics* 394: 221–232.

Artyushkov EV (1973) Stresses in the lithosphere caused by crustal thickness inhomogeneities. *Journal of Geophysical Research* 78: 7675–7708.

Ashby MF and Verall RA (1978) Micromechanisms of flow and fracture, and their relevance to the rheology of the upper mantle. *Philosophical Transactions of the Royal Society of London* 288: 59–95.

Austrheim H and Boundy T (1994) Pseudotachylytes generated during seismic faulting and eclogitization of the deep crust. *Science* 265: 82–83.

Barrell J (1914) The strength of the Earth's crust. Part I: Geologic tests of the limits of strength. *Journal of Geology* 22: 28–48.

Bassi G (1995) Relative importance of strain rate and rheology for the mode of continental extension. *Geophysical Journal International* 122: 195–210.

Bayer R, Carozzo MT, Lanza R, Miletto M, and Rey D (1989) Gravity modelling along the ECORS-CROP vertical seismic reflection profile through the Western Alps. *Tectonophysics* 162: 203–218.

Block L and Royden LH (1990) Core complex geometries and regional scale flow in the lower crust. *Tectonics* 9: 557–567.

Bills BG, Currey D, and Marshall GA (1994) Viscosity estimates for the crust and upper mantle from patterns of lacustrine shoreline deformation in the Eastern Great Basin. *Journal of Geophysical Research* 99(B11): 22059–22086.

Biot MA (1961) Theory of folding of stratified viscoelastic media and its implications in tectonics and orogenesis. *Geological Society of America Bulletin* 72: 1595–1620.

Bird P (1991) Lateral extrusion of lower crust from under high topography in the isostatic limit. *Journal of Geophysical Research* 96: 10275–10286.

Bos B and Spiers CJ (2002) Frictional-viscous flow in phyllosilicate-bearing fault rock: Microphysical model and implications for crustal strength profiles. *Journal of Geophysical Research* 107(B2): 2028 (doi:10.1029/2001JB000301).

Bott MHP (1993) Modelling the plate-driving mechanism. *Journal of the Geological Society of London* 150: 941–951.

Boutelier D, Chemenda A, and Burg J-P (2003) Subduction versus accretion of intra-oceanic volcanic arcs: Insight from thermo-mechanical analogue experiments. *Earth and Planetery Science Letters* 212: 31–45.

Brace WF and Kohlstedt DL (1980) Limits on lithospheric stress imposed by laboratory experiments. *Journal of Geophysical Research* 85: 6248–6252.

Brun J-P (2002) Deformation of the continental lithosphere: Insights from brittle-ductile models. In: De Meer S, Drury MR, De Bresser JHP, and Pennock GM (eds.) *Special Publication-Geological Society London, 200: Deformation Mechanisms, Rheology and Tectonics: Current Status and Future Perspectives*, pp. 355–370. London: Geological Society Publishing House.

Brun J-P, Gutscher MA, and DEKORP-ECORS teams (1992) Deep crustal structure of the Rhine Graben from DEKORP-ECORS seismic reflection data: A summary. *Tectonophysics* 208: 139–147.

Brun J-P, Wenzel F, and the ECORS-DEKORP Team (1991) Crustal structure of the southern Rhine Graben from ECORS-DEKORP seismic reflection data. *Geology* 19: 758–762.

Buck WR (1991) Modes of continental extension. *Journal of Geophysical Research* 96: 20161–20178.

Buck WR (1988) Flexural rotation of normal faults. *Tectonics* 7: 959–973.

Buck WR and Toksöz MN (1983) Thermal effects of continental collisions: Thickening a variable viscosity lithosphere. *Tectonophysics* 100: 53–69.

Burov E (2002) The upper crust is softer than dry quartzite. *Tectonophysics* 361: 321–326.

Burov EB and Diament M (1992) Flexure of the continental lithosphere with multilayered rheology. *Geophysical Journal International* 109: 449–468.

Burov EB and Diament M (1995) The effective elastic thickness (T_e) of continental lithosphere : What does it really mean? *Journal of Geophysical Research* 100: 3895–3904.

Burov EB and Diament M (1996) Isostasy, effective elastic thickness (EET) and inelastic rheology of continents and oceans. *Geology* 24: 419–423.

Burov EB and Guillou-Frottier L (1999) Thermo-mechanical behaviour of large ash-flow calderas. *Journal of Geophysical Research* 104: 23081–23109.

Burov EB, Kogan MG, Lyon-Caen H, and Molnar P (1990) Gravity anomalies, the deep structure, and dynamic processes beneath the Tien Shan. *Earth and Planetary Science Letters* 96: 367–383.

Burov EB, Lobkovsky LI, Cloetingh S, and Nikishin AM (1993) Continental lithosphere folding in Central Asia. Part 2: constraints from gravity and topography. *Tectonophysics* 226: 73–87.

Burov EB, Mareschal J-C, and Jaupart C (1998) Large scale crustal inhomogeneities and lithospheric strength in cratons. *Earth and Planetary Science Letters* 164: 205–219.

Burov EB and Molnar P (1998) Gravity anomalies over the Ferghana Valley (central Asia) and intracontinental deformation. *Journal of Geophysical Research* 103: 18137–18152.

Burov E, Podladchikov Y, Grandjean G, and Burg J-P (1999) Validation of multidisciplinary data using thermo-mechanical modelling: Application to the Western and Nothern Alps. *Terra Nova* 11: 124–131.

Burov EB and Poliakov ANB (2001) Erosion and rheology controls on synrift and postrift evolution: Verifying old and new ideas using a fully coupled numerical model. *Journal of Geophysical Research* 106: 16461–16481.

Burov E and Watts AB (2006) The long-term strength of continental lithosphere: 'Jelly-sandwich' or 'crème-brûlée'? *GSA Today* 16: 4–10.

Burov E and Yamato P (2006) Continental plate collision, P-T-t-z conditions and unstable vs. stable plate dynamics : Insights from thermo-mechanical modelling ''*Lithos*'' Special Volume on Exhumation Processes.

Byerlee JD (1978) Friction of rocks. *Pure and Applied Geophysics* 116: 615–626.

Caristan Y (1982) The transition from high temperature creep to fracture in Marylanddiabase. *Journal of Geophysical Research* 87: 6781–6790.

Carter NL and Tsenn MC (1987) Flow properties of continental lithosphere. *Tectonophysics* 136: 27–63.

Chandrasekhar S (1961) *Hydrodynamic and Hydromagnetic Stability* 704 pp. Oxford: Oxford University Press.

Chapman Y (1986) Thermal gradient in the continental crust. In: Dawson JB, Carswell DA, Hall J, and Wedepohl KH (eds.) *Special Publication Geological Society of London, 24: The Nature of the Continental Crust*, pp. 63–70. Oxford: Blackwell.

Chen W-P and Molnar P (1983) Focal depths of intracontinental and intraplate earthquakes and their implications for the thermal and mechanical properties of the lithosphere. *Journal of Geophysical Research* 88: 4183–4214.

Chester FM (1988) The brittle-ductile transition in a deformation mechanism-map for halite. *Tectonophysics* 154: 125–136.

Chester FM (1995) A rheologic model for wet crust applied to strike-slip faults. *Journal of Geophysical Research* 100(B7): 13033–13044.

Chopra PN and Paterson MS (1981) The experimental deformation of dunite. *Tectonophysics* 78: 453–473.

Chopra PN and Paterson MS (1984) The role of water in the deformation of dunite. *Journal of Geophysical Research* 89: 7861–7876.

Cloetingh S and Wortel R (1986) Stress in the Indo-Australian plate. *Tectonophysics* 132: 49–67.

Cloetingh S and Banda E (1992) Europe's lithosphere – physical properties. Mechanical structure. In: Blundell D, Freeman R, and Mueller S (eds.) *A Continent Revealed: The European Geotraverse*, pp. 80–91. Cambridge, New York: Cambridge University Press.

Cloetingh S and Burov EB (1996) Thermomechanical structure of the European continental lithosphere: Constraints from rheological profiles and EET estimates. *Geophysical Journal International* 124: 695–723.

Cloetingh S, Burov E, and Poliakov A (1999) Lithosphere folding: Primary response to compression ? (from central Asia to Paris Basin). *Tectonics* 18: 1064–1083.

Cochran JR (1980) Some remarks on isostasy and the long-term behavior of the continental lithosphere. *Earth and Planetary Science Letters* 46: 766–2711.

Conrad CP and Molnar P (1997) The growth of Rayleigh–Taylor-type instabilities in the lithosphere for various rheological and density structures. *Geophysical Journal International* 129: 95–112.

Cundall PA (1989) Numerical experiments on localization in frictional materials. *Ingenieur-Archiv* 59: 148–159.

Dahlen FA (1981) Isostasy and the ambient state of stress in the oceanic lithosphere. *Journal of Geophysical Research* 86: 7801–7807.

DallaVia G, Sabadini R, DeNatale G, and Pingue F (2005) Lithospheric rheology in southern Italy inferred from postseismic viscoelastic relaxation following the 1980 Irpinia earthquake. *Journal of Geophysical Research* 110: B06311 (doi:10.1029/2004JB003539).

De Mets C, Gordon RG, Argus DF, and Stein S (1990) Current plate motions. *Geophysical Journal International* 101: 425–478.

Déverchére J, Houdry F, Diament M, Solonenko NV, and Solonenko AV (1991) Evidence for a seismogenic upper mantle and lower crust in the Baikal rift. *Geophysical Research Letters* 18(6): 1099–1102.

Déverchére J, Houdry F, Solonenko NV, Solonenko AV, and Sankov VA (1993) Seismicity, active faults and stress field of the North Muya Region, Baikal Rift: New insights on the rheology of extended continental lithosphere. *Journal of Geophysical Research* 98: 19895–19912.

Doser D and Yarwood DR (1994) Deep crustal earthquakes associated with continental rifts. *Tectonophysics* 229: 123–131.

ECORS-CROP (1989) Deep seismic sounding group. A new picture of the Moho under the western Alps. *Nature* 337: 249–251.

England P and Molnar P (1997) Active deformation of Asia: From kinematics to dynamics. *Science* 278: 647–650.

England PC and Molnar P (2005) Late quaternary to decadal velocity fields in Asia. *Journal of Geophysical Research* 110: B12401 (doi:10.1029/2004JB003541).

England P and Richardson SW (1980) Erosion and age dependence of continental heat flow. *Geophysical Journal of the Royal Astronomical Society* 62: 421–437.

England PC and Houseman GA (1989) Extension during continental convergence, with application to the Tibetan Plateau. *Journal of Geophysical Research* 94: 17561–17579.

Evans B and Goetze C (1979) The temperature variation of hardness of olivine and its implication for polycrystalline yield stress. *Journal of Geophysical Research* 84: 5505–5524.

Evans B and Kohlstedt DL (1995) Rheology of rocks. In: Ahrens TJ (ed.) *AGU Reference Shelf 1: Rock Physics and Phase Relations: A Handbook of Physical Constants*, pp. 149–165. Washington, DC: AGU.

Fleitout L and Froidevaux C (1983) Tectonic stresses in the lithosphere. *Tectonics* 3: 315–324.

Forsyth DW (1985) Subsurface loading and estimates of the flexural rigidity of continental lithosphere. *Journal of Geophysical Research* 90: 12623–12632.

Frei W, Heitzmann P, and Lehner P (1990) Swiss NFP20 research program of the deep structure of the Alps. *Mémoires de la Société Géologique de France* 156: 29–46.

Fuchs K, Bonjer K-P, Gajewski D, *et al.* (1987) Crustal evolution of the Rhinegraben area. Part I: Exploring the lower crust in the Rhinegraben rift by unified geophysical experiments. *Tectonophysics* 141: 261–275.

Gerbault M, Burov EB, Poliakov A, and Dagnieres M (1999) Do faults trigger folding in the lithosphere ? *Geophysical Research Letters* 26(2): 271–274.

Giese P, Nicolich R, and Reutter K-J (1982) Explosion crustal seismic studies in the Alpine-Mediterranean region and their implications to tectonic processes. In: Berckhemer H and Hsu KJ (eds.) *Alpine-Mediterranean Geodynamics*, pp. 347–376. Washington, DC: American Geophysical Union.

Gleason GC and Tullis J (1995) A flow law for dislocation creep of quartz aggregates determined with the molten salt cell. *Tectonophysics* 247: 1–23.

Gratier J, Guiguet R, Renard F, and Jenatto L (2006) Experimental pressure solution creep of quartz by indenter technique. *Eos Transactions of American Geophysical Union, Fall Meeting Supplement* 87(52): T23D-0525.

Goetze C and Evans B (1979) Stress and temperature in bending lithosphere as constrained by experimental rock mechanics. *Geophysical Journal of the Royal Astronomical Society* 59: 463–478.

Govers R, Wortel MJR, Cloetingh SAPL, and Stein CA (1992) Stress magnitude estimates from earthquakes in oceanic plate interiors. *Journal of Geophysical Research* 97: 11749–11759.

Handy MR and Brun JP (2004) Seismicity, structure and strength of the continental lithosphere. *Earth and PlanetaryScience Letters* 223: 427–441.

Hirth G and Kohlstedt DL (1996) Water in the oceanic upper mantle: Implications for rheology, melt extraction and the evolution of the lithosphere. *Earth and Planetary Science Letters* 144: 93–108.

Houseman GA, McKenzie DP, and Molnar P (1981) Convective instability of a thickened boundary layer and its relevance for the thermal evolution of continental convergent belts. *Journal of Geophysical Research* 86: 6135–6155.

Humphreys ED, Hessler E, Dueker K, Farmer GL, Erslov E, and Atwater T (2003) How Laramide-age hydration of North American lithosphere by the Farallon slab controlled subsequent activity. *International Geology Review* 45: 575–595.

Huismans RS, Buiter S, and Beaumont C (2005) Effect of plastic-viscous layering and strain softening on mode selection during lithospheric extension. *Journal of Geophysical Research* 110: B02406 (doi:10.1029/2004JB003114).

Hull D and Bacon DJ (1984) *Introduction to Dislocations* 3rd edn. 255 pp. Oxford: Pergamon Press.

Jackson J (2002) Strength of the continental lithosphere: Time to abandon the jelly sandwich? *GSA Today* 12: 410.

Jaeger JC and Cook NGW (1976) *Fundamentals of Rock Mechanics* 2nd edn. 585 pp. New York: Chapman and Hall.

Jaupart C and Mareschal JC (1999) The thermal structure and thickness of continental roots. *Lithos* 48: 93–114.

Ji S, Wirth R, Rybacki E, and Jiang Z (2000) High-temperature plastic deformation of quartz-plagioclase multilayers by layer-normal compression. *Journal of Geophysical Research* 105(B7): 16651–16664.

Jolivet L, Faccenna C, Goffé B, *et al.* (1998) Mid-crustal shear zones in post-orogenic extension: The northern Tyrrhenian Sea case. *Journal of Geophysical Research* 103: 12123–12160.

Jordan TA and Watts AB (2005) Gravity anomalies, flexure and the elastic thickness structure of the India-Eurasia collisional system. *Earth and Planetary Science Letters* 236: 732–750.

Judge A and McNutt MK (1991) The relationship between plate dip and elastic plate thickness: A study of the Peru-Chile Trench. *Journal of Geophysical Research* 96: 16625–16639.

Karato S (1986) Does partial melting reduce the creep strength of the upper mantle? *Nature* 319: 309–310.

Karato S (1998) Effects of pressure on plastic deformation of polycrystalline solids: Some geological applications. *Materials Research Society Symposium Proceedings* 499: 3–14.

Karato S-I, Paterson MS, and FitzGerald JD (1986) Rheology of synthetic olivine aggregates: Influence of the grain size and water. *Journal of Geophysical Research* 91: 8151–8176.

Katayama I, Karato S-I, and Brandon M (2005) Evidence for high water content in the deep upper mantle inferred from deformation microstructures. *Geology* 33(7): 613–616.

Kirby SH (1983) Rheology of the lithosphere. *Reviews of Geophysics* 21: 1458–1487.

Kirby SH and Kronenberg AK (1987) Rheology of the lithosphere: Selected topics. *Review of Geophysics* 25: 1219–1244 (correction 1680–1681).

Kirby SH, Durham W, and Stern L (1991) Mantle phase changes and deep-earthquake faulting in subducting lithosphere. *Science* 252: 216–225.

Kirby SH, Stein EA, Okal EA, and Rubie DC (1996) Metastable mantle phase transformations and deep earthquakes in subducting oceanic lithosphere. *Reviews of Geophysics* 34: 261–306.

Kissling E and Spakman W (1996) Interpretation of tomographic images of uppermost mantle structure: Examples from the Western and Central Alps. *Journal of Geodynamics* 21: 97–111.

Klemperer S and Hobbs R (1991) *The BIRPS Atlas*, 124 pp. Cambridge: Cambridge University Press.

Kachanov LM (1971) *Foundations of the Theory of Plasticity*, 324 pp. Amsterdam: North-Holland Publications.

Kohlstedt DL, Evans B, and Mackwell SJ (1995) Strength of the lithosphere: Constraints imposed by laboratory experiments. *Journal of Geophysical Research* 100: 17587–17602.

Kruse S and Royden L (1994) Bending and unbending of an elastic lithosphere: The Cenozoic history of the Apennine and Dinaride fordeep basins. *Tectonics* 13: 278–302.

Kusznir NJ (1991) The distribution of stress with depth in the lithosphere: Thermo-rheological and geodynamic constraints. *Philosophical Transactions of the Royal Society of London* A337: 95–110.

Kusznir NJ and Matthews DH (1988) Deep seismic reflections and the deformational mechanics of the continental lithosphere. *Journal of Petrology* 10: 63–87.

Kusznir NL and Park RG (1986) Continental lithosphere strength: The critical role of lower crustal deformation. In: Dawson JB, Carswell DA, Hall J, and Wedepohl KH (eds.) *Special Publication-Geological Society, 24,: The Nature of the Lower Continental Crust, 79–94*. Oxford: Blackwell.

Lanchenbruch AH and Morgan P (1990) Continental extension, magmatism and elevation; formal relations and rules of thumb. *Tectonophysics* 174: 39–62.

Lambeck K (1983) Structure and evolution of intracratonic basins in central Australia. *Geophysical Journal of the Royal Astronomical Society* 74: 843–886.

Lavier LL, Buck WR, and Poliakov ANB (2000) Factors controlling normal fault offset in ideal brittle layer. *Journal of Geophysical Research* 105: 23431–23442.

Le Pichon X, Francheteau J, and Bonnin J (1973) *Plate Tectonics*, 300 pp. Amsetrdam: Elsevier Scientific, 1973.

Le Pourhiet L, Burov E, and Moretti I (2004) Rifting through a stack of inhomogeneous thrusts (the dipping pie concept). *Tectonics* 23(4): TC4005 (doi:10.1029/2003TC001584).

Lobkovsky LI and Kerchman VI (1992) A two-level concept of plate tectonics: Application to geodynamics. *Tectonophysics* 199: 343–374.

Lokhner DA (1995) Rock failure. In: Ahrens TJ (ed.) *AGU Reference Shelf 1: Rock Physics and Phase Relations: A Handbook of Physical Constants, 127–147*. Washington, DC: AGU.

Lowry AR and Smith RB (1994) Flexural rigidity of the basin and range-Colorado Plateau-Rocky Mountain transition from coherence analysis of gravity and topography. *Journal of Geophysical Research* 99: 20123–20140.

Mackwell SJ, Zimmerman ME, and Kohlstedt DL (1998) High-temperature deformation of dry diabase with applications to tectonics on Venus. *Journal of Geophysical Research* 103: 975–984.

Maggi A, Jackson JA, Priestley K, and Baker C (2000) A re-assessment of focal depth distributions in southern Iran, the Tien Shan and northern India: Do earthquakes occur in the continental mantle ? *Geophysical Journal International* 143: 629–661.

McAdoo DC, Martin CF, and Polouse S (1985) Seasat observations of flexure: Evidence for a strong lithosphere. *Tectonophysics* 116: 209–222.

McKenzie DP and Fairhead D (1997) Estimates of the effective elastic thickness of the continental lithosphere from Bouguer and free-air gravity anomalies. *Journal of Geophysical Research* 102: 27523–27552.

McNutt MK and Menard HW (1982) Constraints on yield strength in the oceanic lithosphere derived from observations of flexure. *Geophysical Journal of the Royal Astronomical Society* 71: 363–395.

Meissner R and Bortfeld RK (eds.) (1990) *DEKORP-Atlas, Results of Deutsches Kontinentales Reflexionsseismisches Programm,* (18p and 80 plates). New York: Springer Verlag.

Melosh HJ (1990) Mechanical basis for low-angle normal faulting in the basin and range province. *Nature* 343: 331–335.

Molnar P and Houseman GA (2004) The effects of bouyant crust on the gravitational instability of thickened mantle lithosphere at zones of intracontinental convergence. *Geophysical Journal International* 158: 1134–1150.

Molnar P and Lyon-Caen H (1988) Some simple physical aspects of the support, structure, and evolution of mountain belts. *Geological Society of America, Special Paper* 218: 179–207.

Molnar P and Tapponnier P (1981) A possible dependence of the tectonic strength on the age of the crust in Asia. *Earth and Planetary Science Letters* 52: 107–114.

Monsalve G, Sheehan A, Schulte-Pelkum V, Rajaure S, Pandey MR, and Wu F (2006) Seismicity and one-dimensional velocity structure of the Himalayan collision zone: Earthquakes in the crust and upper mantle. *Journal of Geophysical Research* 111: (doi:10.1029/2005JB004062).

Montesi LGJ (2004) Controls of shear zone rheology and tectonic loading on post seismic creep. *Journal of Geophysical Research* 109: B10404 (doi:10.1029/2003JB002925).

Morley CK (1989) Extension, detachments, and sedimentation in continental rifts (with particular reference to East Africa). *Tectonics* 8: 1175–1192.

Müller B, Zoback ML, Fuchs K, *et al.* (1992) Regional patterns of stress in Europe. *Journal of Geophysical Research* 97: 11783–11803.

Nadai A (1963) *Theory of Flow and Fracture of Solids,* vol. 2, 705 pp. New York: McGraw-Hill.

O'Reilly SY and O'Reilly WL (1996) 4-D lithosphere mapping; methodology and examples. *Tectonophysics* 262: 1–18.

Parsons BE and Sclater JG (1977) An analysis of the variation of ocean floor bathymetry and heat flow with age. *Journal of Geophysical Research* 82: 803–827.

Passey QP (1981) Upper mantle viscosity derived from the difference in rebound of the Provo and Bonneville shorelines, Lake Bonneville basin. *Journal of Geophysical Research* 86: 11701–11708.

Peltier WR (1974) The impulse response of a Maxwell Earth. *Reviews of Geophysics and Space Physics* 12: 649–669.

Peltier WR and Andrews JT (1976) Glacial-isostatic adjustment. PartI: The forward problem. *Geophysical Journal of the Royal Astronomical Society* 46: 605–646.

Pérez-Gussinyé M and Watts AB (2005) The long-term strength of Europe and its implications for plate-forming processes. *Nature* 436: (doi:10.1038/nature03854).

Petrini K and Podladchikov Y (2000) Lithospheric pressure-depth relationship in compressive regions of thickened crust. *Journal of Metamorphic Geology* 18: 67–78.

Pinet C, Jaupart C, Mareschal J-C, Gariepy C, Bienfait G, and Lapointe R (1991) Heat flow and lithospheric structure of the Eastern Canadian shield. *Journal of Geophysical Research* 96: 19923–19941.

Price NJ and Cosgrove JW (1990) *Analysis of Geological Structures*. New York: CambridgeUniversity Press.

Poirier JP (1985) *Creep of Crystals*, 260 pp. New York: Cambridge University Press.

Poliakov ANB, Cundall P, Podladchikov Y, and Laykhovsky V (1993) An explicit inertial method for the simulation of visco-elastic flow: An evaluation of elastic effects on diapiric flow in two- or three-layers models. In: Stone DB and Runcorn SK (eds.) *Dynamic Modelling and Flow in the Earth and Planets Series: Flow and Creep in the Solar System: Observations, Modelling and Theory*, pp. 175–195. Norwell, MA: Kluwer.

Pollitz FF, Wicks C, and Thatcher W (2001) Mantle flow beneath a continental strike-slip fault: Postseismic deformation after the 1999 Hector Mine earthquake. *Science* 293: 1814–1818.

Ranally G and Murphy D (1987) Geological stratification of the lithosphere. *Tectonophysics* 132: 281–295.

Ranalli G (1995) *Rheology of the Earth* 2nd edn. 413 pp. London: Chapman and Hall.

Regenauer-Lieb K, Yuen DA, and Branlund J (2001) The initiation of subduction: Criticality by addition of water? *Science* 294(5542): 578–580.

Rice JR and Tse ST (1986) Dynamic motion of a single degree of freedom system following a rate and state dependent friction law. *Journal of Geophysical Research* 91: 521–530.

Rupke LH, Morgan JP, Hort M, and Connolly JAD (2002) Are the regional variations in Central American arc lavas due to

differing basaltic versus peridotitic slab sources of fluids? *Geology* 30: 1035–1038.
Rutter EH and Brodie KH (1991) Lithosphere rheology – a note of caution. *Journal of Structural Geology* 13: 363–367.
Sabadini R and Vermeersen LLA (2004) *Modern Approaches Geophysics, 30: Global Dynamics of the Earth: Applications of Normal Mode Relaxation Theory to Solid-Earth Geophysics*. New York: Springer.
Salveson JO (1978) Variations in the geology of rift basins: A tectonic model, *Conference Proceedings of the Los Alamos National Laboratory*, 7487, pp. 82–86, Los Alamos, New Mexico.
Scholtz CH (1990) Mechanics of faulting. *Annual Review of Earth and Planetary Sciences* 17: 309–334.
Sclater JG, Jaupart C, and Galson D (1980) The heat flow through oceanic and continental crust and the heat loss of the Earth. *Journal of Geophysical Research* 18: 269–311.
Seno T and Seito A (1994) Recent east African earthquakes in the lower crust. *Earth and Planetary Science Letters* 121: 125–135.
Shelton G and Tullis JA (1981) Experimental flow laws for crustal rocks. *Transactions Of the American Geophysical Union* 62: 396.
Shudofsky GN (1985) Source mechanisms and focal depths of east African earthquakes using Rayleigh-wave inversion and bodywave modelling. *Geophysical Journal of the Royal Astronomical Society* 83: 563–614.
Shudofsky GN, Cloetingh S, Stein S, and Wortel R (1987) Unusually deep earthquakes in east Africa: Constraints on the thermo-mechanical structure of a continental rift system. *Geophysical Research Letters* 14(7): 741–744.
Sibson RH (1992) Transient discontinuities in ductile shear zones. *Journal of Structural Geology* 2: 165–171.
Stacey FD (1992) *Physics of the Earth*, 513 pp. Brisbane: Brookfield Press.
Stephenson RA and Cloetingh S (1991) Some examples and mechanical aspects of continental lithospheric folding. *Tectonophysics* 188: 27–37.
Tirel C, Brun J-P, and Burov E (2004) Thermo-mechanical modeling of extensional gneiss dome. In: Whitney DL, Teyssier C, and Siddoway CS (eds.) *Geological Society of America Special Paper , 380: Gneiss Domes and Orogeny*, pp. 67–78. Boulder, CO: Geological Society of America.
Toussaint G, Burov E, and Jolivet L (2004) Continental plate collision: Unstable vs. stable slab dynamics. *Geology* 32: 33–36.
Tse ST and Rice JR (1986) Crustal earthquake instability in relation to the depth variation of friction slip properties. *Journal of Geophysical Research* 91: 9452–9472.
Turcotte DL and Schubert G (2002) *Geodynamics* 2 nd edn. 456 pp. New York: Cambridge University Press.
Van Hunen J, Zhong S, Shapiro N, and Ritzwoller HR (2005) New evidence for dislocation creep from 3-D geodynamic modelling of the Pacific upper mantle structure. *Earth and Planetary Science Letters* 238: 146–155.
Vermeer PA (1990) The orientation of shear bands in biaxial tests. *Géotechnique* 40(2): 223–236.
Vermeer PA and de Borst R (1984) *Heron, vol. 29(3): Non-Associated Plasticity for Soils, Concrete and Rocks,* pp. 1–75. Rijswijk, The Netherlands: Stevin-laboratory of Civil Engineering, University of Technology, Delft Institute TNO for Building Materials and Building Structures.
Walcott RI (1970) Isostatic response to loading of the crust in Canada. *Canadean Journal of Earth Sciences* 7: 716–727.
Watts AB (1978) An analysis of isostasy in the world's oceans. Part 1: Hawaiian-emperor seamount chain. *Journal of Geophysical Research* 83: 5989–6004.
Watts AB (1992) The elastic thickness of the lithosphere and the evolution of sedimentary basins. *Basin Research* 4: 169–178.
Watts AB (2001) *Isostasy and Flexure of the Lithosphere*, 458 pp. Cambridge, NY: Cambridge University Press.
Watts AB and Burov E (2003) Lithospheric strength and its relationship to the elastic and seismogenic layer thickness. *Earth and Planetary Science Letters* 213: 113–131.
Watts AB, Sandwell D, Smith WH, and Wessel P (2005) Global gravity, bathymetry and the distribution of submarine volcanism through space and time, T41C-1326. *Journal of Geophysical Research* 111: B080408.
Weinberg RF and Podladchikov Y (1995) The rise of solid state diapirs. *Journal of Structural Geolology* 17: 1183–1195.
Wei W, Unsworth M, Jones A, *et al.* (2001) Detection of widespread fluids in the Tibetan crust by magnetotelluric studies. *Science* 292(5517): 716–719 (doi: 10.1126/science.1010580).
Weissel J, Anderson RN, and Geller C (1980) Deformation of the Indo-Australian plate. *Nature* 287: 284–291.
Wever T (1989) The Conrad discontinuity and the top of the reflective lower crust – do they coincide? *Tectonophysics* 157: 39–58.
Wilks KR and Carter NL (1990) Rheology of some continental lower crustal rocks. *Tectonophysics* 182: 57–77.
Wittlinger G, Tapponnier P, Poupinet G, *et al.* (1998) Tomographic evidence for localized lithospheric shear along the Altyn Tagh fault. *Science* 282: 74–76.
Yamato P, Agard P, Burov E, Le Pourhiet L, Jolivet L, and Tiberi C (2006) Burial and exhumation in a subduction wedge: Mutual constraints from thermomechanical modeling and natural P-T-t data (Sch. Lustrés, W. Alps). *Journal of Geophysical Research* 8: 08714.
Zoback ML (1992) First- and second-order patterns of stress in the lithosphere: The World Stress Map project. *Journal of Geophysical Research* 97: 11703–11728.
Zoback MD, Apel R, Baumgartner J, Brudy M, *et al.* (1993) Upper-crustal strength inferred from stress measurements to 6 km depth in the KTB borehole. *Nature* 365: 633–635.
Zoback MD and Townend J (2001) Implication of hydrastatic pore pressures and high crustal strength for the deformation of intraplate lithosphere. *Tectonophysics* 336: 19–30.